UNIVERSITÀ DEGLI STUDI DI PALERMO

Dottorato di Ricerca in Biomedicina e Neuroscienze
Dipartimento di Biomedicina, Neuroscienze e Diagnostica Avanzata (BIND)
SSD BIO/16

NEUROINFLAMMATION AND SYNAPTIC IMBALANCE IN ALZHEIMER'S DISEASE

IL DOTTORE
PIETRO SCADUTO

IL COORDINATORE
FABIO BUCCHIERI

IL TUTOR
GIUSEPPA MUDÒ

IL CO TUTOR
AGENOR LIMON

CICLO XXXII
2018-2019

Dedication

A mia nonna Franca,

la donna più forte che abbia mai conosciuto.

Alla sua incredibile fantasia.

Sempre cantava felice.

Acknowledgements

I would like to thank my mentors, Dr. Limon, Dr. Belluardo and Dr. Mudò for advising me, guiding me and for their unconditional support during my PhD.

I would also thank Dr. Cappello and Dr. Taglialatela to be the minds behind this successful combined PhD program between the Universities of Palermo and Galveston.

I want to thank Monica Frinchi, Domenico Nuzzo, Julie Lauterborn for contributing to part of the work presented in this thesis.

A special thanks goes to the "Behavior Guys" of the Department of Physiology at UNIPA for teaching me most of what I know about behavioral tests and for spending a very good time together.

Thanks to Timi (Oluwarotimi Folorunso) for the nights at work doing electrophysiological experiments and eating cookies.

Thanks to the Italian family in Galveston for the good time spent together and for the tons of coffee drank in the conference room.

Special thanks to Claudia Marino, she always supports me with all her passion and patience.

Thanks to my family for understanding and always supporting my choices.

Thanks also to my friends in Bagheria and to the BioNeC Scientists.

Thesis by scientific manuscripts

1) G. Mudò, M. Frinchi, D. Nuzzo, **P. Scaduto**, F. Plescia, M. F. Massenti, M. Di Carlo, C. Cannizzaro, G. Cassata, L. Cicero, M. Ruscica, N. Belluardo, L. M. Grimaldi. Anti-inflammatory and cognitive effects of interferon-β1a (IFN-β1a) in a rat model of Alzheimer's disease. [PMID: 30777084 - J Neuroinflammation. 2019; 16: 44].

2) **P. Scaduto**, A. Sequeira, M. P. Vawter, W. Bunney, A. Limon. Preservation of global synaptic excitatory to inhibitory ratio during long postmortem intervals. [Reference number: NMETH-BC40451- submitted to Nature Methods].

3) J. C. Lauterborn, **P. Scaduto**, G. Lynch, C. M. Gall, C. D. Keene, K. Jennings, A. Limon. Increased Functional Excitatory to Inhibitory Synaptic Ratio in Parietal Cortex of Alzheimer's Disease. [Reference number: NCOMMS-19-539505- submitted to Nature Communications].

Table of Contents

List of Abbreviations

AD: Alzheimer's disease
AMPA: α-amino-3-hydroxy-5-methyl-4-isoxazolepropionic acid
APOE: apolipoprotein ε
APP- β: amyloid β precursor protein
ATP: adenosine tri-phosphate
Aβ: amyloid β
Aβ-42: amyloid β Protein Fragment 1-42
CN: cognitive normal
CNS: central nervous system
ConA: concanavalin A
CSF: cerebral spinal fluid
CTZ: cyclothiazide
DCF: dichlorofluorescein
DCFH-DA: dichlorofluorescein diacetate
DLG4: PSD-95 gene
DMN: default mode network
DS: down Syndrome
E/I ratio: global synaptic Excitatory to inhibitory ratio
EC50: half of the apparent affinity
ELISA: enzyme-linked immunosorbent assay
fAD: familial Alzheimer's disease
FDT: fluorescence deconvolution tomography
GABA: gamma aminobutyric acid
$GABA_A$Rs: gamma aminobutyric acid receptor type A.
GFAP: glial fibrillary acid protein
GPHN: gephyrin gene
IFN: interferon
IFN-β-1a: interferon-β1a
IGluR: glutamate inotropic receptors
τ : time constant
ρ: non-parametric Spearman's
IL: interleukin
Ir: immunoreactivity
MCI: mild cognitive impairment
MDA: malondialdehyde
MRI: magnetic resonance imaging
MS: multiple sclerosis
MSM: microtransplantation of synaptic membranes
MTS: ([3-(4,5-dimethylthiazol-2-yl)-5-(3-carboxymethoxyphenyl)-2-(4-sulphophenyl)-2H-tetrazolium]
NF-kB: transcription factor nuclear factor-kB
NMDA: N-methyl-D-aspartate
PCx : parietal cortex
PET: positron emission tomography
PiB : Pittsburgh Compound B
PLSD: Fisher's Protected Least Significant Difference
PMI: *post-mortem* interval
PNF-kB: phosphorylated NF-kB
PS1: presenilin-1
PS2: presenilin-2
ptau: phosphorylated tau
ROS: reactive oxygen species
SAD: sporadic Alzheimer's disease
SSAD: staging of severity of AD
Syn: synaptophysin
RI%: recognition index
TBA: thiobarbituric acid
TEVC: two electrode voltage clamp
TGF-β1: Transforming growth factor-beta1
TNF-α: tumor necrosis factor

Abstract

Alzheimer's disease (AD) is a progressive neurodegenerative disease and the most common cause of dementia worldwide. AD hallmarks are synaptic dysfunction and toxic oligomers accumulation that ultimately lead to cognitive and memory impairment. In addition to synaptic dysfunction, neuroinflammation also plays a central role in AD. Toxic oligomers seem to trigger neuroinflammation and together contribute to impair synaptic function that underlies cognitive decline in AD. Compelling evidence have shown that neuroinflammation, accumulation of toxic oligomers and synaptic dysfunction form a positive feedback cycle that may produce aberrant activity of neuronal circuits. In AD patients, brain regions affected by neuropathology have been shown to be hyperexcitable, which seems to contribute to the cognitive decline observed in these patients. However, the mechanism behind this hyperexcitability remains to be understood.

In this thesis, I focus on two of the main AD features: neuroinflammation and synaptic dysfunction. (i) I tested an anti-inflammatory compound (INF-β1a) that reduced neuroinflammation and cognitive decline in an AD rat model. Indicating that neuroinflammation is a valid target for effective therapies. In addition, (ii) by using novel histological and electrophysiological methods I found an imbalance of synaptic excitatory to inhibitory ratio toward pro-excitatory changes in the parietal cortex of the AD brain. This information may help to explain the hyperexcitability in the cortex of AD subjects. Taking all this together, these results provide insights into future strategies to break up the positive feedback loop between oligomers, synaptic dysfunction and neuroinflammation in AD and help to treat patients affected by this devastating disease.

CHAPTER I. INTRODUCTION

Alzheimer's disease

Alzheimer's disease (AD) is an age-related neurodegenerative disorder with a long prodromal phase (around 20 years), that ultimately leads to dementia and death [1]. It is characterized by over-production and aggregation of brain derived proteins prone to misfold such as β-Amyloid (Aβ) and tau, and by synaptic dysfunction which in turn leads to a progressive impairment of cognitive functions [2], [3]. Aβ is a 39–43 amino acid long peptide that have a role in neuronal survival and in synaptic excitability [4], [5]. Tau is a microtubule-associated protein highly abundant in neurons that is involved in cell transport and microtubules stabilization [6]. Protein misfolding is a common cellular event that may be caused by genetic mutations, translational errors, abnormal protein modifications, thermal or oxidative stress, and incomplete complex formations [7]. Misfolded forms of Aβ and tau lead to their aggregation and accumulation. Aβ is considered the trigger of the AD pathology and tau species accumulation increase accordingly to AD severity [8]. However, cognitive decline correlates better with synaptic loss [3], [9]. Histopathologically, AD is characterized by progressive brain shrinking and limbic and cortical degeneration (Figure 1, [10]).

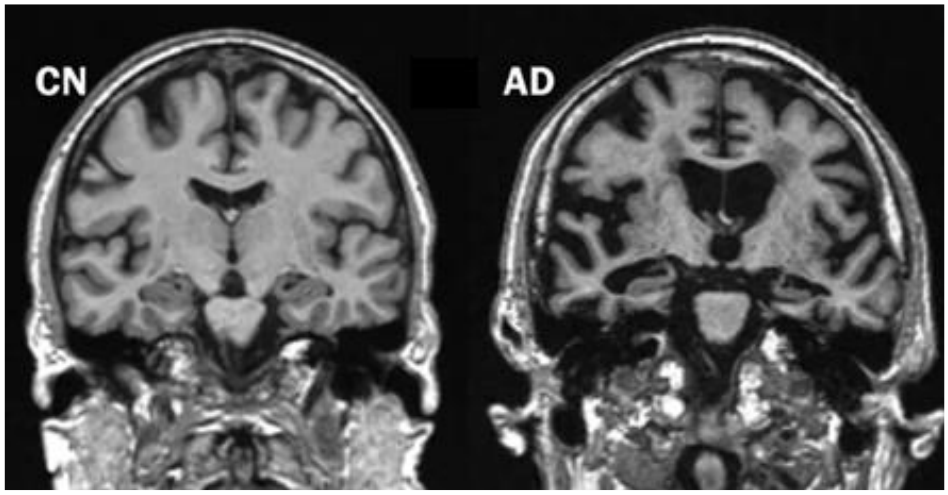

Figure 1. Magnetic resonance imaging (MRI) scan. Coronal section from a cognitive normal (CN) and an Alzheimer's disease (AD) subjects. Modified figure from [10].

The clinical diagnosis of potential AD is established by testing cognitive function as memory, problem solving, attention, counting, and language; or by measuring Aβ and tau accumulation in cerebrospinal fluid (CSF); or by molecular imaging as positron emission tomography (PET)-amyloid and –tau assays and structural magnetic resonance imaging (MRI) in the brain [11], [12].

AD is the most common form of dementia worldwide. In U.S, there are 5.8 million of Alzheimer's cases, and this number is projected to rise nearly to 3 times in the next 30 years [1], [13], [14]. In 2018, the cost of caring for the U.S medical system for those with Alzheimer's and related dementias is estimated to total $290 billion [15]. Currently, there are no effective therapies to treat AD due to the pour knowledge about the mechanisms of neurodegeneration.

Molecular lesions caused by toxic protein accumulation in the aging brain seem to lead to inflammatory damage and excitability impairment: both resulting in synaptic dysfunction. However, recent evidence suggests that neuroinflammation and aberrant brain excitability are not passive systems activated by emerging senile plaques and neurofibrillary tangles, but instead contribute as much as toxic oligomers to AD pathogenesis [16]–[18]. Toxic oligomers production, inflammation and aberrant brain excitability are reciprocally influenced in a positive feedback loop [19]–[25].

History of Alzheimer's disease

AD was first described in the early 1900's by Dr. Aloysius Alzheimer and collaborators [26], by reporting the first clinical case of a "paranoiac with progressive sleep and memory disturbance, aggression, and confusion symptoms". After several decades, in 1984, a task force group composed of leading experts intended to establish and describe a clinical criteria for the diagnosis of AD [27]. AD was thus defined as a brain disorder characterized by progressive dementia. Its pathologic characteristics are degeneration of neurons; presence of neuritic plaques, characterized by Aβ aggregates surrounded by a dense network of nerve cell processes; and intracellular neurofibrillary tangles that are product of the misfolding and aggregation of tau protein (Figure 2, [28]). Moreover, AD was defined as a clinical-pathologic entity, which is diagnosed definitely at autopsy and in life as possible or probable AD [27]. Over the last three decades, researchers have worked to improve the AD diagnosis accuracy in alive people, trying to avoid errors derived from misinterpreting prototypical clinical syndromes without neuropathological verification.

In 1991, Heiko and Eva Braak studied 83 brains from non-demented and demented individuals. Histological sections from these brains were examined for extracellular amyloid deposits and intraneuronal neurofibrillary changes to develop the first classification of AD brain region and severity progression, also known as Braak staging [29]. This classification is still widely accepted to evaluate the severity of the disease on post-mortem brain, and it is mainly based on neurofibrillary tangles distribution. The pathology is divided in 6 stages: the first two earlier stages (transentorhinal phase) were characterized by mild or severe transentorhinal alteration, 3rd and 4th stages (limbic phase) were defined by the spread of the neurodegeneration in the proper entorhinal cortex, and 5th and 6th stages (isocortical phase) were marked by destruction of many cortical association areas [29].

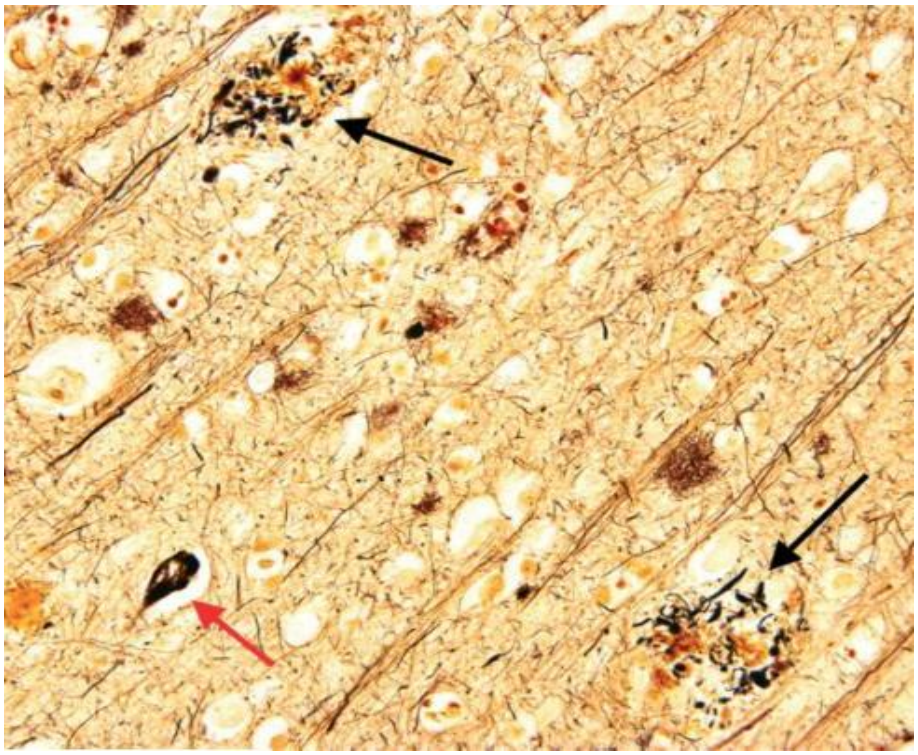

Figure 2. Temporal cortex of a patient with Alzheimer's disease (modified Bielschowski stain; original magnification, 100×). Numerous senile (neuritic) plaques (black arrows) and neurofibrillary tangles (red arrow) are shown. (Figure reference [28])

Despite the considerable progress over the years, the mechanisms behind the neurodegeneration in AD are still not fully understood. Importantly, AD lacks disease-modifying therapies. Many clinical trials preventing aggregation or inhibiting pathways related to amyloid and tau aggregation had failed, and current treatments are only palliative [30]. There are 4 drugs approved by the Federal Drug Administration (FDA) that are currently used for the symptomatic treatment for AD: donepezil, rivastigmine, galantamine, and memantine. The first 3 drugs target the cholinergic system. Memantine is an uncompetitive antagonist of the N-methyl-D-aspartate (NMDA) glutamate receptor. All of them have a temporary modest effect on AD symptoms but are unable to stop or reverse the progression of dementia [31], [32].

Classification of AD pathologies

AD can be classified as familial (fAD) or sporadic (sAD), depending of the pathogenesis. The incidence of fAD is lower than 5% and is associated to mutations in three different genes: presenilin-1 (PS1), presenilin-2 (PS2), and amyloid-β precursor protein (APP-β) [14], [33]. All known fAD mutations are related to the biological cascade controlling either the biosynthesis or the processing of APP [34]–[36]. Down syndrome, characterized by an extra copy of chromosome 21 in which is located the APP gene, is another genetic risk

factor contributing to AD pathogenesis [37]. Sporadic AD (>95%) has a multifactorial onset and the main risk factor is aging with the prevalence of AD rising exponentially after 65 years of age [38]. AD incidence doubles every 5 years after 65 years of age, and even if AD is not always the outcome of aging, after 85 years of age, one in every three subjects is diagnosed with AD [39]. There are other risk factors for AD: lower education, female sex, head trauma, heart disease, smoking, diabetes type 2 and the presence of either 1 or 2 copies of the ε4 allele of the gene for apolipoprotein E (*APOE*) [40]. ApoE is a protein involved in lipid metabolism and consisting in 3 known isoforms: ApoE2-4. ApoE3 is the physiological variant while ApoE4 seems to contribute to an increased risk for AD and ApoE2 has been shown to be protective. Also physical activity and Mediterranean diet seems to a protective role as well. [41], [42].

Despite the effort to characterize distinct pathological stages, AD pathology is considered as a *continuum.* After a preclinical asymptomatic phase, the first signs of cognitive impairment appear and then there is a progressive worsening of symptoms. Subjects with genetic risks of AD or showing positive AD biomarkers without fAD mutations in the early stage of the disease, present a cognitive performance below the expected range. These subjects, which are diagnosed with mild cognitive impairment (MCI, table 1, [43]), are considered to be at an intermediate clinical stage between cognitively intact and AD type dementia [44], [45].

Recent evidence suggests that early cognitive alterations are detectable years before meeting criteria for MCI and may allow to predict the progression to dementia. The study of asymptomatic fAD subjects is critical to elucidate the early impairment of AD. Asymptomatic fAD subjects have shown accumulation of tau and Aβ-42 (considered the most toxic isoform of Aβ) in CSF and in the brain parenchyma [46], [47], and impairment of synaptic excitability [17], [48] years before the onset of clinical AD. Interestingly, the excitability impairment in these individuals produces hyperexcitability of the cerebral cortex and hippocampus, increases the frequency of the seizures, and disrupts functional connectivity in the brain (described in details in “Synaptic excitability in AD” paragraph below)..

Syndromal Cognitive Stage				
Biomarker Profile		**Cognitively unimpaired**	**MCI**	**dementia**
	$A^- T^- (N)^-$	normal AD biomarkers, cognitively unimpaired	normal AD biomarkers with MCI	normal AD biomarkers with dementia
	$A^+ T^- (N)^-$	Preclinical Alzheimer's pathologic change	Alzheimer's pathologic change with MCI	Alzheimer's pathologic change with dementia
	$A^+ T^- (N)^+$	Alzheimer's and concomitant suspected non Alzheimer's pathologic change, cognitively unimpaired	Alzheimer's and concomitant suspected non Alzheimer's pathologic change with MCI	Alzheimer's and concomitant suspected non Alzheimer's pathologic change with dementia
	$A^+ T^+ (N)^-$	Preclinical Alzheimer's disease	Alzheimer's disease with MCI (Prodromal AD)	Alzheimer's disease with dementia
	$A^+ T^+ (N)^+$			

Table 1. Schematic AD continuum biomarker profile in cognitive unimpaired, MCI and demented subjects [43]. A, β amyloid deposition; T, pathologic tau; N, neurodegeneration.

Neuroinflammation in AD

Neuroinflammation in AD is crucial for the progression of synaptic degeneration. In the past two decades, compelling evidence (rev. in [25]) suggests a central role of glial cells such as microglia and astrocytes, and their cytokines as IL-1β, TNF-α, IL-6, IL-18 in the neurodegeneration caused by AD.

Microglia are resident immune cells of the CNS. They are activated during acute and chronic insults providing surveillance and scavenging functions. High levels of activated microglia has been found around abnormal protein deposits in AD suggesting that they possibly participate in the process of Aβ and tau clearance [49]. Microglia also modulates synapses during neurodevelopmental processes such as neurogenesis and synaptic pruning. In the adult brain, microglia and neurons are in a functional reciprocal interaction: chemically, through ATP and CD200 signaling; and physically, through processes connecting resting microglia and highly active neurons [50]–[52]. CD200 is a membrane glycoprotein seem to be involved in neuroprotection and is typically expressed in neurons, oligodendrocytes and astrocytes. The target receptor of CD200 is CD200R, expressed only in microglia and macrophages. CD200 signaling steer microglia activation state playing a critical role in neuronal protection, and interesting, is impaired in multiple sclerosis (MS) and Alzheimer's disease [53]–[55]. In addition, activated microglia can remove inhibitory synapses from neural soma increasing the excitatory transmission [56].

Astrocytes are the largest cell population in mammalian central nervous system (CNS). They became active as a result of an insult in a process known as reactive astrogliosis. Active astrocytes undergo to cellular hypertrophy with increased content in glial intermediary filaments mainly composed by glial fibrillary acid protein (GFAP). Astrocytes seems to be implicated in the onset and progression of several neurodegenerative disease such as AD [57]. They are found to co-localize with Aβ aggregates. Similarly to the microglia, astrocytes have been reported to adopt a phagocytic profile capable of internalize Aβ [57], [58]. Astrocytes are intimately in contact with pre- and post- synaptic compartment forming the tripartite synapse [59], [60]. They release neuroactive molecules as glutamate, d-serine, ATP, adenosine,

The source and association of pro-inflammatory cytokine with AD pathogenesis					
Pro-inflammatory cytokine	**CNS origin**	**Effects on neurons**	**Synaptic effects**	**Effects on Aβ**	**Effects on tau**
TNF-α	Microglia, astrocytes, neurons	Pro-apoptotic; prevent apoptosis	Synaptic excitotoxicity; LTP ↓	↑ Aβ synthesis; ↓ Aβ clearance	↑ tau hyperphosphorylation
IL-1β	Microglia, astrocytes	Neuronal death and damage↑	LTP ↓ synaptic plasticity↓	↑ Aβ synthesis	↑ tau phosphorylation
				↓ Aβ-related pathology	↓ tau pathology
IL-6	Microglia, astrocytes, endothelial cells	Rescue neurons	LTP ↓ prevents synaptic loss	↓ Aβ deposition	↑ tau phosphorylation
IL-18	Activated microglia, astrocytes and ependymal cells	Pro-apoptotic	↓ the induction of LTP	↑ production of APP ↑Aβ	↑ hyperphosphorylation of tau

Table 2. Pro-inflammatory cytokines effects on key AD features. CNS, central nervous system; TNF-α, tumor necrosis factor alpha; IL, interleukin; LTP, long term potentiation; Aβ, amyloid beta; ↑↓, increase or decrease (Modified table from [65]).

GABA, tumor necrosis factor α (TNFα), that can influence neuronal and synaptic physiology[60] and seems to participate in the elimination of synapses [61].

As a result of neuronal insults glial cells release to the extracellular compartment soluble inflammatory molecules such as cytokines. The cytokines, binding their own receptors, activate pro- or anti- inflammatory responses. Recent evidence, reviewed in [62], indicates that pro-inflammatory cytokines modulate brain excitability. Interleukin-6 (IL-6) and interleukin-1 receptor antagonist (IL-1ra) are increased in CSF and plasma of patients with recent tonic–clonic seizures [63], and in animal models pre-treatment with IL- 1β increase the susceptibility to seizures [64].
In AD, pro-inflammatory cytokines, as IL-1β, TNF-α, IL-6 and IL-18 are overproduced and affect the normal neuronal activity (table 2, [65]).

Synaptic imbalance in AD

Neural excitability depends largely on the synaptic activity [66], and AD is considered a disease of the synapses [67]. Contrary to the past reports [67], not only excitatory (glutamatergic) signaling is disrupted in AD, but also inhibitory (gamma aminobutyric acid or GABAergic) signaling [68], [69]. The vast majority of the synapses in human brain use glutamate or GABA as neurotransmitters, and together with their own synaptic receptors, these neurotransmitters are critical for slow neurotransmission via metabotropic receptors, and fast neurotransmission via ionotropic receptors. In this study, I will focus on the fast-synaptic transmission.

Glutamate inotropic receptors (iGluRs) are the major mediators of the fast-excitatory synaptic transmission in the mammalian brain. They are transmembrane ligand-gated ion channels composed by a combination of four subunits. IGluRs, based on their subunit composition, have different physiological properties and are divided in 3 subclasses: α-amino-3-hydroxy-5-methyl-4-isoxazolepropionic acid receptors (AMPARs), kainate receptors, and NMDARs. All of them are permeable to cations. Importantly, AMPARs and NMDARs are known to bind Aβ oligomers, thus causing the opening of the receptors [70].
$GABA_A$ receptors ($GABA_ARs$) are the major mediators of the fast-inhibitory synaptic transmission in the mammalian brain. They are pentameric transmembrane receptors forming a central pore permeable to chloride ions. $GABA_ARs$ are made by the arrangement of five of the nineteen possible subunits, giving to this receptor a large variability of isoforms [71]. Moreover, Aβ oligomers reduce inhibitory post-synaptic currents in neurons via $GABA_AR$ [72].

Glutamatergic and GABAergic synaptic transmissions are constantly tuned to each other during the neurogenesis, adulthood and senescence of the individual[73], [74]. This complex process is named excitation to inhibition balance. It can be defined as the average amount of depolarizing to hyperpolarizing neuronal synaptic currents (global synaptic E/I ratio or just E/I ratio) in a particular region [75]. E/I ratio is critical for coherent neural coding [76] and its impairment has been associated with the onset of disorders such as schizophrenia, autism and AD [77], [78]. Animal models of AD and epilepsy show brain hyperexcitability due to E/I imbalance [21], [79], possibly as a result of alteration of glutamatergic and GABAergic neurotransmission [19]. Tau seems to be essential in this process [20]. Furthermore, evidence reviewed in [80] shows that Aβ oligomers increase calcium permeability in neurons and glia that could lead to disruption of brain circuits, hyperexcitability and increase of cytokines production [81]–[83].

Aberrant excitability has been reported in pre-clinical AD, MCI and AD suggesting that synaptic alterations precedes cognitive symptoms and persist over time. Functional MRI analysis revealed that pre-clinical AD in APOE ε4 positive subjects shows temporal and parietal cortex hyperactivity during cognitive challenge tasks. The hyperactivation correlated with the degree of decline in memory among subjects who were

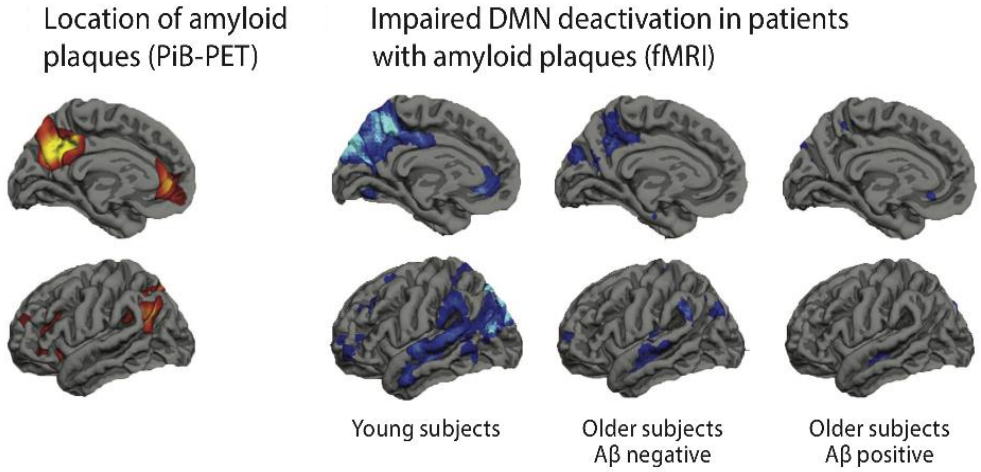

Figure 3. Deactivation of the default mode network (DMN) is reduced with aging and Aβ burden. Modified figure taken from[90]. Anatomic distribution of Aβ burden (yellow and red) detected using Pittsburgh Compound B (PiB) and positron emission tomography (PET). On the right, demonstrating significant task-related decreases in fMRI activity (deactivation shown in blue) during successful encoding of face-name.

retested two years later [48]. Also, pre-clinical AD, carrying fully-penetrant genetic alterations in PS1, have shown hyperactivation of hippocampus [17]. MCI patients present fMRI hyperactivation in hippocampus during memory task performing, and interestingly, it negatively correlates with temporal and parietal thickness [84]. Reducing the hyperexcitability in MCI patients using an atypical anti-epileptic improved their cognition [45], [85]. Subjects with full-blown AD have 6- to 10-fold increase risk of seizures [86],

and show similar medial temporal hyperactivity described before (rev. in [87]). In AD subjects, medial temporal hyperactivity correlates with parietal degeneration, and dysconnectivity between medial temporal lobe and parietal cortices [88].

Interestingly, brain areas in which Aβ start to accumulate are also hyperactive in AD. These areas are functionally interconnected and form a functional network named: *default mode network (DMN)* [89]–[91]. The structural core region of DMN are the posterior medial and parietal cerebral cortices as well as distinct temporal and frontal modules [92]. DMN is active at a resting state but needs to be deactivated when the subject is required to perform a task that involve directing attention to an external stimulus [93]. The efficient deactivation of this brain network is critical for attention, memory and language processing [94]–[96]. Emerging evidence using PET-scan has shown that in AD subjects the accumulation of β-amyloid starts in areas of the DMN causing impairment of the connectivity and deactivation failure (figure 3)[90], [97]. DMN is currently considered as a primary locus of AD pathology [98].

Interferon β-1a

Interferons (IFN) are a family of cytokines involved in the regulation of innate and adapted immunity and IFN-β, a member of this family, was the first approved therapy for multiple sclerosis., IFN-β-1a is the most used isotype of IFN-β for clinical purposes. It inhibits the production of cytokines particularly expressed during the inflammatory response in neurodegenerative diseases (IL-1β, TNF-α, IFN-γ and IL-6) [99]. It also decreases the activation of glial cells and reduce oxidative stress [100].

IFN-β also plays an important role in synaptic transmission by directly modulating glutamatergic neurotransmission. In striatal middle spiny neurons, IFN-β modulates calmodulin-dependent protein kinase II (CaMKII) to inhibit glutamate neurotransmission [101]. CaMKII is a kinase activated by intracellular Ca^{2+} levels, it also regulates and interacts with glutamate NMDA receptors [102]. However, IFN-β seems to produce different effects, depending of the brain region [101], [103]–[105].

Interestingly, administration of IFN-β1a significantly prevented cognitive decline in a large cohort of patients with multiple sclerosis, thus suggesting that modulation of neuroinflammatory pathways may prevent cognitive decline in humans [106], [107], as well as cortical atrophy associated with cognitive impairment in patients with multiple sclerosis [108]. A preliminary evaluation of IFN-β1a safety and efficacy was done in subjects affected by mild-to-moderate AD in a phase 2a study [109], and although not statistically significant, they observed a reduction in disease progression during follow-up as measured by the AD Physical Self-Maintenance Scale.

CHAPTER 2. SPECIFIC AIMS

As mentioned before, AD is the most common cause of dementia and is a multifactorial disease with a complex interplay of genetics and environmental factors [16], [110]. This dissertation aims to better understand two of the key features that has been strongly associated with AD onset: neuroinflammation and synaptic imbalance. These two events, together with toxic oligomers, seems to reinforce themselves through a feedback loop that exponentially worsens the AD behavioral outcome over time.

Neuroinflammation has been widely recognized as a possible pathological contributor to AD, usually including activation of glial cells, such as microglia and astrocytes, and release of cytotoxic compounds (e.g., cytokines and ROS) able to cause neuronal damage and death [25], [111]. Because suppression of neuroinflammation may have therapeutic effects for AD, several approaches have been tested to smolder inflammatory processes by using anti-inflammatory drugs [112]–[115] in AD models [116]. However, anti-inflammatory strategies tested in AD patients have not achieved satisfactory results, indicating the need for a better understanding of the role of the immune system in cerebral proteinopathies and the strategies to modulate it [117]. Nevertheless, intervention with drugs modulating pro-inflammatory cytokine production is still considered a potentially useful strategy to slow down the disease course of this dreadful disease.
I hypothesized that interferon β1a, an anti-inflammatory drug (discussed in chapter 1) is capable to reduce neuroinflammation and to improve cognition in an animal model of AD pathogenesis.

Excitability impairment in AD is observed as increase in the prevalence of seizures and hyperexcitability in imaging studies. Clinical studies and experiments with animal models suggest that synaptic loss may disturb the excitatory to inhibitory balance in circuits vulnerable to AD pathology [118]–[121], which in turn could lead to the cortical hyperexcitability that is associated with cognitive impairment [118], [119], [122], [123]. Moreover, electrophysiological evidence from animal model studies indicates that the activity and strength of excitatory and inhibitory synapses in the cerebral cortex are highly correlated across different cortical activity patterns [76], [124], [125]. Thus, synaptic currents, through excitatory AMPARs and $GABA_A$Rs, are tightly regulated to preserve the global synaptic E/I ratio within a range that allows for normal network level operations.

I hypothesized that brain regions affected by AD pathogenesis, known to be hyperexcitable, will show an imbalance of the E/I ratio toward pro-excitatory changes.

To test these 2 hypotheses, I completed the following aims:

Aim.1. Evaluate anti-inflammatory and cognitive effects of interferon-β1a (IFN-β1a) in a rat model of Alzheimer's disease. I obtained a rat model of AD by intra-hippocampal injection of Aβ-42 peptide. Using novel object recognition and elevator plus maze tests I assessed the cognitive functions. We also studied neuro-inflammation testing levels of ROS, SOD, cytokines and lipid peroxidation using a combination of immunohistochemistry and biochemical techniques. Finally, I tested INF β-1a, an anti-inflammatory drug, on the AD rat model to determine whether the drug produced an improvement of neuro-inflammation and cognitive functions.

Aim.2.1. Determine the preservation of global synaptic Excitatory to Inhibitory ratio during long postmortem intervals. First, I assessed the effect of the *post-mortem* interval on the global postsynaptic excitatory to inhibitory balance (E/I ratio) of a non-demented individual, and in rat brain cortices, using microtransplantation of synaptic membranes (MSM) into *Xenopus laevis* oocytes. I used two electrode voltage clamp (TEVC) on microtransplanted oocytes, to record electrophysiologically the maximum amplitude and agonist affinity of synaptic excitatory iGlu and inhibitory $GABA_A$Rs. These experiments helped to determine the preservation status of the E/I ratio after death.

Aim.2.2. Determine whether an increased functional Excitatory to Inhibitory synaptic ratio is present in the parietal cortex of Alzheimer's disease subjects. Second, I determined the E/I ratio in the parietal cortex from AD subjects. This region was chosen because it is known to be first affected by β -amyloid accumulation and to be overly active and functionally impaired in AD. We compared AD subjects with Down syndrome and control subjects. Down syndrome patients also have AD neuropathology but the parietal cortex is less affected compared to AD in imaging studies. Moreover, using fluorescent deconvolution tomography and flow cytometry assays, I evaluated the relative number of excitatory and inhibitory synapses and their sizes in this region. This information helps to explain the role of synaptic imbalance in the aberrant activity of the parietal cortex in AD.

CHAPTER 3. METHODS

Aim 1. Anti-inflammatory and cognitive effects of interferon-β1a (IFN-β1a) in a rat model of Alzheimer's disease

Animals

Adult female Wistar rats (3 months old) were used. Rats were housed in a specific pathogen-free environment, three per polypropylene cages in controlled temperature (23 ± 2 °C), humidity (50–55%), and light (12-h light/dark cycle), with access to food and water *ad libitum*. Procedures involving animal were carried out in accordance with the Italian institutional guidelines (D. LGS. no. 26, GU n.61, March 2014). All applicable international, national, and/or institutional guidelines for the care and use of animals were followed. No other methods to perform the described experiments were found.

Experimental design

For this study, we used the following experimental groups (N=6 each group): (1) a control group treated with saline only (control); (2) a sham-operated control group and treated with saline (sham); (3) an Aβ-42 peptide-treated group; (4) an interferon-β1a (IFN-β1a)-treated group; and (5) an Aβ-42 peptide + IFN-β1a-treated group. Rats received two bilateral intra-hippocampal injections of 23 μg/2 μl of Aβ-42 peptide dissolved in 0.9% physiological saline solution. IFN-β1a was given subcutaneously (s.c.) at a dose of 3.6 μg (1 M Units, Rebif, Merk Serono, London) in a volume of 0.1 ml of 0.9% of saline solution. We used female rats because in AD disproportionately the female/male ratio is 2:1, although the biological basis of these sex-based differences in AD onset and progression remains elusive [126], [127].

Aβ-42 peptide preparation and toxicity

Aβ-42 protein was produced according to Carrotta et al. [128]. For the kinetics of aggregation, the sample of Aβ-42 protein was loaded in a 96 black multi-well and added with 8 μM of thioflavin-T. The multi-well was read to the plate reader every 30 s at 450–485 nm wavelength for 8 h at 37 °C. After the 8 h of incubation, the formation of Aβ-42 protein aggregates was also evaluated at the fluorescence microscope (Leica Microsystems, Heidelberg, Germany). In addition, the mean size of the Aβ-42 plates was measured by fluorescence microscopy software (Leica QFluoro V1.1 software, Heidelberg, Germany).

LAN5 cells were cultured with RPMI 1640 medium (Celbio srl, Milan, Italy) supplemented with 10% fetal bovine serum (Gibco-Invitrogen, Milan, Italy) and 1% antibiotics (50 mg mL − 1 penicillin and 50 mg ml − 1 streptomycin). Cells were maintained in a humidified 5% CO_2 atmosphere at 37 ± 0.1 °C. For

dose-effect studies of Aβ-42 toxicity, cells were treated with 50, 75, and 100 μM of Aβ-42 for 24 h, and thereafter, their viability was evaluated by MTS assay ([3-(4,5-dimethylthiazol-2-yl)-5-(3-carboxymethoxyphenyl)-2-(4-sulphophenyl)-2H-tetrazolium]; Promega Italia, S.r.l., Milan, Italy) and morphological analyses. After 24 h of cell treatment with Aβ-42, 20 μl of the MTS solution was added to each well for 3 h at 37 °C, 5% CO2. The absorbance was read at 490 nm on the Microplate reader (WallacVictor 2 1420 Multilabel Counter) (PerkinElmer, Inc. Monza, Italy).

Aβ-42 intra-hippocampal injection

The Aβ-42 peptide intra-hippocampal injection was performed as described by Mudò et al. [129]. Shortly, rats were anesthetized with mixture of 1:1 of Zolazepam + tiletamine 15 mg/kg b.w. (Zoletil, Virbac) and xilazine 9 mg/kg b.w. (Nerfasin, ATI, Italy), placed in a David Kopf stereotaxic apparatus, and received two bilateral intra-hippocampal injections of 23 μg/2 μl of Aβ-42 peptide, using the following stereotaxic coordinates from the Bregma, according to Paxinos and Watson (1998): first injection AP = − 3.6, L = 2, and V = 4.5; second injection AP = − 4.2, L = 2.4, and V = 4.5. The sham group was intra-hippocampal-injected with 2 μl of 0.9% physiological saline. Injections were performed by 30-gauge injector cannula that was connected by a piece of polyethylene tube to the 10 μl Hamilton syringe. Each injection was performed over 3 min, and following injection, the needle remained in the target location for 3 min to avoid Aβ-42 peptide reflux along the needle tract and to achieve a proper diffusion of the drug. After surgery, each rat was treated with penicillin (100,000 U/i.m.) to prevent infection.

Behavioral testing

Using the novel object recognition (NOR) test, we evaluated changes in cognitive function of the experimental animals (for this experiment we used 8 animals in each group). Rats were tested in an open field Plexiglas square box, in a mean light intensity (100 lx) illuminated chamber. All experimental groups were subjected to a 5-min training session when they were presented two identical non-toxic objects (i.e., two metal cans) placed against a wall in the open field arena. To prevent coercion to explore the objects, rats were released against the opposite wall with the back to the objects. The time spent on exploring each object was recorded using ANY MAZE Video Tracking System (Ugo Basile, Italy); a 2-cm^2 area surrounding the objects was defined such that nose entries were recorded as time exploring the objects. After the training session, animals were placed in their home cage for a 24-h retention interval. Then, they were returned to the arena containing two objects: one was identical to the familiar one but previously unused (to prevent olfactory cues and the necessity to wash objects during experimentation) and the other was a novel object (metal, glass, or hard plastic items). Time spent on exploring each object was recorded along 5-min session. Objects were randomized and counterbalanced across animals. The objects and arena

were thoroughly cleaned at the end of each experimental session. The recognition index (RI), which is the time spent on investigating the novel object, divided by the total amount of exploration time of the novel (TN) and familiar objects (TF), [RI = TN/(TN + TF)], is a measure of novel object recognition and the main index of retention. If RI percentage is higher than 50%, it indicates more time spent on inquiring into the novel object, whereas less than 50% indicates that time was prevailingly spent on exploring the familiar object, and 50% indicates a null preference.

Immunohistochemistry

The rats under deep anesthesia were perfused through the aorta with 0.9% saline and the brain was dissected afterwards. The left side of the brain was used for histological evaluation and the right side for molecular analysis. Immuno-histochemical experiments were performed as described by Di Liberto et al. [130]. The left side of brain was fixed with 4% of paraformaldehyde in 0.1 M phosphate buffer (pH 7.4) for 2 days and then immersed in the sucrose 10% solution for 1 day and in sucrose 20% for 2 days. Subsequently, brains were frozen in cooled isopentane and 20-μm-thick coronal sections at hippocampal level were prepared and processed for immunohistochemistry as free-floating sections. Sections were washed for 5 min in 0.1 M PBS and incubated for 15 min with BSA (5 mg/ml) and Triton X-100 (0.3%) in PBS 0.1 M. Mouse monoclonal antibody anti-glial fibrillary acidic protein (anti-GFAP; diluted 1:400; MAB360 Chemicon) or rabbit anti-ionized calcium-binding adapter molecules-1 (anti-Iba-1; diluted 1:300 Wako Catalog No. 019-19741) was added to sections that were then incubated at 4 °C overnight. After two washing steps with PBS for 5 min, the sections were incubated at RT for 1 h with specific Cy2-conjugated secondary antibodies diluted 1:250 (711225152 and 115-165-003; Jackson Immuno Research, West Grove, PA, USA). Following two washing steps with PBS, the sections were counterstained by incubation for 10 min in 0.5 mg/ml of the fluorescent nuclear dye Hoechst 33258 (bisbenzimide, Sigma–Aldrich, Seelze, Germany). Following a short washing with PBS, sections were cover-slipped in a glycerol-based medium and slides were examined under a fluorescence microscope (DMRBE, Leica Microsystems, Wetzlar, Germany).

Western blotting

Rats were sacrificed at the end of experimental procedures by an overdose of anesthesia, and the hippocampi were rapidly removed from their brain, collected, and stored at − 70 °C for later use. Dissected hippocampal tissue was homogenized in cold radio-immunoprecipitation assay (RIPA) buffer (50 mM Tris, pH 7.4, 150 mM NaCl, 1% Triton, SDS 0.1%), supplemented with protease inhibitor cocktail (Sigma-Aldrich P8340) and phosphatase inhibitor cocktail (Sigma–Aldrich P5726). Samples were sonicated (30 pulsations/min), quantified by the Lowry method [131], and stored at − 80 °C. Western blotting was performed as previously described by Frinchi et al. [132]. Protein samples (50 μg per lane) and molecular

weight marker (161-0376 BIO-RAD) were run on 10% or 12% polyacrylamide gel and electrophoretically transferred onto nitrocellulose membrane (RPN303E, Hybond-C-extra, GE Healthcare Europe GmbH). The membranes were incubated for 1 h in blocking buffer, 1x TBS, 0.1% Tween-20, and 5% w/v nonfat dry milk, with gentle shaking overnight at − 4 °C with specific antibody in blocking buffer. For detection of superoxide dismutase-1 (SOD1) and superoxide dismutase-2 (SOD2), the following antibodies were used: rabbit polyclonal anti-SOD1 1:1000 (Sc-11407 Santa Cruz Biotechnology); mouse anti-SOD2 1:500 (SOD2; sc-137254, Santa Cruz Biotechnology). For detection of GFAP and Iba-1, the following antibodies were used: mouse monoclonal antibody anti-GFAP 1:2000 (MAB360 Chemicon), rabbit anti-Iba-1 1:1000 (Wako Catalog No. 019-19741). The day after, the membranes were washed three times for 10 min with TBS/T and then incubated for 1 h at room temperature with goat anti-rabbit IgG (sc-2004 Santa Cruz Biotechnology) or goat anti-mouse IgG (Sc.7076 Cell Signaling Technology) horseradish peroxidase-conjugated diluted 1:10000. After three washings with TBS-T, immune complexes were visualized with a chemiluminescence reagent (RPN2236, GE Healthcare Europe GmbH) according to the manufacturer's instructions. The Hyperfilm (ECL-films 28906837, GE Healthcare Europe GmbH) were developed using Kodak developer and fixer (catalog no. 1900984 and 1902485, Kodak GBX, Eastman Kodak). For the normalization of quantitative evaluation of bands, each membrane was stripped at 65 °C for 30 min in buffer containing NaCl 137 mM, TrisHCl 20 mM pH 7.6, and β-mercaptoethanol 0.01%. After two washings with TBST, the membranes were reprobed with an anti-β-actin antibody (sc-47778, Santa Cruz Biotechnology). The densitometric evaluation of bands was performed by measuring the optical density (O.D.) using the Image J software (Rasband WS, ImageJ, U.S. National Institutes of Health, Bethesda, Maryland, USA, https://imagej.nih.gov/ij/, 1997–2018).

Measurement of pro-inflammatory or anti-inflammatory cytokines by ELISA assay

Concentrations of interleukin-1β (IL-1β), interleukin-6 (IL-6), interleukin-10 (IL-10), and transforming growth factor-beta1 (TGF-β1) were measured in the hippocampus homogenates (20 mg of tissue sample) using enzyme-linked immunosorbent assay (ELISA) kits for rat (Cloud-Clone Corp, Wuhan, Hubei) according to the manufacturers' protocols and as reported by Zizzo et al. [133].

Reactive oxygen species analysis

To assess reactive oxygen species (ROS) generation by fluorimeter analysis, 10 mg of tissue from rat hippocampus was weighed and suspended on 1000 µl of PBS1X with 10 µL of protease inhibitors (Amersham Life Science, Munich, Germany). Samples were then incubated with 1 mM dichlorofluorescein diacetate (DCFH-DA) for 10 min at room temperature in the dark. The conversion of non-fluorescent DCFH-DA to the highly fluorescent compound 20,70-dichlorofluorescein (DCF) by esterase activity was

used to monitor the presence of peroxides due to the oxidative burst in the brain [133]. The samples were analyzed by fluorimetry (Microplate reader WallacVictor 2 - 1420 Multilabel Counter; PerkinElmer, Inc.), using the excitation filter set at 485 nm and the emission filter set at 530 nm. Relative ROS production was expressed as the change in fluorescence of the experimental groups compared with that of the control group (100%).

SOD activity levels

The hippocampus of rats was homogenized in PBS with protease inhibitors (Amersham Life Science, Munich, Germany). To remove insoluble material, tissue lysates were sonicated and centrifuged (14,000 rpm, at 4 °C, for 30 min). In the supernatant, total proteins were quantified by the Lowry method [131]. Volume corresponding to 50 μg of protein was used for total SOD enzymatic activity measurement, by using the SOD assay kit (Sigma–Aldrich) according to manufacturer's instructions [133]. Absorbance was measured by using the iMark™ Microplate Absorbance Reader at 450 nm.

Lipid peroxidation assay

The lipid peroxidation assay kit (Sigma Aldrich) was used to detect the concentration of malondialdehyde (MDA), a final product of lipids peroxidation. Ten milligrams of hippocampal tissues was homogenized in 300 μl of MDA lysis buffer (supplied in the kit), and colorimetric reaction with thiobarbituric acid (TBA) was read on an iMark™ Microplate Absorbance Reader at 532 nm, according to manufacturer's instructions [133].

Cell counting

The number of Iba-1 and GFAP-positive cells was estimated by counts made by systematic sampling of brain sections, every third section of total 10 sections, in the hippocampal region of rat brain. All counts were made in four rats for each group and were carried out double-blindly. Labeled cells were evaluated using ImageJ software (Cell Counter plugin; Rasband, W.S., ImageJ, U.S. National Institutes of Health, Bethesda, Maryland, USA, http://imagej.nih.gov/ij/, 1997–2018). The cell count values obtained from three to five random fields per section, in 10 sections examined, were expressed as means ± SEM values per square millimeter of tissue.

Cortisol levels

Rats under anesthesia were sacrificed between 11:00 and 12:00 am, and blood was taken by intracardiac puncture and collected in tubes coated with EDTA. Blood samples were centrifuged at 4000×g at 4 °C for 10 min, and the supernatant was stored at − 80 °C. The plasma levels of cortisol were measured using an

automated electrochemiluminescence immunoassay (Roche Diagnostics Elecsys Cortisol II assays and COBAS E801), and values were expressed in nanograms per milliliter. The minimum level of detection for assays of cortisol was 0.15 ng/ml [134].

Statistical analysis

Data analysis was performed using the GraphPad Prism 6 software (GraphPad Software, Inc., La Jolla, CA, USA). Results are presented as mean ± SEM, and in some cases are expressed as arbitrary units, with controls equal to 1, or as percentage of control. For the novel object recognition task, the parameter chosen to assess rats' ability to discriminate novelty from familiar features was the recognition index (RI) and was calculated using the following formula: [RI = TN/(TN + TF)]. Statistical evaluations were performed by one-way ANOVA, followed by Fisher's Protected Least Significant Difference (PLSD) test, with the exclusion of behavioral data for which we used the Tukey's multiple comparison test. Differences in P value less than 0.05 were considered statistically significant.

Aim 2.1. *Preservation of global synaptic Excitatory to Inhibitory ratio during long postmortem intervals*

Human tissue

The right frontal hemisphere from a 39 years old male control subject (PMI=15h) was obtained post-mortem from the University of California Irvine Brain Bank (UCIBB) in accordance with the university's Institutional Review Board after obtaining consent from next of kin. A psychological autopsy was completed based on family informant information, medical and psychiatric records, toxicology reports, and the subject's medication history. The UCIBB autopsy protocol is based largely on procedures validated by Kelly and Mann [135], and includes questions concerning the decedents' demographics, medical history, psychiatric symptoms, medication use, hospitalizations, substance use, physical health. The human brain dissection and freezing protocol is described in detail elsewhere [136]. Briefly, after collection, frontal cortex samples were either frozen in isopentane at -40 C (PMI 15h) or kept at 2°C at different time intervals (18, 21, 27, 39, 63, and 87h) before freezing, to simulate different PMIs.

Rat brain cortex

Briefly, adult male Wistar rats, 2 months old, were euthanized at the same time following procedures in accordance with the National Institutes of Health Guide for the Care and Use of Laboratory Animals and IACUC at University of California, Irvine (IACUC: 1998-1388), and kept at 2°C or 21°C for different time intervals: 0, 6, 16, 24, 48, or 120 h (N=2 each experimental group). The body temperature of the rats was measured by putting a small digital temperature logger (ibutton; thermochron; Baulkham Hills, Australia) outside the chest of the animals. At the specified time brains were surgically removed; the cortex was isolated and frozen by immersion in liquid nitrogen and stored at -80°C.

Synaptosomes isolation

Synaptosomal enriched preparations were extracted from 50 mg of human DLPFC or 60 mg of dissected rat cortex using Syn-PER reagent protocol (Thermo Scientific, Rockford, IL) following the manufacturer's instructions. All the synaptosomes preparations for rats were done at the same time, from frozen tissue for each PMI time point. A similar strategy was done in the human case to avoid batches effects. Three fractions were isolated, stored at -80 C, and used for downstream protocols as specified below. The S1 fraction, that contains soluble cytosolic elements, was used to extract and quantify mRNA. The P1 fraction, which contains mostly nuclei, myelin, and large non-homogenized tissue, was used as a reference for synaptosomes enrichment in P2 fractions by Western Blot analysis. All the procedures of centrifugation

were performed at 4°C using proteinase inhibitors (Thermo fisher, cat #A32955) to reduce proteolysis and denaturation. The P2 fraction was re-suspended in Syn-Per buffer solution and the amount of protein was quantified by DeNovix QFX fluorometer instrument (DeNovix Inc. Wilmington, USA) and Qubit reagents (Invitrogen, cat# Q33212).

Western blotting

Twenty µg of proteins from P2 fractions were run in a polyacrylamide gel (Invitrogen precast gradient gels 4-12% bis-tris plus) at 155 V. To reduce the variability multiple proteins were detected by re-blotting the membrane with different antibodies and without a stripping protocol between blottings. Proteins were transferred from the gel to a nitrocellulose membrane (Invitrogen, cat#LC2000) and unspecific blocking was reduced by incubating membranes for 1h at room temperature with Odyssey blocking buffer (LI-COR Biosciences - U.S.). Next, membranes were treated for 1h at room temperature, or overnight at 4°C, with the following primary antibodies. Mouse anti-synaptophysin (Abcam cat# ab8049, dilution 1:2000), mouse anti-PSD-95 antibody (Thermo Fisher cat# MA1-045, dilution 1:2500), rabbit anti-gephyrin antibody (Abcam cat# ab32206, dilution 1:1600), rabbit anti-NeuN antibody (Abcam, cat#ab177487, rabbit, and dilution 1:2000), rabbit anti-GAPDH antibody (Abcam cat# ab9485, rabbit, and dilution 1:3000). GAPDH was selected because is minimally affected by PMI [137]. To visualize the primary antibody membranes were incubated with fluorescent secondary antibody (Li-Cor anti-rabbit cat#926-32213 and anti-mouse cat#926-68072 dilution 1:2000 for both) and imaged with an Odyssey infrared imager (Li-Cor Odyssey 9120 Infrared Imaging System, Lincoln, Nebraska USA). The intensities of the bands were analyzed with Image J software.

Analysis of pH

Rat brain cortex (60 mg) were homogenized at 4°C in 600 µL of ddH_2O at pH 7 (w/v 1:10) as previously described [138]. After 30 minutes, the pH was measured using a micro pH electrode and the Accumet AE150 pH Benchtop Meter (Thermo Fisher Scientific Inc.). Three readings per sample were taken. Intraclass correlation coefficient [ICC] was calculated using R studio software, ICC= 0.999,95% confidence interval [CI] within samples.

Microtransplantation of synaptic membranes (MSM) and TEVC

For MSM experiments 50 nL of P2 fractions at 2 µg/µL were injected into stages V-VI *Xenopus laevis* oocytes as previously described [139] and recorded by TEVC the day after the microinjection (20-28 hrs). TEVC experiments were performed using an Oocyte Clamp OC-725C amplifier at holding potential of −80 mV. Currents were filtered by a dual variable filter Kemo at 20 Hz. GABA was from Sigma (St. Louis,

MO, USA) and kainate from Tocris (Minneapolis, MN, USA) All the drugs were dissolved into Ringer solution (NaCl 115mM, KCl 2mM, $CaCl_2$ 1.8mM, HEPES 5mM, pH=7.4).

Isolation and injection of RNA

Total RNA was extracted from the P2 fraction from each rat experimental group using PureLinkTM RNA Mini Kit (Invitrogen by Thermo Fisher Scientific). Extracted RNA was quantified using NanoDrop 2000/2000c and was later injected into the oocytes (2 mg/mL). Electrophysiological recordings of oocytes injected with total RNA were performed 24 h after injection. Quality of isolated RNA was determined by RIN value using an Agilent 2100 bioanalyzer.

Aim 2.2. Increased functional Excitatory to Inhibitory synaptic ratio in parietal cortex of Alzheimer's disease subjects

Cases and tissue samples.

AD and DS parietal cortex tissue was provided by the UCI Institute for Memory Impairments and Neurological Disorders through the UCI-Alzheimer's Disease Research Center (ADRC). Control tissue was provided by the NINDS/NIMH sponsored Human Brain and Spinal Fluid Resource Center at the VA West Los Angeles Healthcare Center, Los Angeles, CA. All cases were de-identified and coded by the source tissue banks. For the present studies, the samples were recoded and processed for all analyses with the experimenter blind to subject and group. The study was reviewed by the Institutional Review Boards of the University of California at Irvine and the University of Texas Medical Branch and categorized as a non-human subject study.

Postmortem human PCx tissue blocks, that included a well-defined sulcus with portions of gyri present on both sides, were obtained from 5 controls, 5 AD cases and 6 DS cases, with both males and females included in the analyses (Table 3). While effort was made to match age and postmortem interval (PMI) as closely as possible, the control group contained longer PMIs; in preliminary studies PMIs up to ~25 h did not significantly affect FDT- or MSM- based synapse measures, consistent with earlier work [140] and with our study evaluating the effects of postmortem interval on synaptic metrics (please see Aim 2.1). All DS and AD cases underwent formal neuropathological evaluation in the ADRC Neuropathology Core and demonstrated Braak stage VI neurofibrillary degeneration [141] and Consortium to Establish a Registry for Alzheimer's Disease (CERAD) as frequent in cerebral cortex neuritic plaque density [142]. Functional levels of independence were comparable between the two groups as determined by the modified version of the Bristol Activities of Daily Living Scale (mBADLS) that was collected within the last 1-2 years of life [143] (Table 3). In addition, in a recent study we used Western blotting and antibodies to AT8 to assess the levels of hyperphosphorylated (p)-tau in tissue sections obtained from the same tissue blocks used here [144]. Those data are presented here again for each sample in order to directly compare a hallmark of AD pathology with measures of excitation and inhibition for each case.

For both FDT and MSM analyses, each fresh-frozen tissue block was cut on a cryostat at 20 µm perpendicular to the tissue surface and sections were collected. For FDT, sections were slide-mounted, methanol-fixed, and stored at -20°C prior to processing for double-labeling immunofluorescence. For MSM

analyses, a single tissue section was collected into a microcentrifuge tube and stored at -80°C until processed as described below.

DIAGNOSIS	N	AGE	SEX	PMI (H)	AD PATHOLOGY	M-BADLS
CONTROL	5	57.2 ± 4.9	4M/1F	15.4 ± 4*		
AD	5	57.8 ± 2.2	2M/3F	3.8 ± 1	Stages VI/C	27.4 ± 13.7
DS	6	56.3 ± 3.5	3M/3F	4.1 ± 1	Stages VI/C	33.2 ± 9.3

Table 3. Summary of demographics, pathology, and cognitive skills for study groups. Values for age, postmortem interval (PMI), and the modified version of the Bristol Activities of Daily Living Scale (mBADLS) are mean ± SD. ANOVA test showed significant difference (*) of PMI of CTRL compared to the two pathological groups ($p<0.05$). See text for further details.

Fluorescence deconvolution tomography (FDT)

Tissue sections were processed for double-labeling immunofluorescence as described [145], using antisera directed against the excitatory synapse scaffold protein PSD-95 to label excitatory synapse postsynaptic densities (PSDs) [146] in combination with antisera directed against the inhibitory synaptic marker gephyrin as previously described [147], [148]. Antibodies used were mouse anti-PSD-95 (1:1000; Thermo Scientific, #MA1-045) and rabbit anti-GPHN (1:1000; Abcam, ab32206), with species-specific Alexafluor488 and Alexafluor594 conjugated secondary antibodies (1:1000 each; Thermo Fisher Scientific) for visualization. For FDT, image z-stacks of layer 1 and layer 2 parietal cortex were collected using a 1.4 NA 63X objective through a depth of 2 µm with 0.2 µm steps using a Leica DM6000 epifluorescence microscope equipped with a Hamamatsu ORCA-ER digital camera; the sample field size for each cortical layer measured 42,840 μm^3. Both layers 1 and 2 were assessed for analyses because depth placement of the sample field, relative to the cortical surface, could be reliably replicated, and to compare a relatively cell sparse versus cell dense layer. Numbers of immunolabeled synapses in the two layers ranged from 25,000-30,000 per stack. For each layer, 10-12 image stacks from three sections per brain were taken from within the sulcus of each sample, and then processed for iterative deconvolution using Volocity 4.1 (Perkin Elmer). Deconvolved images were analyzed using in-house software to quantify all labeled puncta within the size constraints of synapses as previously described [145], [147]–[149]. Background staining variations in the deconvolved images were normalized to 30% of maximum background intensity

using a Gaussian filter, and object recognition and measurements of immunolabeled puncta were automated using in-house software built using Matlab R2007, Perl, and C that allows for detailed analysis of objects reconstructed in 3D. Pixel values (8-bit) for each image were multiply binarized using a fixed-interval intensity threshold series followed by erosion and dilation filtering to reliably detect edges of both faintly and densely labeled structures. Object area and eccentricity criteria were then applied to eliminate elements, including lipofuscin granules, that do not fit the size and shape range of synaptic structures from the quantification. Counts of immunolabeled objects were averaged across sections to produce mean values per subject. Statistical comparisons to identify the effect of group used a one-way ANOVA followed by Newman-Keuls Multiple Comparison test for post-hoc paired comparisons (GraphPad Prism, Version 5.0). If variances across groups were not equal, as determined by Bartlett's test, then the Welch ANOVA or nonparametric Kruskal-Wallis test was used followed by Dunn's Multiple Comparison test. In other comparisons, repeated-measures ANOVA was used followed by Student Newman Keuls post-hoc test. In all cases, $p<0.05$ was considered significant. Pearson product-moment was used for all the linear correlations using JMP version 14 (SAS Institute, Cary, NC).

Microtransplantation of synaptic membranes and flow cytometry.

Membrane preparations were isolated from a single 20 µm slice of frozen PCx from each brain donor using Syn-PER method (Thermo Fisher Scientific); on average, the tissue blocks ranged in size from ~25-35 mm (length) by 15-20 mm (width). Briefly, a tissue slice was placed in an Eppendorf tube and stored at -70^{o} C until processed. To make synaptic membranes, each slice was suspended in 500 µl of Syn-PER extraction reagent, transferred to 2 mL glass/Teflon Dounce and stroked slowly for 15 times. The homogenate was then transferred to 1.5 mL Eppendorf and centrifuged at 1200 g (4° C) for 10 min. The supernatant (S1) was transferred to a new Eppendorf and centrifuged at 15,000 g for 20 min. The pellet enriched in synaptosomes (P2 fraction) was resuspended in 15 µL of Syn-Per solution, aliquoted and stored at -80° C until further use for electrophysiology experiments. The amount of protein was determined using the Qubit protein assay reagent kit (Thermo Fisher Scientific). Numbers of particles within the size of synaptosomes were counted as described previously [150]–[152], using appropriate size standards (Spherotech, Inc), in a Guava EasyCyte flow cytometer (EMD Millipore) and analyzed using Incyte software (EMD Millipore). Synaptosomes were sonicated in iced-water 3 times for 5 seconds, at 1 min intervals between sonications, to create small proteoliposomes that can fuse to the oocytes' extracellular membrane. One day before electrophysiological recordings the synaptic membranes were injected into stage V-VI *Xenopus laevis* oocytes using protocols previously published for cellular membranes[140], [153], [154]. Each oocyte was injected with 50 nL of synaptic proteoliposomes (2 mg/mL protein concentration).

Electrophysiological recordings

Ion currents elicited by agonist perfusion were recorded by the two-electrode voltage clamp (TEVC) method between 18-36 h post injection [154]. Microelectrodes were filled with 3 M KCl and resistance of the microelectrodes ranged from 0.5–3.0 MΩ. Piercing and recording took place in a chamber (volume ≈0.1 ml) continuously perfused (6 ml/min) with Ringer's solution [115 mM NaCl, 2 mM KCl, 1.8 mM $CaCl_2$, 5 mM Hepes (pH 7.4)] at room temperature (19–21°C). Oocytes were voltage clamped to −80 mV. Ion currents were recorded and stored with WinEDR ver 2.3.8 Strathclyde Electrophysiology Software (John Dempster, Glasgow, United Kingdom). Kainic acid, s-AMPA were purchased from Tocris (Minneapolis, MN). All other reagents were from Sigma (St. Louis. MO). Working solutions were made by diluting stock solutions in Ringer's solution. A total of 7 frogs were used for MSM experiments. For all measures, for each subject, electrophysiological recordings were done at least in triplicate (three oocytes) in batches of oocytes from 2-4 different frogs, balancing the groups for equal number of subjects in each experimental run. Statistical comparisons to identify the effect of diagnosis used the mean of each metric, for each subject, as experimental unit in a one-way ANOVA, followed by post-hoc Dunnett's multiple comparisons versus control test (JMP, version 14). If variances across groups were not equal, then the Welch ANOVA or nonparametric Kruskal-Wallis test was used followed by Dunn's comparison vs control test. As a matter of confirmation, we also implemented a nested ANOVA with random effects mixed model, wherein the subjects were nested within diagnosis, and subject was tested as a random effect using the expected mean squares method. In all cases, $p<0.05$ was considered significant. Pearson product-moment was used for linear correlations, and Spearman's rank for non-parametric correlations, using JMP version 14.

CHAPTER 4. RESULTS AND DISCUSSION

Aim 1. Anti-inflammatory and cognitive effects of interferon-β1a (IFN-β1a) in a rat model of Alzheimer's disease

Aβ-42 peptide abnormal production is associated with the development and maintenance of neuroinflammation and oxidative stress in brains from AD patients. Suppression of neuroinflammation may then represent a suitable therapeutic target in AD. We evaluated the efficacy of IFN-β1a in attenuating cognitive impairment and inflammation in an animal model of AD.

A rat model of AD was obtained by intra-hippocampal injection of Aβ-42 peptide (23 μg/2 μl). After 6 days, 3.6 μg of IFN-β1a was given subcutaneously (s.c.) for 12 days. Using the novel object recognition (NOR) test, we evaluated changes in cognitive function. Measurement of pro-inflammatory or anti-inflammatory cytokines, reactive oxygen species (ROS), Superoxide dismutase (SOD) activity levels was performed in the hippocampus. Data were evaluated by one-way ANOVA with Fisher's Protected Least Significant Difference (PLSD) test.

We showed that treatment with IFN-β1a was able to reverse memory impairment and to counteract microglia activation and upregulation of pro-inflammatory cytokines (IL-6, IL-1β) in the hippocampus of Aβ-42-injected rats. The anti-inflammatory cytokine IL-10, significantly reduced in the Aβ-42 animals, recovered to control levels following IFN-β1a treatment. IFN-β1a also reduced ROS and lipids peroxidation and increased SOD1 protein levels in the hippocampus of Aβ-42-injected rats.

This study shows that IFN-β1a is able to reverse the inflammatory and cognitive effects of intra-hippocampal Aβ-42 in the rat. Given the role played by inflammation in AD pathogenesis and the established efficacy of IFN-β1a in the treatment of inflammatory diseases of the central nervous system such as multiple sclerosis, its use may be a viable strategy to inhibit the pro-inflammatory cytokine and oxidative stress cascade associated with Aβ deposition in the hippocampus of AD patients.

Exp 1.1 – β-amyloid oligomers

Aβ-42 oligomers, prepared as reported in Carrotta et al. [128], were aggregated by incubation for 8 h at 37 °C. The results of aggregation kinetics of Aβ-42 oligomers are shown in Figure 4a–c. The Aβ-42 oligomers aggregation was also evaluated by fluorescence microscopy, and the Aβ-42 plate's mean size was measured by fluorescence microscopy software; results are shown in Figure 4d. For Aβ-42 cell toxicity, LAN5 cells were treated with 50, 75, and 100 μM of Aβ-42 for 24 h and the cell viability was evaluated using MTS assay; results are shown in Figure 4e, f. Based on the present aggregation and toxicity data of Aβ-42 oligomers and on data of neurotoxicity dependent on the types and sizes of Aβ-42 oligomers [155],

[156], it was decided to inject Aβ-42 oligomers aggregates, formed after 8 h of incubation and at concentration of 75 μM, in the dorsal hippocampus.

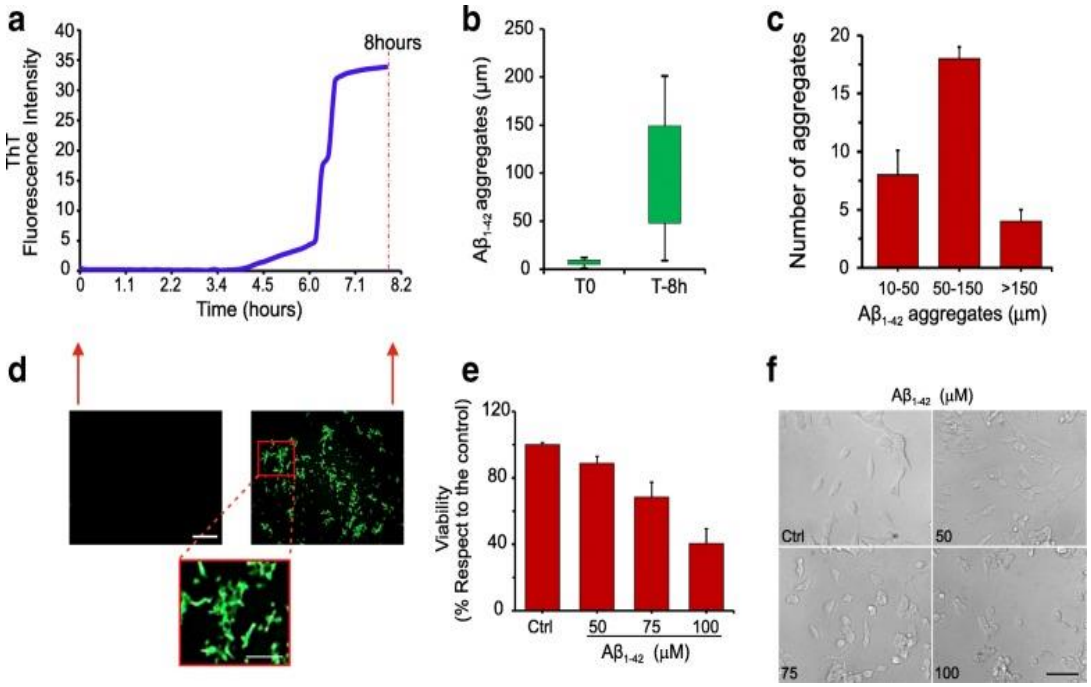

Figure 4. Aβ1-42 oligomers aggregation and toxicity. a.–c. Aggregation kinetics of Aβ1-42 oligomers. **d.** Fluorescence imaging of Aβ1-42 plates. **e., f.** Aβ1-42 cell toxicity in LAN5 cells treated with 50, 75, and 100 μM of Aβ1-42 for 24 h: cell viability (**e.**) and dose-effect of cell morphological changes (**f.**). Scale: upper panels 100 μm; lower panel 50 μm.

In Figure 5a, the stereotaxic position of injection site in the dorsal hippocampus is shown. Figure 5b shows the scheme of treatment performed. The amount of Aβ-42 protein aggregates injected was 23 μg/2 μl according to toxicity data of previous experimental models [157], [158]. The scheme of dose and time of IFN-β1a treatment was based on previous work using a similar experimental rat model [100] or a rat model of autoimmune encephalomyelitis [159]–[161].

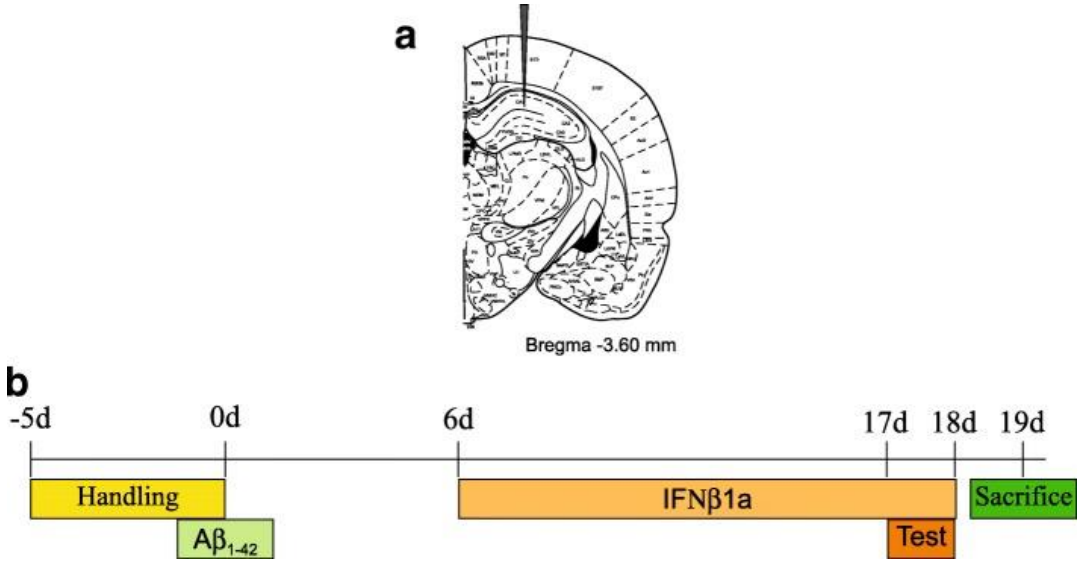

Figure 5. Aβ1-42 intra-hippocampal injection and IFNβ1a treatment. a. Stereotaxic position of Aβ1-42 injection in the dorsal hippocampus. **b.** Scheme of Aβ1-42 and IFNβ1a treatment performed.

Exp. 1.2 - IFN-β1a treatment rescues cognitive performances impaired by intra-hippocampal injection of Aβ-42 peptide

Using the NOR test, we evaluated changes in cognitive function induced by intra-hippocampal injection of Aβ-42 peptide. At scheduled time (Figure 5b), rats were tested in an open field arena in order to assess declarative memory as assessed by the recognition index of novel objects from familiar ones. When rats were trained with two identical objects, a one-way ANOVA did not show (Figure 6a) any statistical variation in the recognition index (RI%) ($F(4,35) = 0.6122$; $p = 0.6566$) among the experimental groups (Figure 6a). Twenty-four hours after the training, rats' preference toward a novel object was evaluated. A one-way ANOVA showed (Figure 6b) a significant effect of treatment ($F(4,35) = 5.971$; $p < 0.001$). The post hoc analysis conducted by Tukey's multiple comparison test showed a significant reduction of RI% in the Aβ-42 group as compared to the control ($p < 0.01$), to Aβ-42 + IFN-β1a ($p < 0.01$), and to IFN-β1a ($p < 0.05$) groups (Figure 6b). In the Aβ-42 + IFN-β1a group, the treatment with IFN-β1 fully counteracted the RI% reduction observed in the Aβ-42 group. In the IFN-β1a and sham groups, the RI% did not change as compared to control.

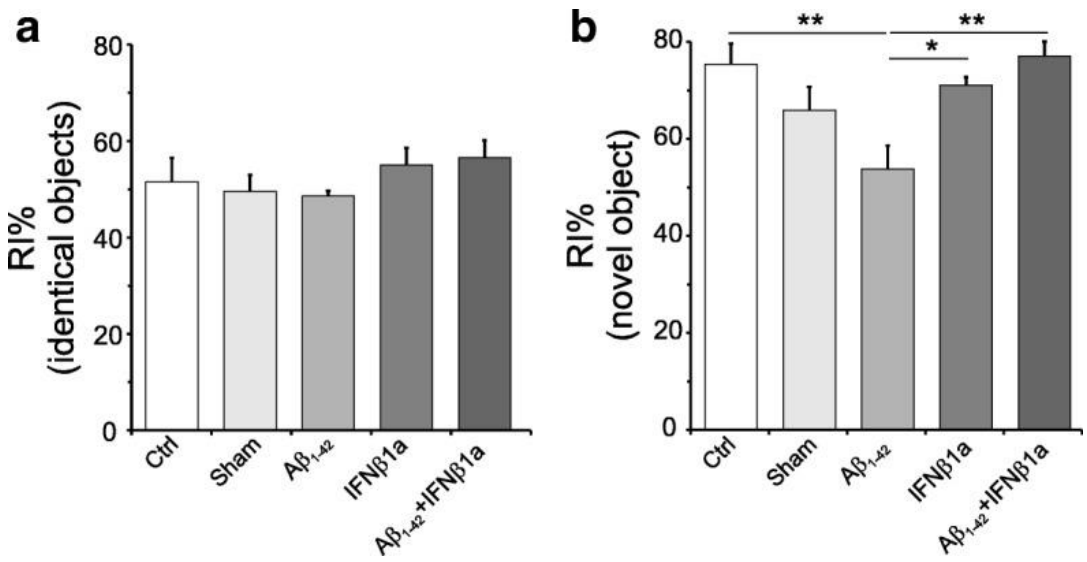

Figure 6. Cognitive evaluation by NOR test. a. Rats (n = 8 per group) exposed to the training with two identical objects did not show any statistical variation in the RI% (F (4,35) 0.6122; p = 0.6566) among the experimental groups. **b.** Twenty-four hours after the training was the evaluation of rats' preference toward novel object. The results of one-way ANOVA showed a significant effect of treatment (F (4,35) = 5.971; p < 0.001). The post hoc analysis conducted by Tukey's multiple comparison test showed a significant reduction of RI% in the Aβ1-42 group with respect to control (p < 0.01), Aβ1-42 + IFNβ1a (p < 0.01), and IFNβ1a (p < 0.05) groups. In the Aβ1-42 + IFNβ1a group, the treatment with IFNβ1a full counteracted the RI% reduction observed in the Aβ1-42 group. In the IFNβ1a and sham groups, the RI% did not change as compared to control. *P < 0.05, **P < 0.01.

Exp 1.3 - Body weight and cortisol levels

Rats' body weight was measured at the beginning and the end of the experimental period (Figure 5b). Two-way repeated ANOVA measurements showed no significant differences in body weight (Figure 7a) both among the various experimental groups and in each group at the end of the experimental period as compared to the beginning of the experiment. Although corticosterone is considered the main glucocorticoid involved in the regulation of stress responses in rodents, we preferred to measure cortisol in consideration of procedure availability in our laboratory and of good correlation between serum cortisol and corticosterone [162]. The results are reported in Figure 7b: one-way ANOVA did not show significant change in cortisol level among experimental groups.

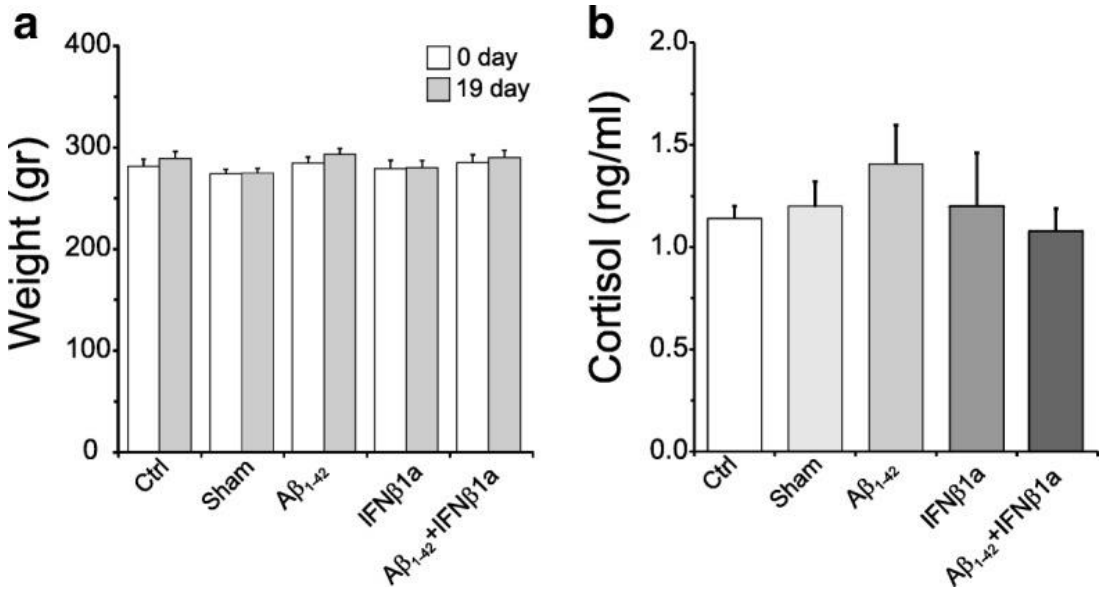

Figure 7. Body weight and cortisol levels. a. Two-way repeated measurement ANOVA showed not significant differences in the body weight, both among the experimental groups and each group at the end of experimental period as compared to starting body weight. **b.** One-way ANOVA did not show significant change in cortisol level among the experimental groups.

Exp.1.4 - IFN-β1a effects on glial cell activation by Aβ-42 protein injection in the hippocampus

Since one of the features of AD pathology is activation of microglia and astrocytes induced by Aβ deposits, we analyzed by immunohistochemistry and Western blot Iba-1 and GFAP markers for microglia and astrocyte activation. As shown in Figure 8a, b, the count of Iba-1-positive cells was significantly increased in the hippocampus of the Aβ-42-treated group ($F(4,22) = 26.97$, $p < 0.0001$) as compared to the control ($p < 0.0001$) and sham groups ($p < 0.001$). However, in the Aβ-42 + IFN-β1a group, the treatment with IFN-β1a significantly counteracted the effect of Aβ-42 injection as shown by the Iba-1-positive cell number significantly reduced as compared to the Aβ-42 group ($p = 0.02$). However, the cell number in the Aβ-42 + IFN-β1a group was still significantly increased when compared to the control group ($p < 0.0001$) but not compared to the sham group (Figure 8a, b). The sham group, but not the IFN-β1a group, showed a significant increase of Iba-1-positive cell number as compared to the control group ($p < 0.001$). Quantitative Western blot analyses of Iba-1 protein levels clearly showed a significant increase in the Aβ-42 group as compared to both control ($p < 0.05$) and sham ($p < 0.05$) groups. In the Aβ-42 + IFN-β1a group, the treatment with IFN-β1a counteracted the Aβ-42 effect on Iba-1 protein levels. Indeed, Aβ-42 + IFN-β1a Iba-1 protein levels are not significant when compared to the Aβ-42 group, but they are also not significant when compared both to control and sham groups (Figure 8c). This means that treatment with IFN-β1a in the Aβ-42 + IFN-β1a group counteracted the increase of Iba-1 protein levels induced by Aβ-42, as shown by its loss of significance with respect to controls, although it does not bring them back to the levels detected

in the control and sham groups (Figure 8c). Iba-1 protein levels in the IFN-β1a and sham groups did not show significant difference as compared to the control group. The immunohistochemistry analysis of GFAP marker showed a not significant trend toward an increase in the astrocytes number in all experimental groups as compared to control group (Figure 9a, b). By contrast, the quantitative Western blot analyses of GFAP protein levels showed that in the Aβ-42 and in the Aβ-42 + IFN-β1a groups, GFAP protein levels were significantly increased (both $p < 0.0001$) as compared to the control group and in the Aβ-42 + IFN-β1a group as compared to the sham group (Figure 9c). Surprisingly, the treatment with IFN-β1a alone significantly reduced ($p < 0.01$) the GFAP protein levels as compared to the control group. The cell number of the sham group was not significantly different from the control group.

Exp.1.5 - IFN-β1a inhibits pro-inflammatory cytokines increase induced by Aβ-42 protein injection in the hippocampus

We also analyzed by ELISA the hippocampal levels of pro-inflammatory cytokines, IL-1β and IL-6, and anti-inflammatory cytokines, IL-10 and TGF-β1. As shown in Figure 10a, b, we found that both IL-1β and IL-6 levels were significantly increased in the Aβ-42 group as compared to the control ($p < 0.0001$ and $p < 0.01$ respectively) and sham ($p < 0.0001$ and $p < 0.001$ respectively) groups. In the Aβ-42 + IFN-β1a group, the treatment with IFN-β1a counteracted this Aβ-42 effect on IL-1β and IL-6 levels ($p < 0.0001$ and $p < 0.01$ respectively), bringing them back to the levels of control and sham groups. In the IFN-β1a group, the treatment with IFN-β1a did not change the IL-1β levels as compared to the control, whereas it produced a substantial reduction of IL-6 levels as compared to the control and sham groups ($p < 0.05$). In contrast to hippocampal upregulation of IL-1 and IL-6 levels, the anti-inflammatory cytokine IL-10 was found significantly reduced in the Aβ-42 group as compared to the control ($p < 0.001$) and sham ($p < 0.001$) groups (Figure 10c). Following IFN-β1a treatment in the Aβ-42 + IFN-β1a group, the IL-10 levels recovered to control levels, strengthening the anti-inflammatory property of IFN-β1a. The TGF-β1 levels were significantly reduced in the IFN-β1a group as compared to control or sham group ($p < 0.01$ and $p < 0.001$ respectively) and Aβ-42 group as compared to sham ($p < 0.05$) group (Figure 10d), whereas surprisingly in the Aβ-42 + IFN-β1a group, TGF-β1 levels recovered to the control group levels. In the sham group, we did not find significant changes in both IL-10 and TGF-β1 levels as compared to the control group.

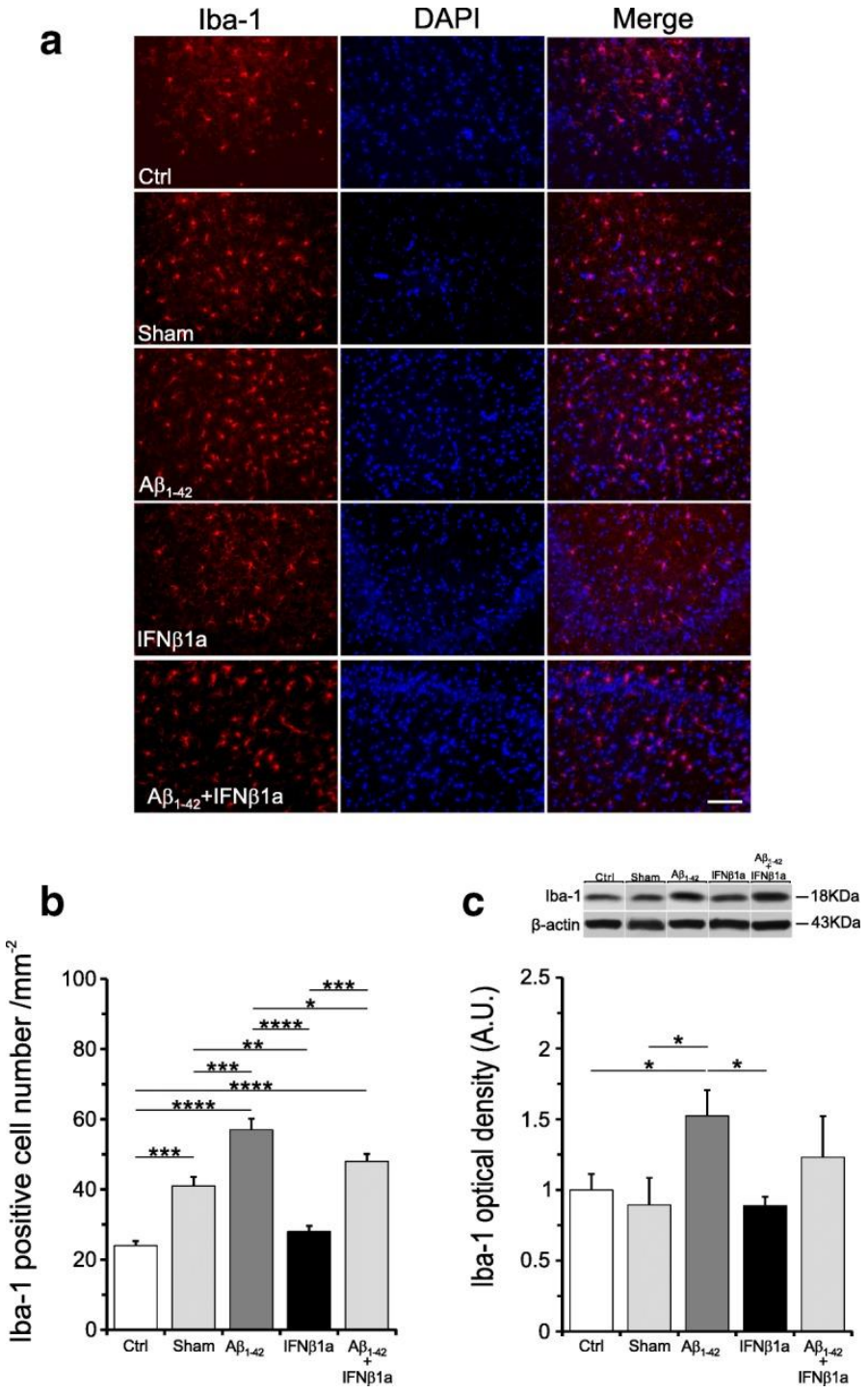

Figure 8. IFNβ1a effects on microglial cell activation by Aβ1-42. a. Iba-1 immunohistochemistry in the hippocampus. **b**. Count of Iba-1-positive cells showed a significant increase of cell number in the hippocampus region of the Aβ1-42-treated group (n = 6) and treatment with IFNβ1a (n = 6) significantly counteract this effect in the Aβ1-42+ IFNβ1a group (n = 6) as compared to sham group but not to the control group (n=6). **c.** Similarly, quantitative Western blot analyses of Iba-1 protein levels showed that in the Aβ1-42 group, Iba-1 protein levels were significantly increased and treatment with IFNβ1a significantly counteract this effect in the Aβ1-42 + IFNβ1a group. Scale: 100 μm. *P < 0.05, **P < 0.01, ***P < 0.001, ****P < 0.0001.

Exp. 1.6 - IFN-β1a treatment effects on ROS levels and SOD1 or SOD2 proteins and activity levels

SOD1 levels (Figure 11a) were increased in the Aβ-42 + IFN-β1a group as compared to the control ($p < 0.05$) and sham ($p < 0.05$) groups, whereas SOD2 levels (Figure 11b) were significantly reduced in the same group as compared to the control ($p < 0.05$) and sham ($p < 0.01$) groups. The SOD2 levels were significantly lower in the IFN-β1a group as compared to the sham group ($p < 0.05$) but not to the control group, suggesting that IFN-β1a per se may negatively regulate the SOD2 levels. In the sham group, we did not find significant changes in both SOD1 and SOD2 levels as compared to the control group.

Concerning the SOD activity (Figure 11c), we found that SOD activity levels were significantly decreased in the Aβ-42 group as compared to control ($p < 0.01$). In the Aβ-42 + IFN-β1a group, the treatment with IFN-β1a counteracted the decrease of SOD activity level bringing it back to the control level. In the IFN-β1a group, the treatment with IFN-β1a did not change the SOD activity levels as compared to the control and sham groups. In the sham group, we did not find significant changes in SOD activity levels as compared to the control group.

Concerning the oxidative stress analysis (Figure 11d), we found that ROS levels were significantly increased in the Aβ-42 group as compared to control ($p < 0.0001$) and sham ($p < 0.01$) groups. In Aβ-42+ IFN-β1a group, the treatment with IFN-β1a counteracted the increase of ROS levels bringing them back to the control level. ROS levels were substantially similar in the IFN-β1a, control, and sham groups.

Lipid peroxidation is the degradation of lipids that occurs as a result of oxidative damage, typically by reactive oxygen species, resulting in a well-defined chain reaction with the production of end products such as MDA. According to previous data [163] showing that Aβ-42 injection induces ROS levels, we analyzed the level of lipid peroxidation in the hippocampus by measuring the concentration of MDA. The analysis (Figure 11e) revealed a significant increase of MDA levels in the Aβ-42 group as compared to control ($p < 0.0001$) and sham ($p < 0.01$) groups. This increase of MDA levels was positively correlated n with the increased levels of ROS. In the Aβ-42 + IFN-β1a group, the treatment with IFN-β1a completely blocked the increase of MDA levels observed in the Aβ-42 group. Interestingly, in the IFN-β1a group, the MDA levels were found significantly reduced as compared to control ($p < 0.01$) and sham ($p < 0.001$) groups. However, the MDA levels were found also significantly increased in the sham as compared to control group ($p < 0.05$).

These results indicate that the short treatment with IFNβ1a was able to reverse memory impairment and to suppress microglia activation and the upregulation of pro-inflammatory cytokine (IL-6, IL-1β) levels and oxidative stress in the hippocampus produced by toxic oligomers, and suggest a protective effect of IFNβ1a against Aβ1-42-induced functional alterations in the hippocampus of this rat AD model. IFNβ1a anti-inflammatory effects have been clearly defined within the peripheral immune system but its role in the

central nervous system function has been little explored. Indeed, the only data available in this field, in addition to the already mentioned anti-inflammatory effect of IFN-β1a in patients with multiple sclerosis [164]–[166], derived from studies on experimental autoimmune encephalomyelitis, an animal model of multiple sclerosis. Indeed, IFNβ1a treatment prevents and reduces the progression of the experimental CNS demyelination [161], [167], [168] by inhibiting pro-inflammatory cytokines (IL-6, IL-1β, TNF-α, IFN-γ), astrocytes activation, and inducible nitric oxide synthase expression [100]. However, adverse effect of type I interferon (IFN-I) has been reported that in the aging brain chronically elevated IFN-I activity contributes to the pathology of various human CNS diseases and in animal models, including aging microglial phenotype, neurodegeneration, and microgliosis [169].

Our results showed the beneficial effects of IFNβ1a in a model of AD pathology, but it is still unclear how it exerts this effect within the CNS, since its passage from the bloodstream to the brain parenchyma is significantly restricted by the blood–brain and blood–cerebrospinal fluid barriers [170]–[173].

In this context, the effects of IFNβ1a in the brain have been associated with possible modulation of brain inflammatory events at capillaries level [160] or with a decreased permeability of the blood–brain barrier to inflammatory cell entry into to the brain [174], thus reducing CNS inflammatory response. Interesting, it was demonstrated that IFN-β modulate glutamatergic neurotransmission [101], [103]–[105].

Several studies have demonstrated anti-inflammatory effect of IFNβ1a outside the CNS [164]–[166]. Indeed, IFNβ1a regulates several immunological functions, including decrease in T cell activation, induction of cytokine shifts in favor of an anti-inflammatory effect, prevention of T cell adhesion, and extravasation across the blood–brain barrier, as well as induction of T-regulatory cells, all occurring within the peripheral immunological organs [100], [164], [165]. Recently, several pathways for the transport of cytokines from systemic circulation into the brain have been reviewed [173], but the mechanisms by which IFNβ1a treatment may affect pro-inflammatory response induced by Aβ1-42 peptide injection in the hippocampus need further investigations. Anyway, in the present work, it is possible to exclude a role of glucocorticoid in mediating anti-inflammatory effects, since we did not observe any significant change in cortisol levels among the experimental groups.

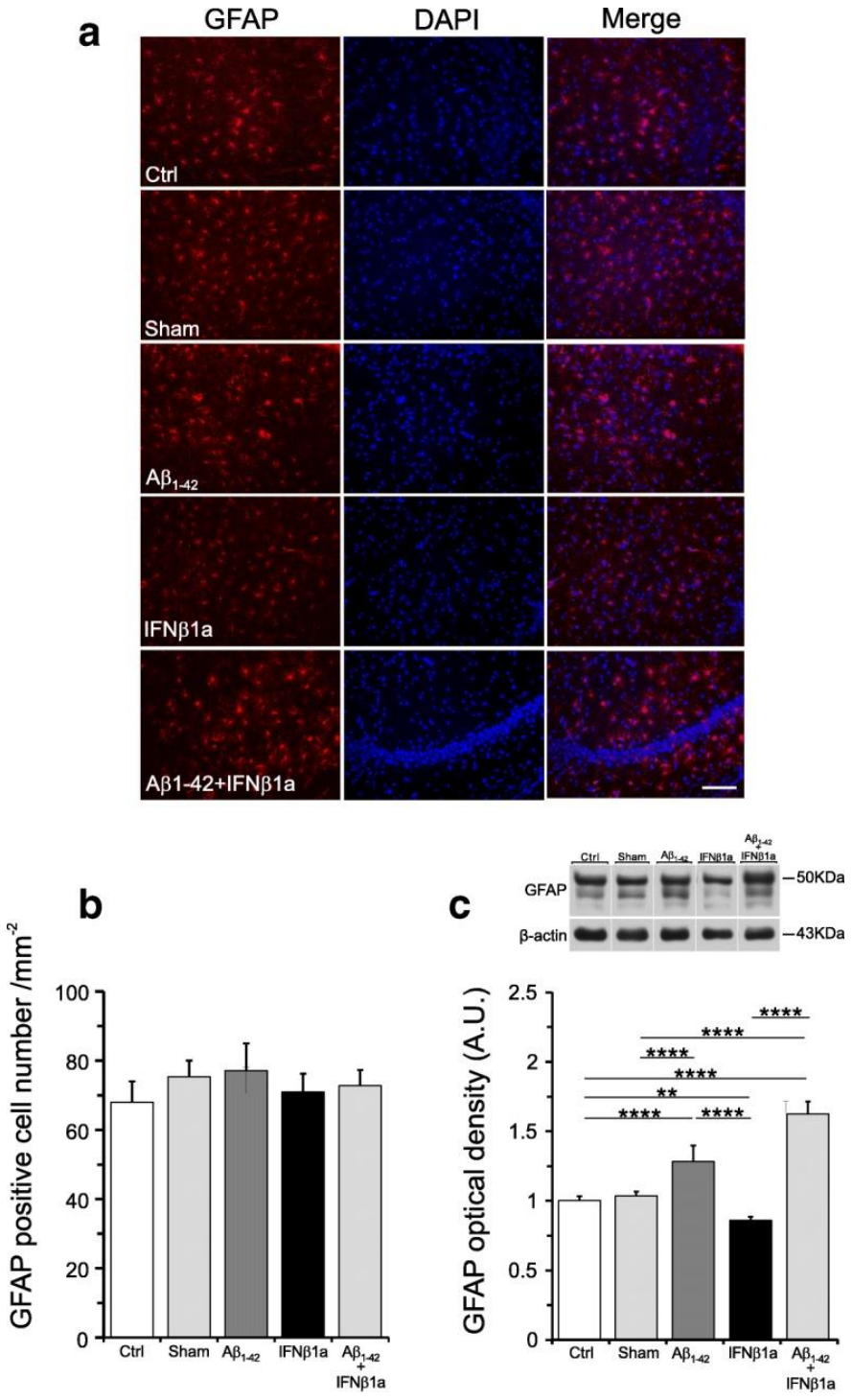

Figure 9. IFNβ1a effects on astroglial cell activation by Aβ1-42. a. GFAP immunohistochemistry in the hippocampus. **b.** Count of GFAP positive cells and **c.** quantitative Western blot analyses of GFAP protein levels. **b.** Count of astrocytes number showed no significant changes in all experimental groups. **c.** By contrast, the quantitative Western blot analyses of GFAP protein levels revealed that in the Aβ1-42 group (n = 6), GFAP protein levels were significantly increased and this increase was not counteracted by treatment with IFNβ1a (n = 6) in the Aβ1-42 + IFNβ1a group (n = 6). Note IFNβ1a alone significantly reduced the GFAP protein levels as compared to the control group. Scale: 100 μm *P < 0.05, **P < 0.01, ***P < 0.001, ****P < 0.0001

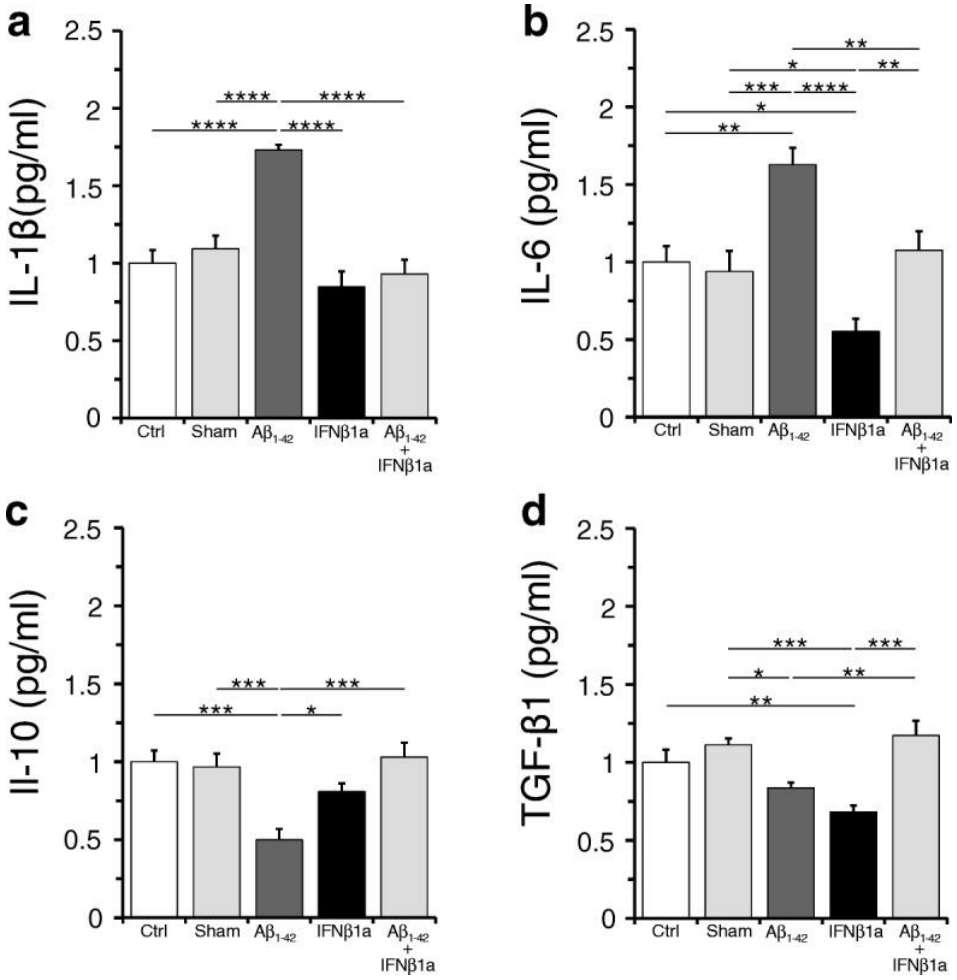

Figure 10. IFNβ1a effects on inflammatory cytokines in the hippocampus. a, b. Hippocampal levels of pro-inflammatory cytokines, IL-1β and IL-6. Note that IL-1β and IL-6 levels were significantly increased in the Aβ1-42 group (n = 5 respectively) and this increase was counteracted by treatment with IFNβ1 (n = 5 respectively) in the Aβ1-42 + IFNβ1a group (n = 5 respectively). **c., d.** Hippocampal levels of anti-inflammatory cytokines, IL-10 and TGF-β1. Note IL-10 and TGF-β1 levels showed significant reduction in the Aβ1-42 group (n = 5 respectively) and following IFNβ1a (n = 5, respectively) treatment in the Aβ1-42 + IFNβ1a group (n = 5, respectively) were recovered to control (n = 5 and n = 6, respectively) levels. *P < 0.05, **P < 0.01, ***P < 0.001, ****P < 0.000

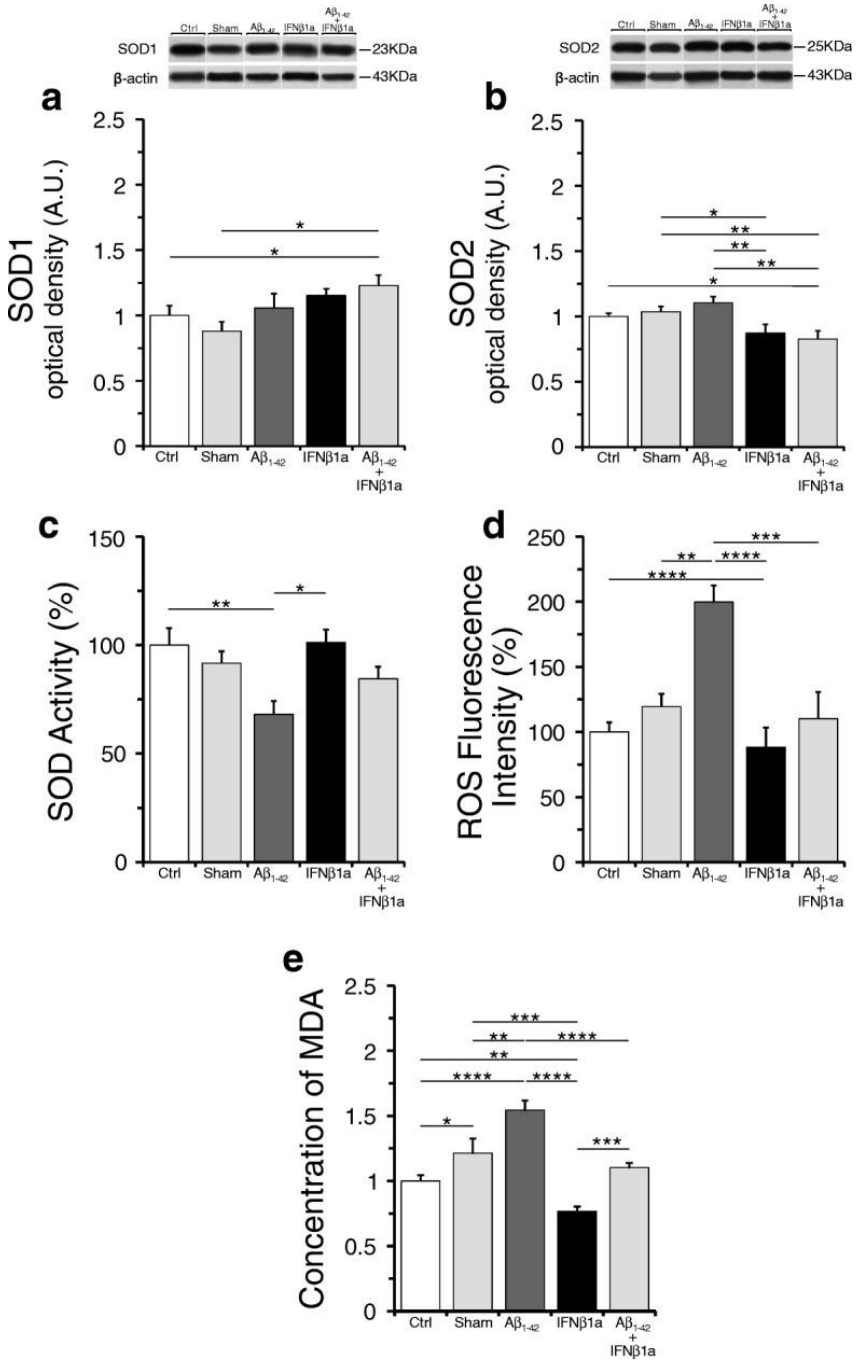

Figure 11. IFNβ1a effects on ROS and lipid peroxidation levels and SOD1 or SOD2 proteins and activity levels in the hippocampus. a., b. The levels of SOD1 showed significant increase in the Aβ1-42 + IFNβ1a group (n = 5), whereas those of SOD2 appear significantly reduced in the same group (n = 5). **c.** Total SOD activity levels showed significant decrease in Aβ1-42 group (n = 5), and this decrease was counteracted in the Aβ1-42 + IFNβ1a group (n = 5) by treatment with IFNβ1a. **d.** ROS levels were significantly increased in the Aβ1-42 group (n = 5), and this increase was counteracted by treatment with IFNβ1a (n = 5). **e**. The analysis of lipid peroxidation levels, measured as concentration of MDA, revealed a significant increase of MDA levels in the Aβ1-42 group (n = 5) that was completely blocked by IFNβ1a treatment in the Aβ1-42 + IFNβ1a group (n = 5). *P < 0.05, **P < 0.01, ***P < 0.001, ****P < 0.0001

Aim 2.1 Preservation of global synaptic Excitatory to Inhibitory ratio during long postmortem intervals

Study of global synaptic excitation to inhibition (E/I ratio) imbalances, thought to underlie many human brain diseases, is hampered by time-dependent postmortem degradation of synaptic receptors. We show that near-simultaneous recording of synaptic receptors after simulated morgue conditions allows the determination of the E/I ratio with no changes in receptors affinity for at least 120h after death, expanding the availability and use of human diseased tissue stored in brain banks.

The excitation to inhibition balance has been defined as the average amount of depolarizing to hyperpolarizing neuronal synaptic currents (global synaptic E/I ratio or just E/I ratio) in a particular brain region [75]. Because the E/I ratio emerges from complex processes that are critical for physiological coding by neural circuits ensembles [76] alterations of this balance have been proposed to underlie neuropsychiatric and neurodegenerative disorders such as schizophrenia, autism and dementias [21], [77]. However, disturbances of the E/I ratio are equalized by synaptic scaling [175], heterosynaptic plasticity [176] and changes of synaptic function [177]; thus, synaptic E/I imbalance cannot be implied from observing dysfunction in only one component. Simultaneous measures of excitatory and inhibitory components are needed for such assertion. This information is critical for understanding the pathophysiology of brain disorders whose major clinical manifestations emerge from abnormal synaptic function. Whereas the E/I ratio has been measured at the neuronal level in animal models, the global synaptic ratio in a particular region is still not well known. In humans the E/I ratio is even less understood due to the difficulty to measure the simultaneous activity of synaptic excitatory AMPARs and inhibitory $GABA_A$Rs in alive people. Reactivation of post-mortem tissue by MSM, which allows the electrophysiological analysis of postsynaptic AMPARs and $GABA_A$Rs [139], [178]–[180], has opened the possibility to access this information; however, the large variability of ion current responses across microtransplanted cells [154], [181] and the potential degradation of biological activity due to post-mortem interval (PMI) [182], has slowed its implementation in synaptic disorders. Here we show that the global postsynaptic E/I ratio can be estimated from the near-simultaneous recording of post-mortem synaptic AMPARs and $GABA_A$Rs microtransplanted into *Xenopus* oocytes, and that the large variability of responses observed when AMPARs or $GABA_A$Rs are studied in isolation is remarkably minimized when the E/I ratio is used instead. We also demonstrate that the E/I ratio is relatively unaffected by PMI when the tissue is stored at cold temperatures for long periods of time removing one of the barriers preventing its use for electrophysiological analyses.

Exp 2.1.1 – Low temperature prevents the change of brain pH and preserves the integrity of RNA

To test the PMI effects on the E/I ratio, 22 adult Wistar rats were euthanized at room temperature (21°C). The cerebral cortex from 2 rats were immediately removed, snap-frozen in liquid nitrogen and stored at -80°C for downstream applications. These rats were used as controls (PMI=0). The remaining rats were separated in two groups. One group was kept at room temperature (21°C) and the other was stored inside a refrigerator (2°C) to simulate morgue conditions. Cerebral cortices from 2 rats per time point (6, 16, 24, 48 and 120h), per group, were surgically removed and snap-frozen in liquid nitrogen. After euthanasia, the rats body temperature fell exponentially from 38°C to 21°C with a time constant (τ) of 7.5 h, and to 2°C with a τ of 4.8 h (Figure 12). Measurements of pH in brain cortex homogenates showed no significant PMI effects when the rat bodies were kept at 2°C for up to 120h after death (pH= 6.80 ±0.04; F (5,12) = 3.096, p=0.0505; ANOVA; Figure 12). However, a significant acidification at room temperature was observed at 48h and 120h (pH = 6.74 ±0.1; F (5, 12) = 22.53, p<0.0001; ANOVA followed by Dunnett's multiple comparisons test). Changes in pH were similar to changes in the quality of total RNA. RNA integrity (RIN) values were preserved at 2°C for up to 120 h (7.4 ±0.37), and at 21°C for up to 48 h (7.3 ±0.39). Synaptic RNA from rats kept at room temperature was highly degraded by 120h (figure 13).

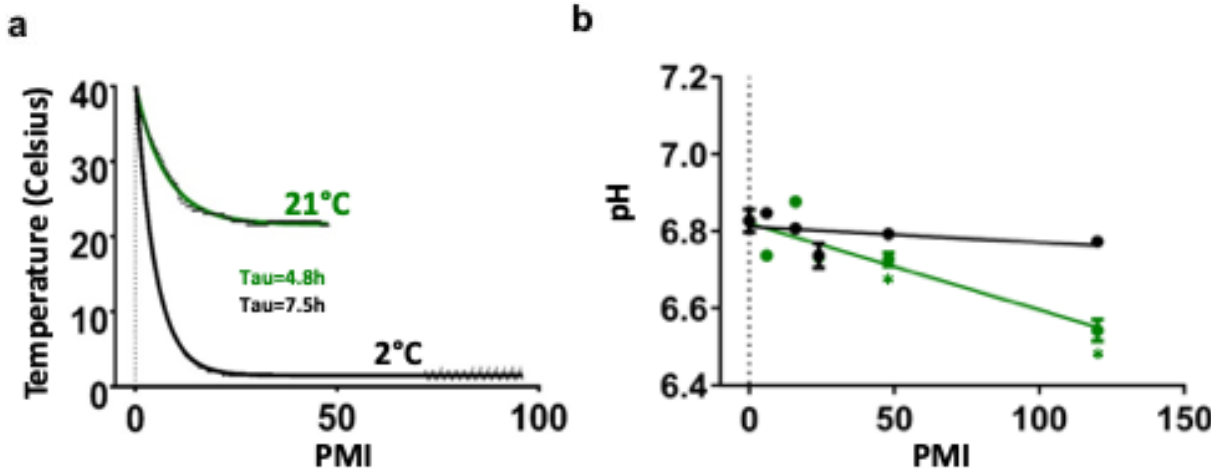

Figure 12. Temperature and pH. a. Temperature was monitored during the PMI. The curves were fitted with a one phase decay non-linear regression. **b.** Measurements of pH showed no difference along the PMI at 2°C. Instead, larger PMI at 21°C (48h and 120h) showed significative acidosis compared to the control at time 0 (ANOVA one-way-Dunnett's multiple comparisons test; 48h p<0.05, 120h p<0.0001, n=3).

Exp.2.1.2 – Morgue temperature reduces the pace of postsynaptic density degradation and preserves the E/I ratio

Degradation levels and loss of biological activity of synaptic receptors synaptosomes were evaluated in synaptosome-enriched P2 membrane preparations. Synaptosome enrichment was determined by the ratio of synaptophysin (Syn) to the nuclear marker NeuN, measured by WB (Syn/NeuN). The Syn/NeuN ratio in the P2 fraction was increased by 603 ±106% at 2°C across all PMIs, and by 622 ± 278 % at 21°C for PMIs up to 48h, compared to the P1 fraction. In agreement with the decline of the quality markers pH and RIN, samples from brains left for 120h at 21°C showed no synaptosome enrichment (Figure 14). With exception of 21°C/120h samples, similar synaptosome enrichment across different PMIs was observed at 2°C and 21°C (2°C $F(11,26) = 4.489$, $p<0.0008$ and 21°C $F(11,20) = 4.423$, $p=0.002$ ANOVA); although a loss of enrichment trend was observed at 21°C ($r=0.916$, Pearson's correlation coefficient). WB analysis of the excitatory and inhibitory postsynaptic density proteins, PSD-95 and gephyrin [183], [184], showed a time-dependent linear reduction of these proteins at 2°C. Notably, the abundance of both proteins was highly correlated across PMIs indicating a uniform degradation; consequently the PSD-95/gephyrin ratio, at 2°C, remained borderline constant up to 120h after death $F(5,26) = 2.419$, $p=0.063$. At room temperature the degradation of PSD and gephyrin was better described by a one phase decay equation, and PSD-95 was more affected compared to gephyrin leading to a significantly lower PSD-95/gephyrin ratio after 24h at room temperature.

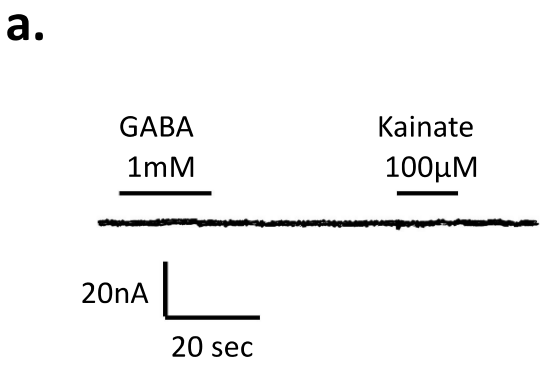

b.

	Sample	RIN
	Ctrl	7.7
4°C	6h	7.3
	16h	7.6
	24h	6.9
	48h	7.9
	120h	7
21°C	6h	7.4
	16h	6.7
	24h	7.7
	48h	7
	120h	2.5

Figure 13. Injection of synaptic RNA. a. Total RNA isolated from synaptosome-enriched fractions was injected in oocytes, no response was elicited by GABA and kainate perfusion after 24h from the injection, suggesting that potential contamination of total RNA does not produce de novo production of neurotransmitter receptors. **b.** RNA integrity number (RIN) showed a good quality of the RNA across the experimental groups except in 21°C/120h.

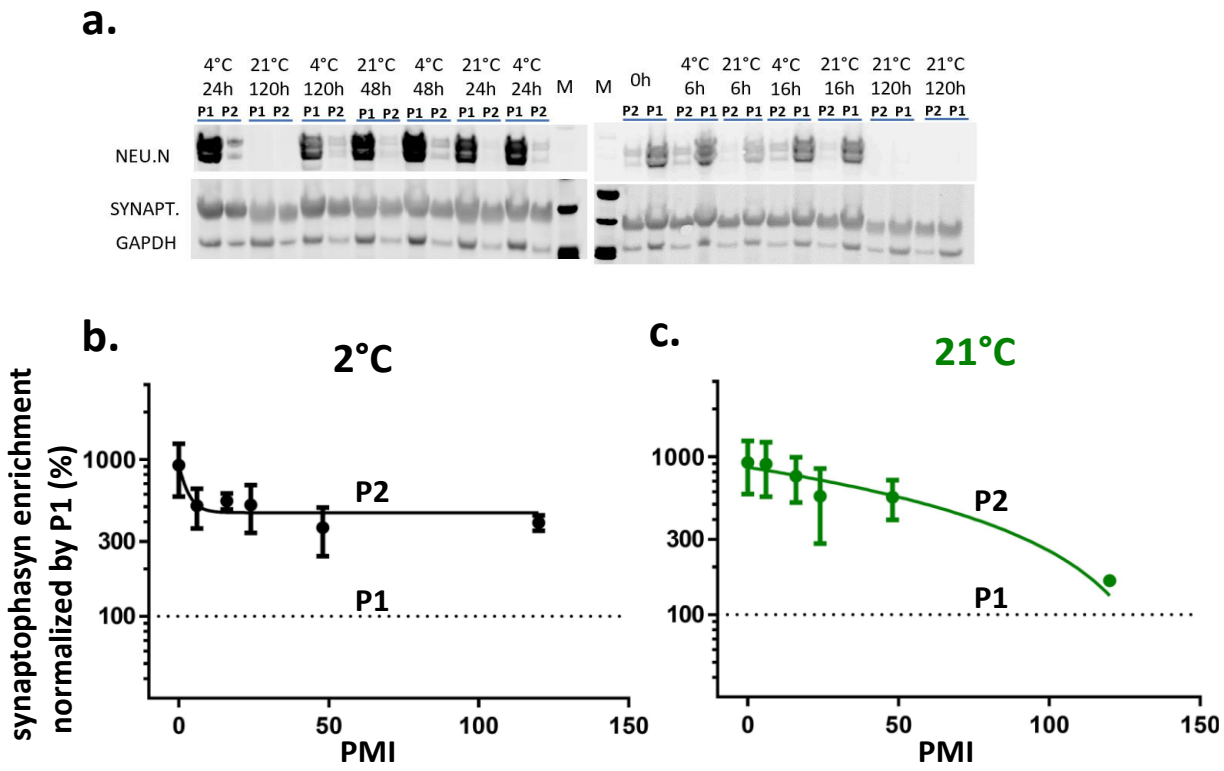

Figure 14. Synaptosome fraction enrichment. a. Representative western blots used for synaptic enrichment quantification. **b.-c.** western blotting analysis of synaptophysin enrichment (calculated by the ratio of synaptophysin/Neu.N levels) in synaptosomes (P2) and nuclear fraction (P1, dotted line). The protein levels are expressed in percentage in a logarithmic scale. PMI time points at 2°C were fitted with one phase decay exponential and at 21°C were fitted with linear regression equation. The enrichment of synaptosomes marker in P2 was significative in each experimental group except 120h/21°C, one-way ANOVA.

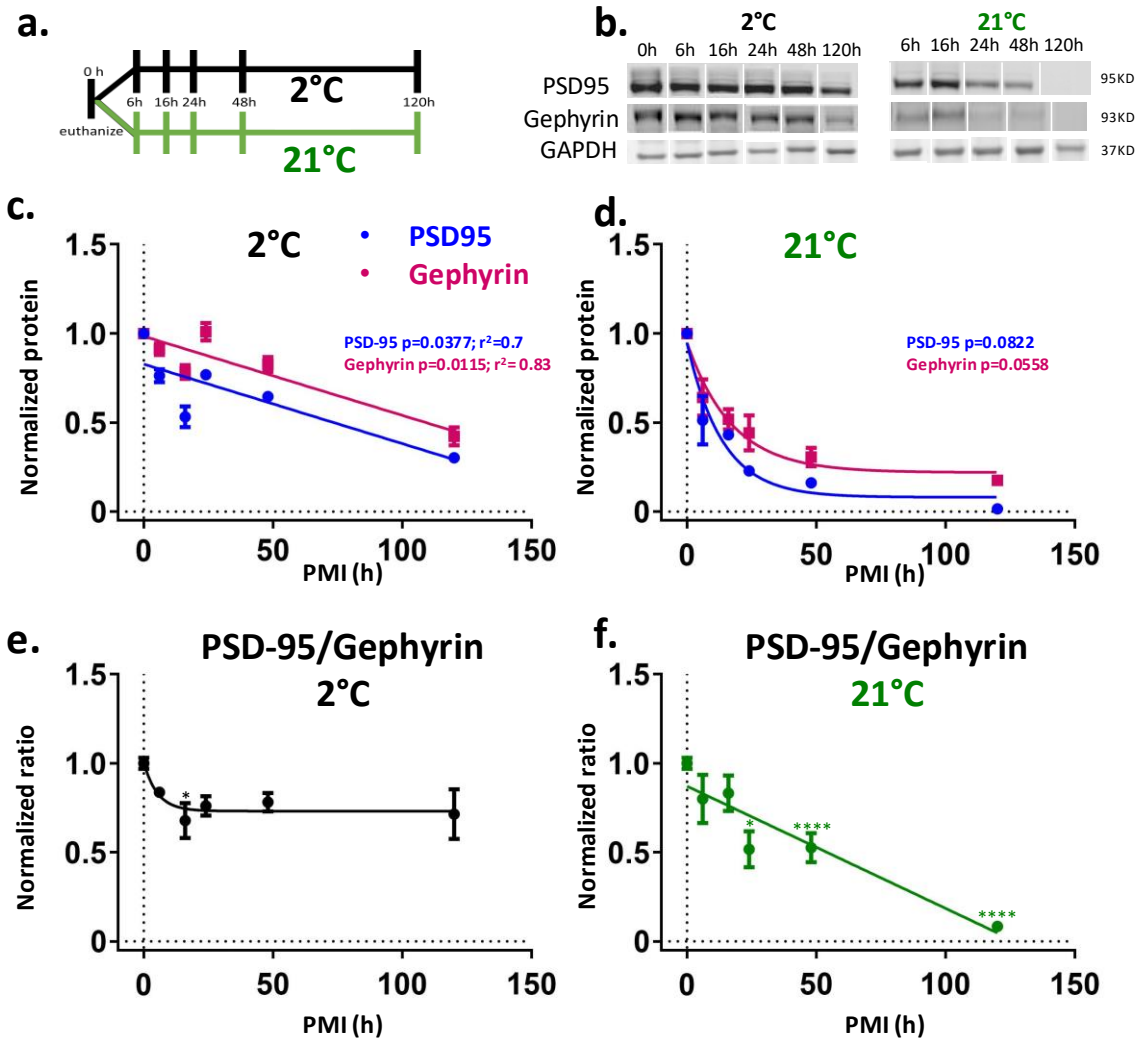

Figure 15. Morgue temperature reduced the rate of synaptic protein degradation and preserved the PSD-95/gephyrin ratio. a. Schematic of PMI experimental schedule. **b.** Representative Western blots of excitatory (PSD-95), inhibitory (gephyrin) postsynaptic markers, and GAPDH that was used as an internal control **c.-d.** Synaptic protein levels of PSD-95 and gephyrin at 2°C and 21°C. Linear regressions (2°C) and one phase decay (21°C) functions were used to fit the means of gephyrin and PSD-95 protein level along the PMI. **e.-f.** The PSD-95/gephyrin normalized ratio shows temperature-dependent relationships across time. At simulated morgue conditions, and after an initial reduction, the PSD-95/gephyrin ratio is preserved at least after 120h. The E/I ratio was fitted with one phase decay at 2°C and with a linear regression at 21°C. Data are reported as means ± SE. *p < 0.05, ***p<0.0001. N=4 for all of them except 0, 6h/21ºC and 6h/4ºC, n=8 statistical test is an ANOVA multiple comparison followed by Dunnet test to the control group (time 0).

Exp.2.1.3 - Synaptic receptor activity, affinity and E/I ratio are preserved by low temperature after long PMI

An electrophysiological metric of global E/I ratio that is useful to compare brain regions/subjects in health and disease in large population cohorts should be simple to calculate, stable within each subject across experiments, and flexible enough to show pharmacological changes. Because changes in excitatory

plasticity are normally followed by homeostatic changes of inhibitory signaling [185], [186] we decided to allow pharmacological flexibility to the excitatory component of the E/I ratio by activating AMPARs with 100 µM kainate, which is near half of the apparent affinity (EC50) for kainate in human microtransplanted AMPARs (Figure 17). Kainate is an agonist of AMPARs that keeps the channel in a non-desensitized state allowing consistent recordings of ion currents via AMPARs [187], produces less intra-subject variation compared to currents elicited by the combination of AMPA + cyclothiazide (CTZ) [188], [189], and due to the low expression of synaptic kainate-type receptors compared to AMPARs in synaptosomes kainate-induced currents in microtransplanted oocytes reflect the activation of AMPARs [144]. For the estimation of the inhibitory component we used 1 mM GABA which is a saturating concentration of $GABA_A$Rs. Thus, shifts of the E/I ratio reflect changes in the number and activity of excitatory or inhibitory receptors and/or small changes in AMPARs EC50 or large changes of $GABA_A$Rs EC50. Figure 16 shows kainate-induced AMPA currents and GABA currents recorded by two electrode voltage clamp (TEVC) in microtransplanted receptors between 20 and 32 h post-injection. We tested weather PMI had an effect on the E/I ratio of rat cortex, and dorsolateral prefrontal cortex (DLPFC) from a human brain with no history of drug abuse, psychiatric or neurodegenerative disorders. Non-injected oocytes, as well as oocytes injected with total RNA extracted from synaptosomal preparations, were unresponsive to these agonists confirming that ion-currents elicited in microtransplanted oocytes were generated by human synaptic receptors (Figure 13a).
Temperature was critical to preserve the amplitude of the currents. No statistical differences with the control were found across PMIs at 2°C, even 120h after death (Kainate $F(5,106) = 2.035$, $p=0.080$; GABA $F(5,50) = 0.9342$, $p=0.47$ ANOVA). In contrast, in samples stored at 21°C ion currents gradually decreased with longer PMIs. After 6 h GABA currents were reduced by 57% and kainate-induced AMPA currents were reduced by 45%. No currents were observed in 21°C/120h samples. Remarkably, due to the uniform loss of activity of excitatory and inhibitory synaptic receptors the global E/I ratio was preserved at least up to 120 h at 2°C, and up to 48h at 21°C (PMIs at 2°C, $F(5,50) = 1.077$; $p=0.38$ and PMIs at 21°C; $F(4,39) = 3.791$, $p=0.01$ using ANOVA. 48h/21°C $p=0.053$; 24h/21°C $p=0.94$ using Dunnett's multiple comparisons). Moreover, the EC50 or slope (Hill coefficient) to kainate and GABA was not significantly affected by PMI or temperature. Similar findings were observed in the DLPFC samples stored at 4°C for different PMIs. The biological activity of AMPA and GABA receptors showed a trend toward reduction by 30% after 87h (AMPA $F(6,33) = 0.2973$, $p=0.93$; GABA $F(6,41) = 0.6263$, $p=0.71$) but the E/I ratio was preserved. These results strongly indicate that inter-subject variability of the E/I ratio is minimal compared to the receptors studied in isolation and it is highly preserved across extremely large PMIs when the tissue is stored at morgue temperature. Thus, they provide strong support for the feasibility of electrophysiological studies of synapses using the invaluable tissue that is stored in brain banks which long PMIs is still unavoidable.

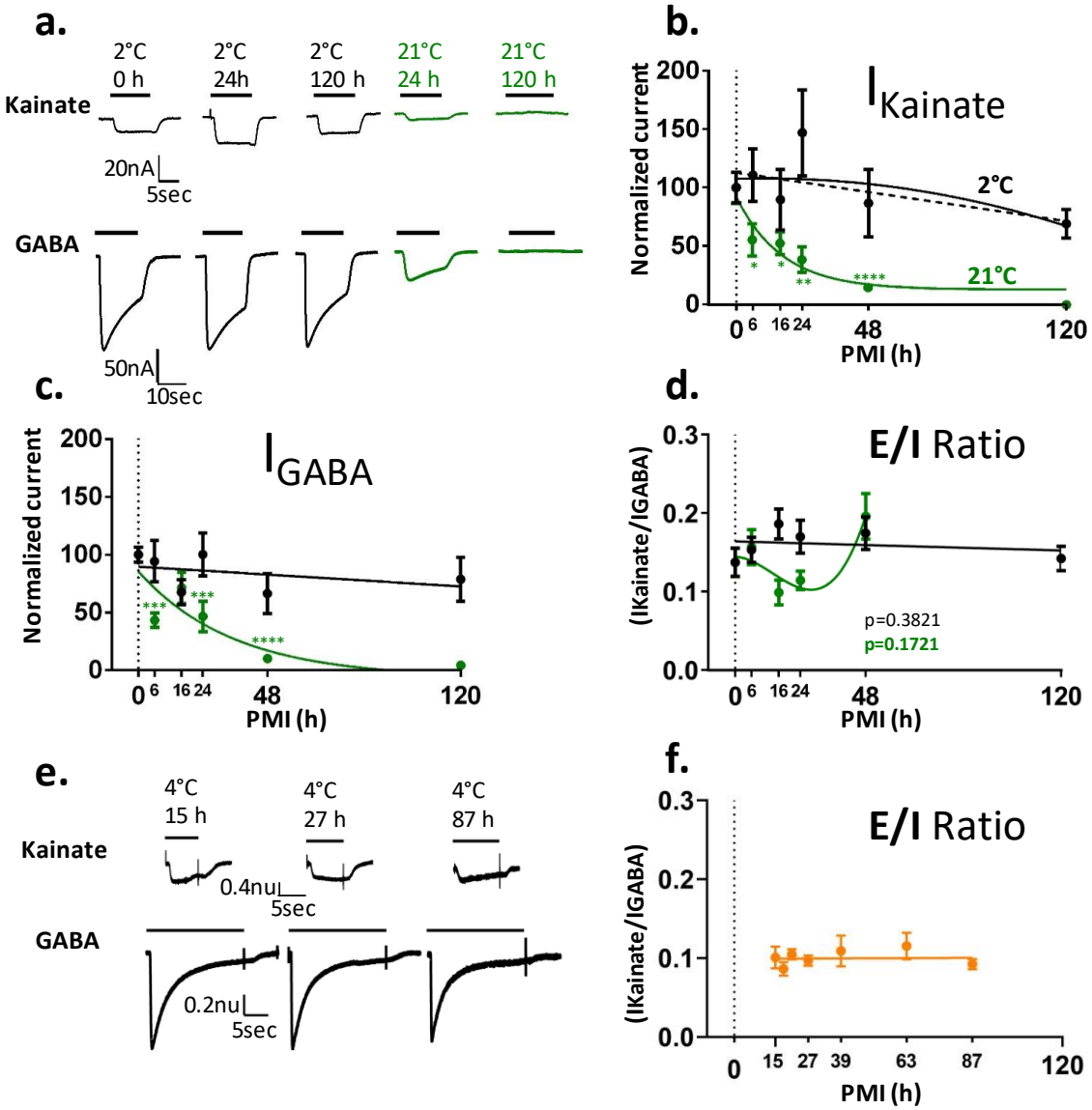

Figure 16. Electrophysiological activity of synaptic receptors is preserved by low temperature. **a.** TEVC, current responses of oocytes microtransplanted with synaptic receptors. **b.-c** Normalized maximum current of synaptic receptors. The currents generated by GABA and glutamate receptors, across PMIs time points, are well preserved at 2ºC but not at 21ºC showing significant differences compared to the control (time 0). **d.** E/I ratio (kainate/GABA current) obtained from the average of the ratio of each single oocyte. No differences were observed across groups. (N=8-11 oocytes per group). Statistical analysis was done using one-way ANOVA test, followed by Dunnett's multiple comparison test where appropriate. Statistical differences where P≤0.05 (*p < 0.05, **p < 0.01; ***p < 0.001; **** p< 0.0001). The mean values of the maximal currents were fitted with linear regression, one phase decay and third order polynomial (cubic). **e.** representative currents recorded from microtransplanted oocytes with human synapses. **f.** Electrophysiological E/I ratio of human synapses.

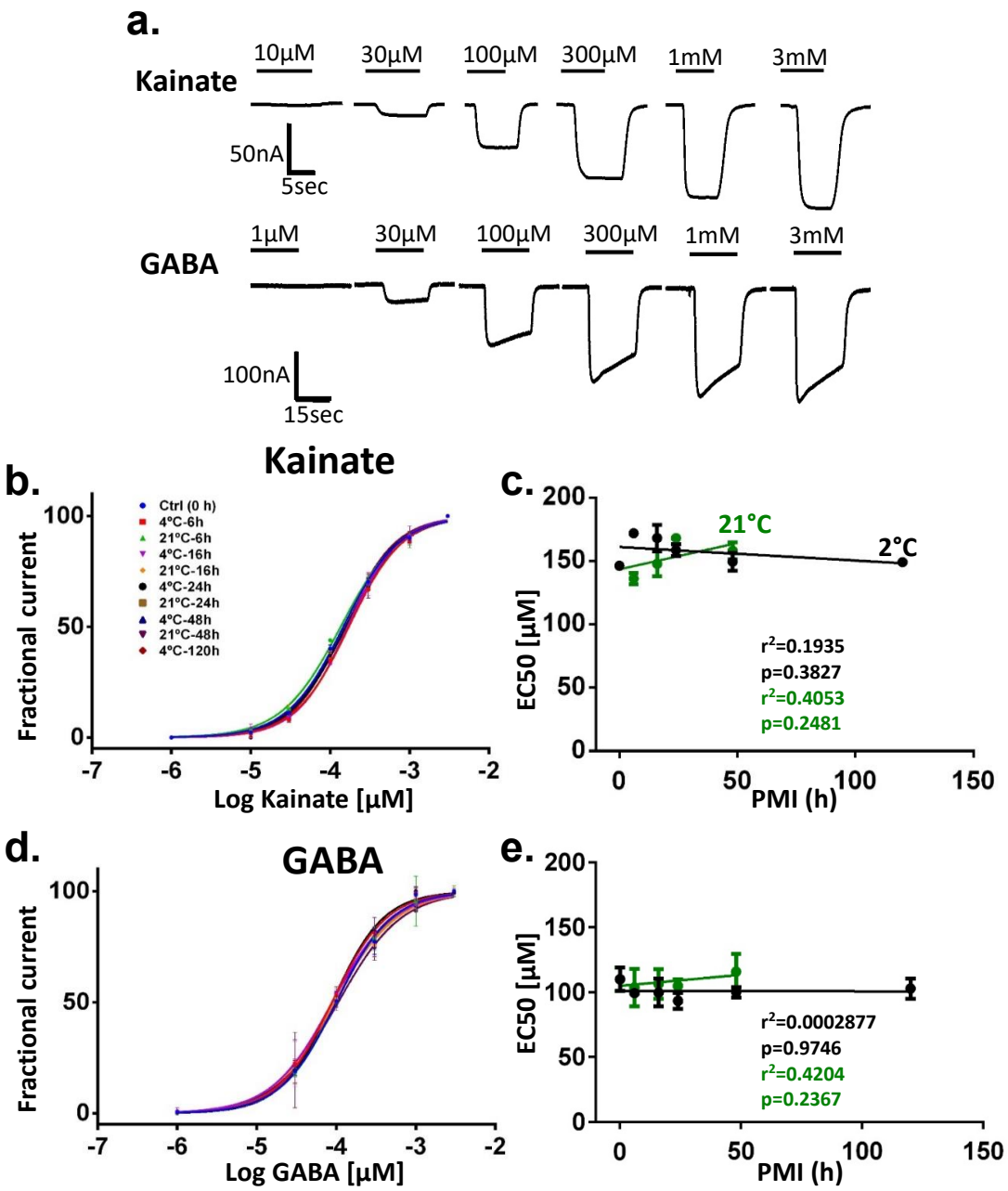

Figure 17. Synaptc receptor affinity is maintained for at least 5 days at 2°C and 2 days at 21°C. a. Ion currents elicited by different concentration of GABA and kainate in two oocytes microtransplanted with rat synaptic receptors. **b.-d.** Concentration response curves for kainate and GABA (each point is calculated as mean of three oocytes microinjected). Curve fitting was done using the Hill equation $I_{current}$=100/[1+10^((LogEC_{50}-[agonist])*HillSlope)]. **c.-e.** EC_{50} (mean ± SEM; n = 3) was calculated for each dose-response curve. 21ºC/120h had no current responses. No significative differences were found within the groups (One-way ANOVA, Dunnett's multiple comparison post hoc test). All the groups were fit with linear regression. n=3.

Aim 2.2 Increased functional excitatory to inhibitory synaptic ratio in parietal cortex of Alzheimer's disease subjects

Clinical studies and experiments with animal models suggest that synaptic loss may disturb the excitatory to inhibitory balance (E/I ratio) in circuits vulnerable to AD pathology [118], [121], [190], which in turn could lead to the cortical hyperexcitability that is associated with cognitive impairment [118], [122], [191]. However, electrophysiological evidence from animal model studies indicates that the activity and strength of excitatory and inhibitory synapses in the cerebral cortex are highly correlated across different cortical activity patterns [76], [125]. Thus, synaptic currents, through AMPARs and $GABA_A$Rs, are tightly regulated to preserve the global synaptic E/I ratio within a range that allows for normal network level operations [76], [125], [192]. Our previous work showed the total activity of functional $GABA_A$Rs, both synaptic and extrasynaptic, is significantly reduced in the temporal cortex of the AD brain, and that this reduction is equal to or greater than the reduction in AMPARs [154]. However, those experiments did not distinguish between synaptic and extrasynaptic $GABA_A$Rs, and thus do not directly address potential changes in the strength of fast inhibitory synaptic currents. Moreover, gene expression for the $GABA_A$R subunit GABRG2 was more affected than that of GRIA2 [154], a result that raises the possibility of AD related shifts in the operating characteristics of synaptic receptors. In all, the issue of whether AD differentially affects inhibitory vs. excitatory synapses, and thus E/I balance in cortex, has yet to be resolved. Such information is critical for refining hypotheses about the origins of AD related pathogenesis and pathophysiology, and for development of effective therapies.

In the present study, we utilized two complementary approaches to assess the global synaptic E/I ratio in the inferior parietal cortex (PCx) of AD subjects. The PCx is part of the default mode network (DMN) that is active during daydreaming, mind wandering, and introspection, but deactivates during demanding goal-directed cognitive tasks [98], [193]. Importantly, baseline DMN activity is increased in AD and fails to deactivate during cognitive tasks, suggesting that the DMN is abnormally and continuously hyperactive in AD [124], [194]. This may be due to disruptions in the E/I balance of principal neurons, although direct evidence is lacking. The present study was therefore undertaken to determine the anatomical E/I ratio in postmortem PCx from middle-aged subjects with AD, Down Syndrome (DS), and normal controls without pathology, using fluorescence deconvolution tomography (FDT) to histologically assess the synaptic levels of markers for excitatory and inhibitory postsynaptic densities: PSD-95 and gephyrin (GPHN), respectively. The DS group was included to compare synaptic effects in two neurological disorders with AD pathology; virtually all DS individuals exhibit AD pathology by 40 years of age [195]. The electrophysiological E/I ratio was then measured by MSM isolated from slices adjacent to those used in FDT experiments. As originally described by Miledi and colleagues [140], [196] , and expanded by others [178], [180], [197],

the MSM technique allows for assessment of human receptors that are still associated with their natural lipid environment and accessory proteins. Results from the present work provide the first evidence that despite a loss of both excitatory and inhibitory synaptic proteins, individuals with AD exhibit a marked shift towards a pro-excitatory perturbation of postsynaptic densities and electrophysiological synaptic E/I balance. Further corroborating evidence for this imbalance in AD parietal cortex was found using publicly available RNA-Seq transcriptional datasets.

Exp.2.2.1 - Anatomical alterations in excitatory and inhibitory synaptic markers in cortical layers of individuals with AD pathology

Quantitative FDT analyses were used to assess levels of PSD-95 and GPHN in parietal cortical layers 1 and 2 from individuals with AD or DS with AD pathology, and from normal controls (Figure 18). Both layers were assessed individually to test for differences in levels of the synaptic markers between the cell body-sparse layer 1 and the adjacent cell body-dense layer 2. Counts of PSD-95 and GPHN immunoreactive puncta in the sample fields from both layers were not significantly different across groups (Figure 18), indicating that the total density (puncta per volume) of excitatory and inhibitory synapses was maintained in parietal cortex of middle-aged individuals including those in the disease states. Nevertheless, in all cases there was evidence of age-related pathology including an accumulation of large lipofuscin deposits often in association with GPHN immunopositive (+) cell bodies. In the AD cases we also observed dystrophic GPHN+ processes (Figure 18d).

Next, we assessed the levels of immunoreactivity (ir) for both synaptic markers within individual synapse-sized puncta and plotted these measures in intensity frequency distributions (Figure 18e-h). Both AD and DS cases were characterized by a reduction in the proportion of excitatory synapses with high levels of PSD-95-ir ($\geq$ 90 immunofluorescence intensity, on a 20-180 scale) and an increase in the proportion of excitatory synapses with lower intensity labeling. These changes were larger in the perikarya-rich layer 2 as compared to layer 1 (Figure 18e, g); RM-ANOVA, $P < 0.0001$ for interaction between groups and intensities for both GPHN and PSD-95 in layer 2, vs $P = 0.0066$ for GPHN and $P = 0.0419$ for PSD-95 in layer 1. Consequently, the ratio of the high-to-low immunoreactivity for excitatory PSDs was significantly reduced in all AD and DS cases (Figure 19a-f). The leftward shift in intensity suggests that a larger proportion of excitatory synapses in AD and DS have smaller postsynaptic densities or disturbances in synaptic scaffolding. The intensity frequency distribution for analysis of GPHN-ir at inhibitory synapses demonstrated that changes in AD and DS cases were similar to those of PSD-95-ir (Figure 18f, h), with there being a marked reduction in the ratio of high-to-low levels of GPHN-ir per synapse in both layers 1 and 2, and stronger effects in layer 2 (Figure 19c-h). The disturbances in both PSD-95 and GPHN

immunoreactivities suggest reductions in both excitatory and inhibitory drive in AD and DS, with effects being relatively greater in the vicinity of perikarya.

Given the marked reductions in levels of synaptic PSD-95-ir and GPHN-ir in both AD and DS groups, we next asked whether these proteins were similarly reduced or if they were differentially affected on a subject by subject basis. The ratio of the peaks of the immunolabeling frequency distributions for PSD-95 to GPHN (PSD-95-ir/GPHN-ir), for each subject, was not different between groups for layer 1 (Welch ANOVA allowing unequal variances, P= 0.22), indicating a similar anatomical E/I ratio for AD and DS versus controls (Figure 20a). However, within layer 2 this ratio was significantly larger in the AD group as compared to controls (Welch ANOVA, P=0.0316; followed by Dunn post hoc test comparing AD and DS vs control); the DS group had a trend in the same direction for layer 2 but this effect did not reach statistical significance due to greater group spread (Fig 20b). These results suggest that while both PSD-95 and GPHN levels are reduced in AD, in layer 2 of PCx the ratio of excitatory to inhibitory postsynaptic elements is significantly elevated in AD versus controls.

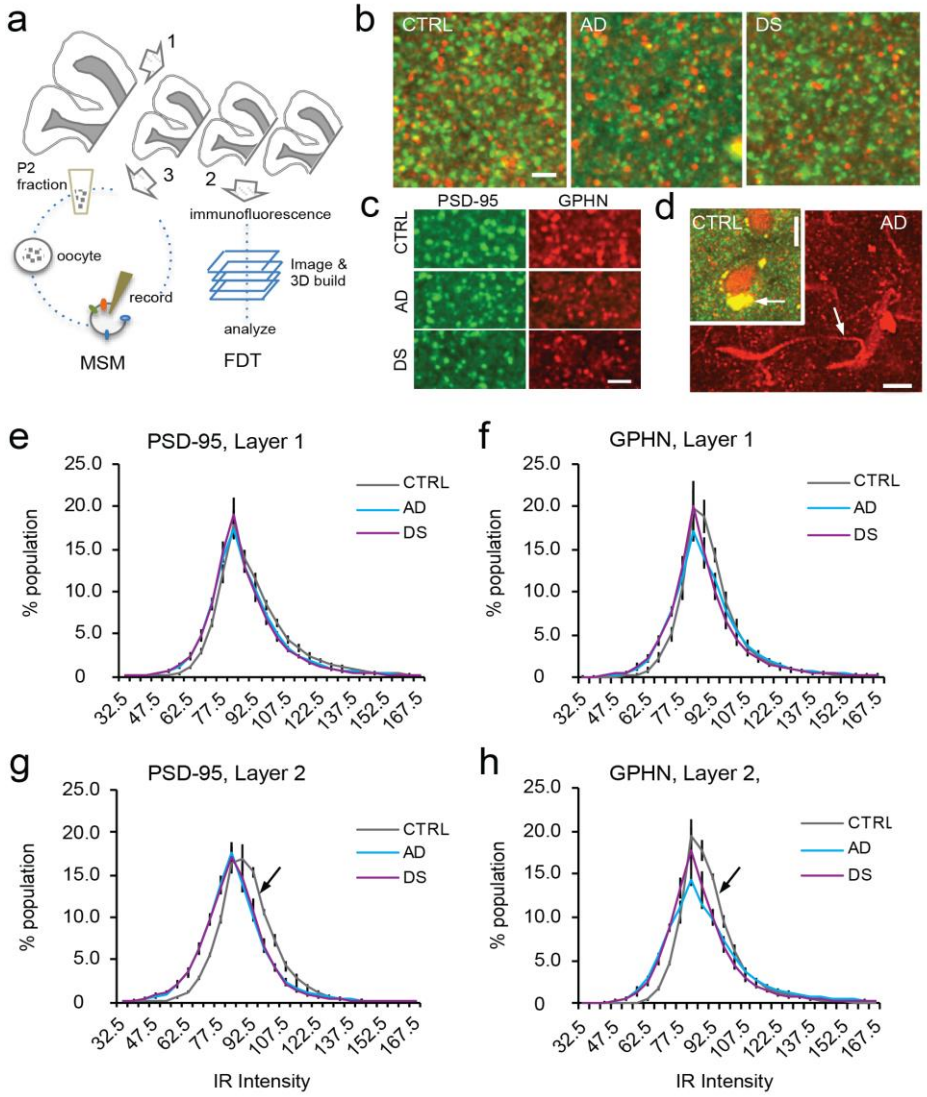

Figure 18 . Approach for analyses and quantification of changes in synaptic protein levels in AD and DS. **a.** Schematic illustrating the methodological approach for processing fresh-frozen parietal cortex subsections from the same tissue block (step 1) for either FDT (step 2) or MSM (step 3) analyses. See Methods for details. **b., c.** Photomicrographs showing PSD-95 (green) and gephyrin (GPHN, red) immunoreactive puncta in layers 1 (**b.**) and 2 (**c.**) parietal cortex from control (CTRL), AD, and DS subjects. Calibration bars, 2 µm (b & c). **d.** Examples of lipofuscin granules (arrow) surrounding gephyrin immunopositive cells in a control case (inset, upper left; calibration bar, 10 µm), and gephyrin+ dystrophic processes (arrow) in an AD case (calibration bar, 5 µm). **e.- h.** Synaptic immunolabeling intensity frequency distributions from the FDT analyses show the proportion of PSDs (Y-axis) in layers 1 (e,f) and 2 (g,h) that were immunolabeled for PSD-95 or GPHN at different intensities (X-axis) for the three groups; data plotted are group mean values ± SEM. Note the leftward skew in the immunolabeling intensity frequency distributions for the AD and DS groups relative to controls; this was most pronounced for layer 2 (RM-ANOVA, $P < 0.0001$ for interaction between groups and intensities for both GPHN and PSD-95 in layer 2; $P = 0.0066$ for GPHN and $P = 0.0419$ for PSD-95 in layer 1). Arrows in panels **g.** and **h.** indicate the control group which have a greater proportion of PSDs with high levels of the synaptic markers versus the AD and DS groups.

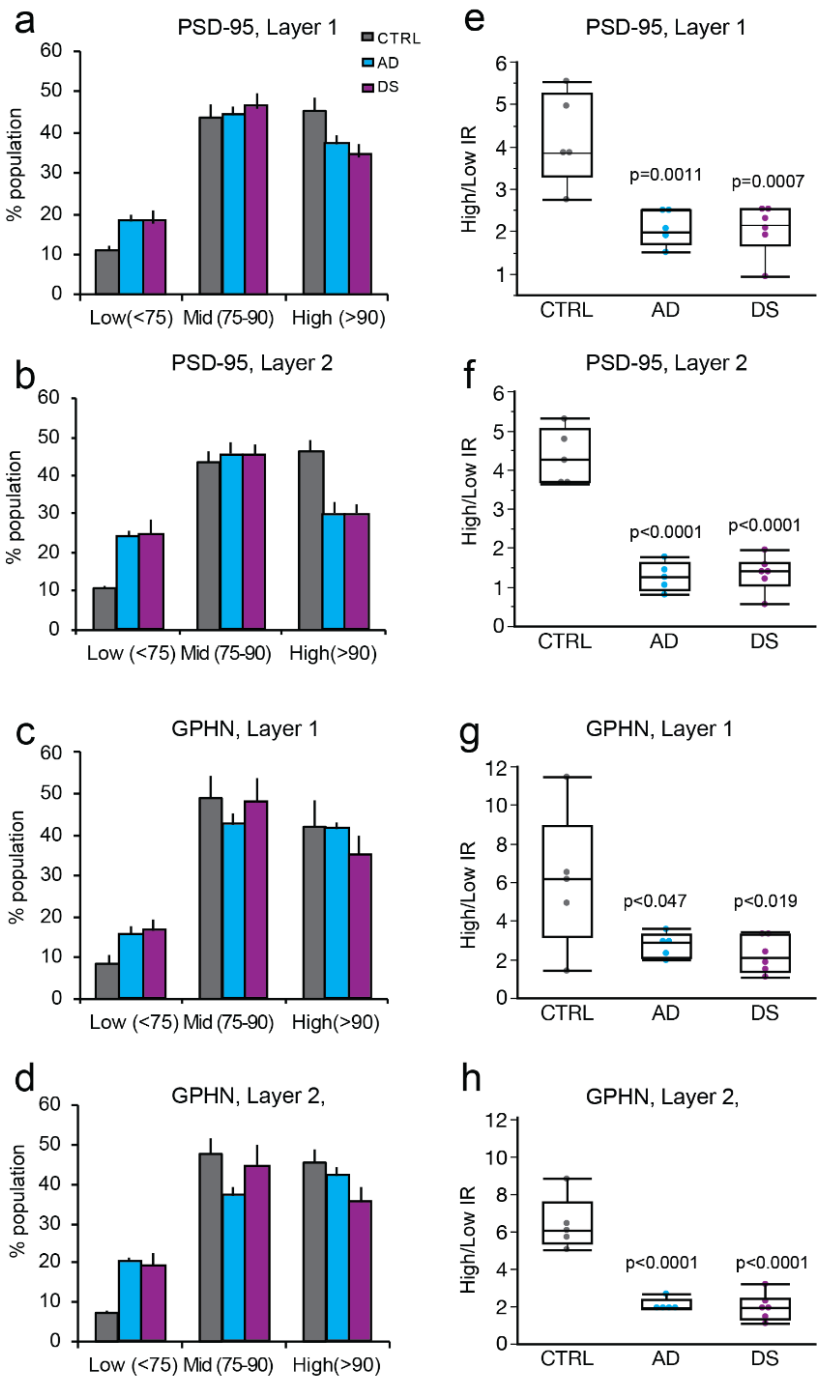

Figure 19. Levels of immunoreactivity for excitatory and inhibitory synaptic proteins are reduced in AD and DS. a.-d. Plots showing the proportion of PSD95+ and gephyrin+ puncta in each layer with immunofluorescence in low, mid or high intensity ranges for each group (group means ± SEM; based on Figure 18 **e.-h.** intensity distributions). RM-ANOVA (group x intensity interaction) indicated a significant effect for layer 2 only: P = 0.0019 for PSD-95 and P = 0.0133 for GPHN. RM-ANOVA for layer 1, P = 0.1027 for PSD-95 and P = 0.4151 for GPHN. (E-H) Box plots show the ratio of high-to-low labeling intensities for each individual case. As shown, all AD and DS cases exhibited significantly lower high-to-low intensity ratios as compared to controls for both postsynaptic proteins in each layer: PSD-95 layer 1, ($F(2,13) = 14.17$, $P < 0.0005$); GPHN layer 1 ($F(2,13) = 5.1$, $P < 0.023$); PSD-95 layer 2, ($F(2,13) = 8.4$, $P < 0.0045$); GPHN layer 2 ($F(2,13) = 37.54$, $P < 0.0001$). P values shown are from the Dunnett's post hoc test comparing AD or DS to control.

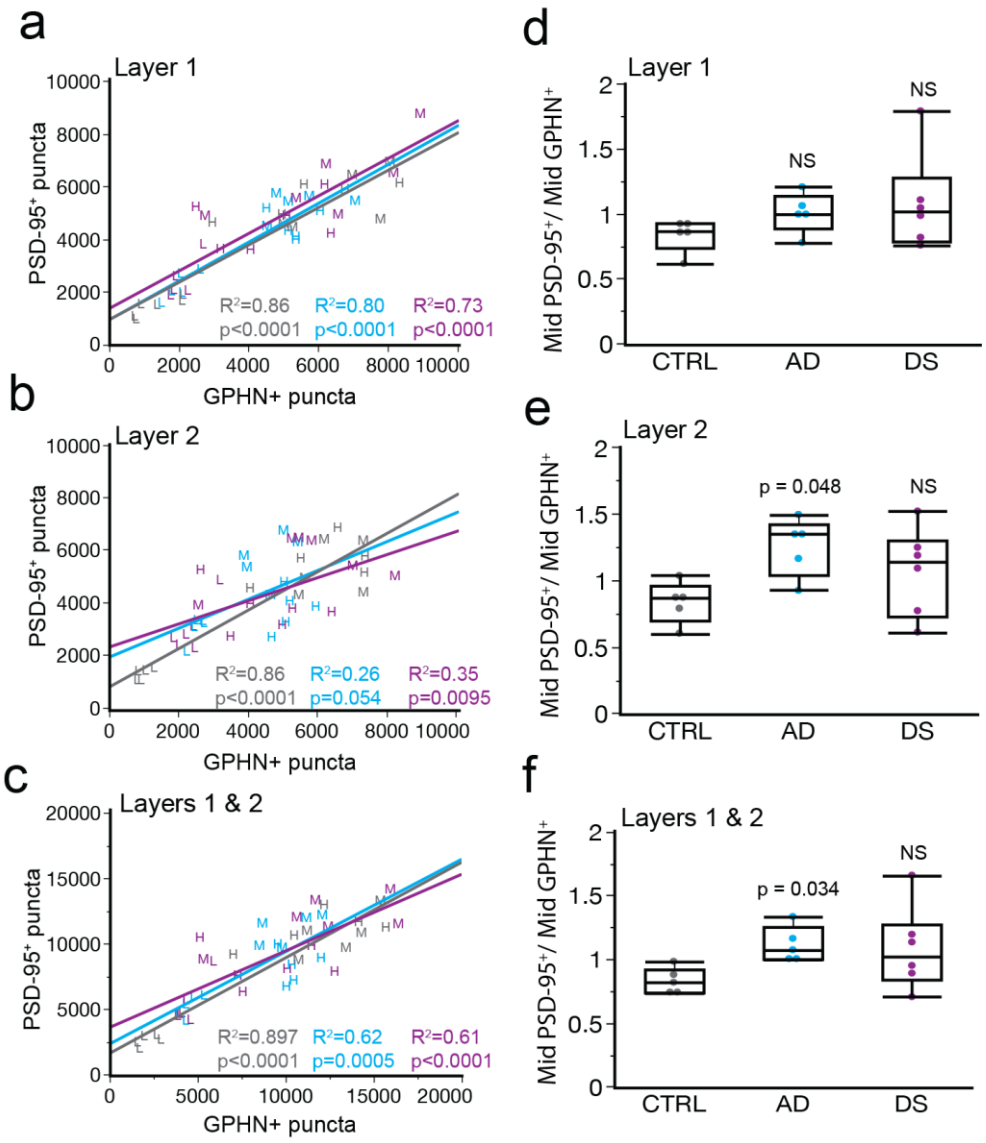

Figure 20. Differential alterations in the excitation-to-inhibition balance in parietal cortex of AD and DS. a.-c. Scatter plots show the ratio of the peak value from the PSD-95 intensity frequency distribution to the peak value from the GPHN distribution to provide a measure of the anatomical E/I balance for layers 1(**a.**) and 2 (**b.**), and for the two layers combined (**c**.) **d.-f.** As shown, the E/I balance (PSD-95/GPHN ratio) was not different between groups in layer 1 (a; Welch ANOVA allowing unequal variances P = 0.22), but it was significantly affected in layer 2 (b; Welch ANOVA; P = 0.0316) with only the AD group exhibiting elevated E/I balance versus controls (P=0.048, non-parametric Dunn's post hoc test). When layers 1 and 2 were combined, the difference between the AD and control groups was even greater (Welch ANOVA p = 0.0173; AD vs CTRL, P = 0.0336 Dunn's post hoc test). Notably, the DS group was highly variable in these E/I balance analyses.

Exp. 2.2.2 - Reduction of synaptosome-like particles in both AD and DS

To determine whether the anatomical E/I synaptic marker protein alterations are indicative of alterations in the abundance of functional synaptic AMPARs and $GABA_A$Rs, P2 fractions enriched in synaptosomes were isolated from a single (20 µm-thick) cryostat section, adjacent to those used in FDT analysis, with the goal of recording the electrophysiological activity of synaptic receptors by MSM. As an intermediate step between FDT and MSM, one aliquot of the P2 fraction was examined by flow cytometry to aid in the interpretation of the immunohistochemical analysis from layers 1 and 2, and the global electrophysiological recording of synapses from the whole slice. Flow cytometry analysis showed a striking 48% and 64% reduction of synaptosome-like particles in the AD and DS groups, respectively, as compared to the control group ($F(2,13) = 15.82$, $p = 0.0003$; Figure 21a, b). Aligning with the loss of synaptosome particles, total protein levels in the P2 fractions were also significantly reduced in the AD and DS groups ($F(2,13) = 21.5$, $p < 0.0001$) (Figure 21b). The amount of protein and the number of synaptosomes were strongly positively correlated $R^2(16) = 0.75$; $P<0.0001$.

These results indicate that preservation of the density of PSD-95+ and GPHN+ synapses in AD and DS, at least in superficial cortical layers, is at the cost of tissue shrinkage. We also observed a leftward shift in the size of recovered synaptosome-like particles from the AD and DS groups indicating that a large proportion of resilient synapses across all cortical layers have smaller-than-control sizes, a finding that is consistent with the reductions in immunoreactivity for both synaptic markers. Further in agreement with the FDT analyses, the ratio of large-to-small synaptosome-like particles was strongly reduced in AD and DS ($F(2,13) = 21.5$, $p < 0.0001$ vs control) (Figure 21f), and the large/small ratio from the whole slice was linearly correlated to the high/low immunoreactivity for PSD-95 and GPHN in layers 1 and 2 combined ($R^2(16)=0.69$, $P<0.0001$) (Figure 21g). Results from flow cytometry strongly suggests that synaptic deficits observed in cell-dense layer 2 identified with FDT are representative of effects in all cell-dense cortical layers, and that the P2 fractions capture those changes.

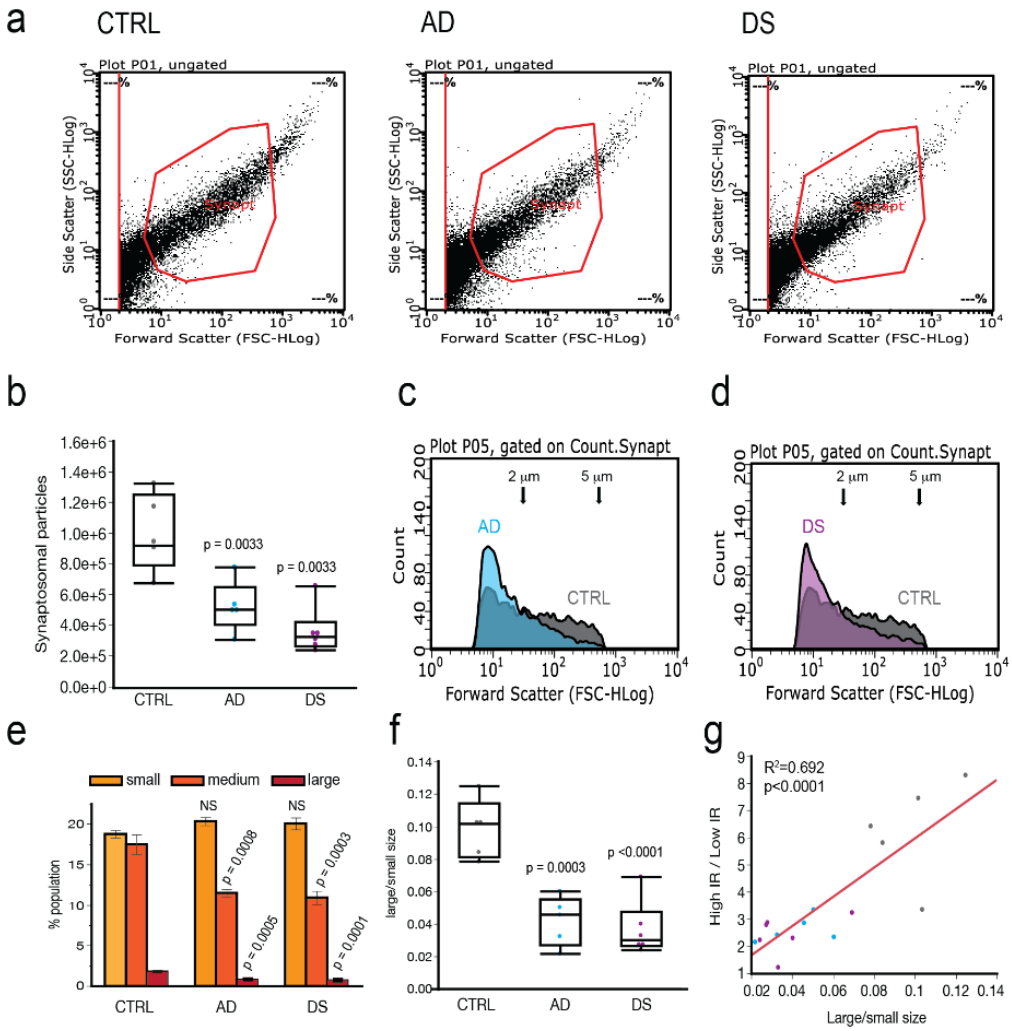

Figure 21. Flow cytometric analysis of synaptosomes in P2 fractions from AD and DS subjects. **a.** Representative plots indicate the gating parameters, based on size (1-5 um), used to quantify synaptosomes in P2 fractions from the parietal cortex of CTRL, AD and DS subjects. **b.** Numbers of particles within the size of synaptosomes were reduced from $1e^{+6} \pm 8.6\ e^{+4}$ in control (mean ± SEM; n = 5) to $5.2\ e^{+5} \pm 8.6\ e^{+4}$ in AD (n=5) and $3.6\ e^{+5} \pm 7.9\ e^{+4}$ in DS (n=6). An analysis of variance showed effect of diagnosis on particle count was significant, F (2,13) = 15.82, p = 0.0003. Post hoc analysis comparing to control using Dunnett's method (AD and DS vs CTRL) indicated that the average number of particles was lower in AD and DS. **c.,d.** Forward scatter plots for synaptosome sized particles from AD and DS subjects compared to controls. Forward scatter plots are representative of particle size and show a shift to smaller size particles in AD and DS compared to control. **e.** Plots showing the proportion of particles within the size range of synaptosomes in P2 fractions that were further identified as being small (1 µm > diameter (∅) < 2 µm), medium (2 um ≤ ∅ ≤ 3 µm) or large (3 µm < ∅ ≤ 5 µm) sized for each group (group means ± SEM; based on c,d size distributions). ANOVA determined that effect of diagnosis was significant for large (F (2,13) = 18.88, p < 0.0001) and medium sized particles (F (2,13) = 16.7, p = 0.0003) but not for the small group (F (2,13) = 1.7, p = 0.2). **f.** All AD and DS cases exhibited significant reductions in the large-to-small size ratios for particles from P2 fractions (F (2,13) = 21.5, P < 0.0001). P values shown in the figures indicate the P value of the Dunnett's post hoc test comparing AD or DS vs control. **g.** Plot showing the correlation between FDT high-to-low immunoreactivity (IR) ratios (PSD-95-ir and GPHN-ir in layers 1 and 2 combined) and the large-to-small for each subject. Each subject is color coded by diagnosis: CTRL (gray), AD (cyan), DS (magenta). The solid line represents the Pearson's correlation; $R^2(15) = 0.692$, P<0.000, showing agreement between intensity and size data from FDT and flow cytometry.

Exp.2.2.3 - Increased electrophysiological E/I ratio in AD but not DS.

Flow cytometry analysis identified a large reduction of synaptosome-particles in P2 fractions in AD and DS; this is in agreement with neuronal loss and synaptic dysfunction found in previous studies. To determine whether changes in postsynaptic markers are associated with changes in AMPARs and $GABA_A$Rs, we microtransplanted the same amount of synaptosomal membranes for each subject and measured the agonist-elicited responses of excitatory and inhibitory receptors in xenopus oocytes. Because it is known that naïve oocytes (non-injected) do not express endogenous AMPARs or $GABA_A$Rs [198], the ion currents elicited by specific-agonists for these receptors in microtransplanted oocytes are mediated by the non-native human receptors. To confirm this point, in each experiment we tested agonists for AMPARs or GABAARs and were unable to elicit currents from non-injected oocytes, as previously reported. In contrast, oocytes microtransplanted with synaptosomes from each of the three groups, and clamped at a voltage of -80 mV, exhibited fast activated currents when perfused with 1 mM GABA (GABA currents) or 100 µM kainate (kainate currents) (Figure 22a). Am mentioned previously, kainate is an agonist of AMPARs that keeps the channel in a non-desensitized state, allowing steady-state measurement of AMPARs currents [199]. Co-perfusion of s-AMPA plus CTZ, after 3 min CTZ preincubation, elicited ion currents with similar amplitude of those produced by kainate alone (kainate vs AMPA+CTZ correlation: $R^2(16) = 0.935$, $P<0.0001$) suggesting that kainate currents are mostly generated by AMPARs. To determine the contribution of kainate-type receptors specifically, we incubated microtransplanted oocytes in concanavalin A (ConA), a positive allosteric modulator of kainate-type receptors [200]. Figure 22c shows no effect of ConA in this preparation, confirming that the contribution of kainate receptors in our recordings was negligible.

Having demonstrated agonist-induced responses in microtransplanted oocytes, we then tested for group differences. Maximal responses to GABA, kainate and AMPA+CTZ were variable across subjects (Figure 22); this was most striking in the DS group, which included some of the largest ion currents recorded. Therefore, although both AMPAR and $GABA_A$R responses tended to be smaller in AD versus control cases, the differences were not statistically significant. It is important to note that this study was not powered to detect differences in the total amplitude of the currents when measured individually (Figure 22b). However, the maximal amplitude of currents through AMPARs and GABAARs were highly correlated across subjects (Figure 22d, e). Because the correlation between ion currents elicited by kainate and GABA ($R^2(16)=0.942$, $P<0.0001$) was higher than that between s-AMPA+CTZ and GABA ($R^2(16)=0.916$, $P<0.0001$), we used kainate and GABA currents to calculate the electrophysiological E/I ratio for each subject. For this, measures were collected and averaged only from oocytes in which both kainate and GABA currents were unambiguously measured. As compared to controls, only the AD group exhibited an increase in electrophysiological E/I balance with the kainate/GABA response ratio being significantly greater than for

controls ($F(2,13) = 4.21$, $p < 0.0387$; Figure 22f); responses from the DS group did not differ from controls. Combined with results from the FDT and flow cytometry analyses, these findings provide the first evidence that individuals with AD have a shift in the E/I balance leading to greater excitatory relative to inhibitory activity in cortex than is the case in controls.

Unlike the AD cases, the electrophysiological E/I ratio was preserved in DS (vs controls) despite these individuals exhibiting severe plaque and tangle pathology that was comparable to the AD group (Table 3). As described above, the DS group exhibited large variability in ion currents that lead us to ask whether this might reflect another aspect of pathology such as levels of phosphorylated (p) tau, which can vary across individuals despite similar AD staging [201]. Thus, we tested if ion currents in the DS group were correlated with ptau levels. Notably, in DS individuals the amplitude of kainate currents was negatively correlated with ptau levels ($\rho(6) = -0.9429$, $p=0.0048$; non-parametric Spearman's ρ to avoid artifactual correlations due to extreme variability). In addition, the numbers of synapses with high levels of PSD-95-ir (layers 1 and 2 combined) were also negatively correlated with AT8-ir denoting ptau levels ($\rho(6) = -0.8857$, $p=0.0188$). Neither the amplitude of GABA currents ($\rho=-0.7714$, $p=0.07$) nor GPHN-ir per synapse ($\rho= -0.09$, $p=0.87$) was significantly correlated with ptau levels. For the AD subjects, ptau levels did not correlate with either measure ($p>0.2$ for all) likely reflecting the small within-group difference in ptau levels.

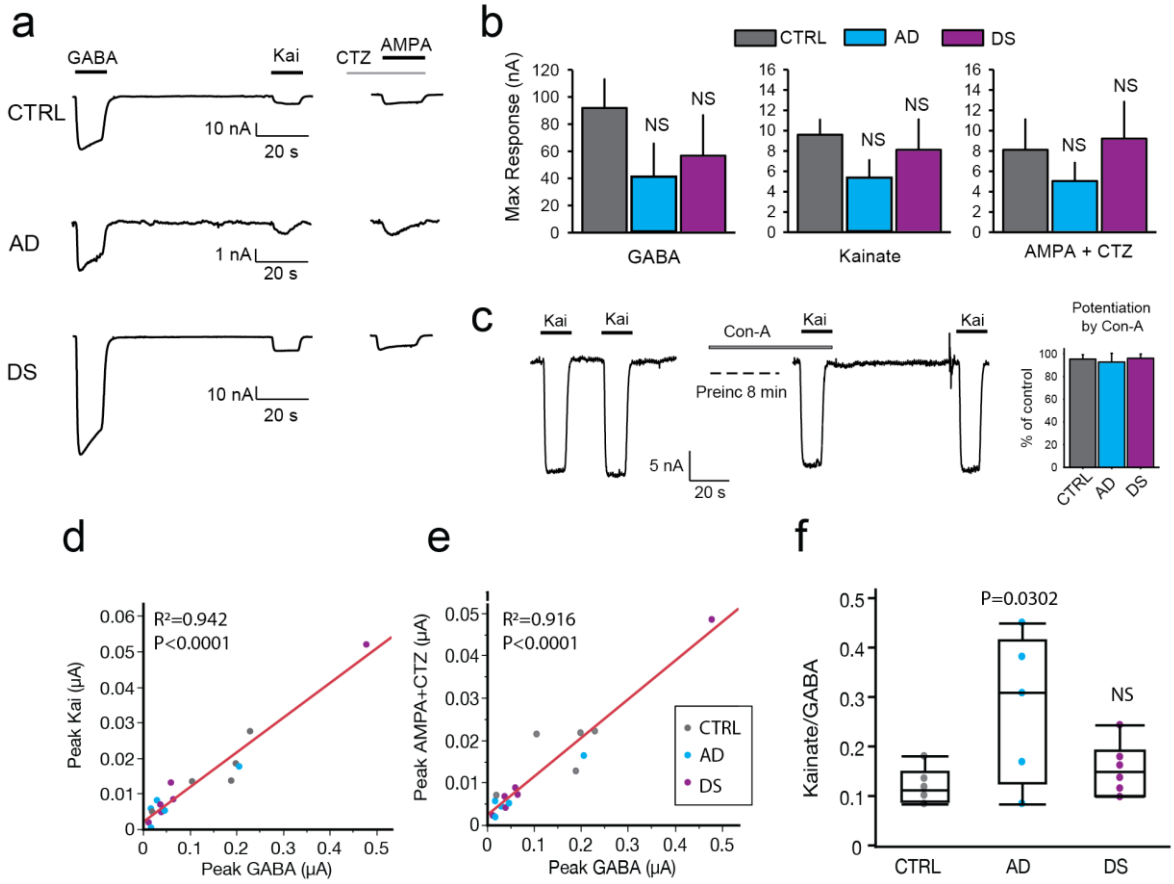

Figure 22. Differential alterations of the excitation to inhibition balance in ion currents of microtransplanted receptors from AD and DS parietal cortex. **a.** Functional responses of microtransplanted synaptic receptors were elicited by application of 1 mM GABA, 100 µM kainate, or 10 µM s-AMPA in combination with 10 µM cyclothiazide (CTZ), after 3 min preincubation with CTZ. **b.** No significant group differences were found in the maximal amplitude of agonist-induced ion currents for any of the responses (Welch ANOVA allowing unequal variances P = 0.27 for kainate, P = 0.09 for AMPA+CTZ, P= 0.34 for GABA). The DS group had both the largest, and some of the smallest, responses indicating a large within-group data spread in this condition. **c.** Kainate-induced responses were not potentiated by concanavalin A (Con-A), a positive allosteric modulator specific for kainate-type glutamate receptors, indicating that the participation of kainate receptors is negligible and kainate-induced receptors are generated by AMPA-type receptors. **d. ,e.** Plots showing the correlation between responses of excitatory receptors activated by kainate or AMPA plus CTZ and those of inhibitory receptors activated by GABA. Each point represents the average of responses from three recordings sessions. The solid lines represent the Pearson's correlation. **f.** Excitation to inhibition ratio, defined as the average of maximum amplitude of kainate- to GABA-induced currents measured from the same oocyte was significantly larger in oocytes microtransplanted with synaptic membranes from AD compared to control brains ($F(2,13) = 4.2$, $p < 0.0387$). P value in plot indicates results from Dunnett's post hoc test.

Exp.2.2.4 - Increased transcriptomic DLG4/GPHN ratio in AD.

To determine whether the E/I imbalance in AD is reflected at the transcriptional level in a larger independent cohort, we used publicly available RNA-Seq data from the ADTBI cohort to calculate the transcriptional E/I ratio in PCx. The transcriptional E/I ratio was defined as the level of mRNA for DLG4, which encodes PSD-95, divided by the level of mRNA for GPHN, which encodes gephyrin. An effect of clinical diagnosis (P=0.00891) was found on DLG4/GPHN ratios when individuals were pooled by signs of dementia (AD type by DSM-IV clinical DX) or non-dementia (Figure 23a). Ageing had no effect (p=0.34566). Further dissection of the transcriptional E/I ratio by staging of severity of AD (SSAD), from "0" for none to "3" for frequent, as defined by the CERAD score, indicated that people with clinical signs of dementia, but without neuritic plaque deposition (SSAD=0), had significantly larger transcriptional E/I ratios in PCx as compared to controls (Figure 23b). There was a trend towards reduced E/I ratios in people with clinical dementia and CERAD 1, but increased amyloid burden (e.g., SSAD=3) was associated with a markedly increased transcriptional E/I ratio. A random forest analysis, combining the transcriptional E/I ratio (DLG4/GPHN) with histopathological data and protein quantification across individuals, identified the transcriptional E/I ratio as a strong predictor effect for dementia status in the ADTBI cohort (Figure 23c).

Taking all these results together, using multiple approaches, we report here the first evidence for a shift of the global E/I synaptic balance in the inferior PCx of the AD brain that favors greater synaptic excitation. While results from FDT studies indicate a reduction in levels of both excitatory and inhibitory synapse markers of middle-aged AD subjects, the ratio of PSD-95 to gephyrin was strikingly altered in layer 2, indicating greater excitatory connectivity in this region. Gene expression analyses for PSD-95 and GPHN transcripts, in a larger cohort of subjects with level of pathology similar to the ones used in FTD studies, provided additional evidence for a shift in E/I imbalance, and suggest that alterations in layer 2 may extend to other cell-dense layers in the PCx. Electrophysiological recordings from the MSM studies also showed unequal deficits in postsynaptic AMPAR- and GABAAR-mediated ion currents, leading to an increase in the global electrophysiological synaptic E/I ratio, which would favor enhanced synaptic excitatory drive. The E/I shift in AD is remarkable in the context of studies showing that synaptic levels of inhibition are generally proportional and scaled in strength to excitation, despite even large variations in the amplitude of excitatory synaptic currents across neurons [125], [176], [185]. Changes in excitatory synapse number and/or strength predicted for Hebbian plasticity during learning and memory is similarly compensated for by synaptic scaling [175], heterosynaptic plasticity [176], and changes in synaptic function within minutes and hours [177]. Indeed, the E/I ratio in our MSM study had minimal variation compared to ion currents

measured individually, indicating that on average the relationship between postsynaptic AMPARs and GABAARs is nearly constant in control individuals, and even in DS.

Our converging evidence suggests that a pro-excitatory synaptic imbalance may underlie the hyperexcitability and reduced resting state deactivation that have been consistently observed in the PCx of AD patients [202], [203]. Further dissection of the transcriptional E/I ratio by amyloid plaque burden severity indicated that those with severe amyloid deposition and dementia had larger transcriptional E/I ratios than those without these clinical manifestations. This suggests that homeostatic mechanisms that maintain the E/I ratio are preserved in so-called "resilient" individuals that remain cognitively intact despite abundant Aβ plaques and NFTs [204], [205]. Importantly, people with dementia but without amyloid deposition also had significantly larger transcriptional E/I ratios compared to controls. These results suggest that pro-excitatory E/I ratios primarily correlate with dementia status, with potential secondary effects reflecting the level and type of pathology. Thus, cortical hyperexcitability may be part of a positive feedback loop whereby higher neuronal activity promotes production and accumulation of toxic Aβ and Tau oligomers [23] resulting in unequal synaptic losses that, in turn, lead to greater excitation. The preservation of a normal synaptic E/I balance in PCx in DS is an interesting finding. To our knowledge whether the default mode network shows signs of hyperactivity in DS is not known. However, comparative imaging studies of DS and control subjects did not find functional differences in the resting-state connectivity within PCx, even in subjects with APOE ε4 vs APOE ε3 variants that denote a higher risk for AD [206], suggesting resilience or persisting homeostatic mechanisms in this region in DS despite AD-like pathology.

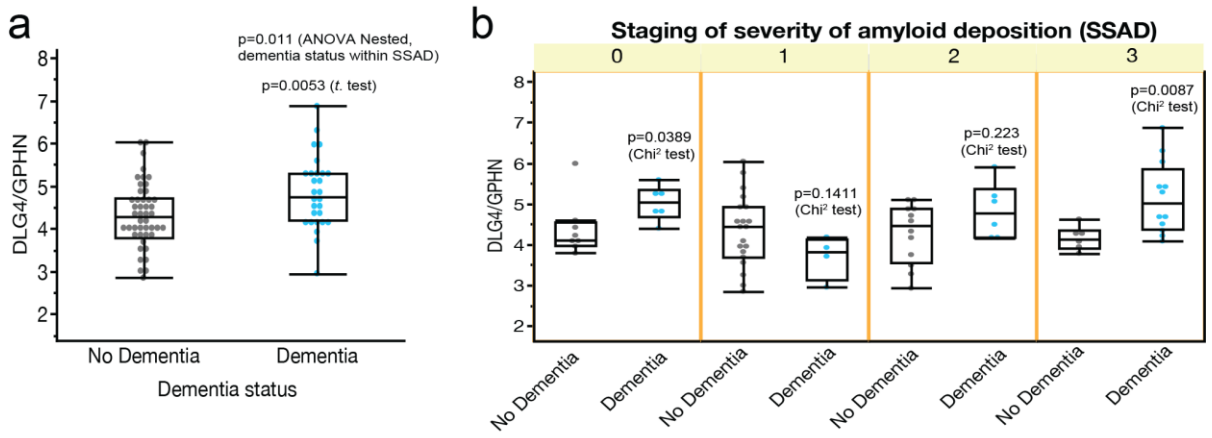

c

	Dementia status			
Predictor	Contribution	Portion		Rank
DLG4/GPHN	1.19294	0.2295		1
ihc_tau2_ffpe	0.56685	0.1091		2
ihc_gfap_ffpe	0.43356	0.0834		3
vegf_pg_per_mg	0.43258	0.0832		4
ab42_over_ab40_ratio	0.41170	0.0792		5
ihc_a_beta	0.29455	0.0567		6
ptau_over_tau_ratio	0.23249	0.0447		7
ptau_ng_per_mg	0.22607	0.0435		8
rantes_pg_per_mg	0.16040	0.0309		9
ihc_iba1_ffpe	0.13526	0.0260		10
il_7_pg_per_mg	0.12507	0.0241		11
ihc_at8_ffpe	0.12214	0.0235		12
mip_1a_pg_per_mg	0.09893	0.0190		13
a_syn_pg_per_mg	0.09629	0.0185		14
il_4_pg_per_mg	0.09236	0.0178		15
tau_ng_per_mg	0.09179	0.0177		16
ihc_ptdp_43_ffpe	0.09132	0.0176		17
il_10_pg_per_mg	0.06291	0.0121		18
ab40_pg_per_mg	0.06070	0.0117		19
ihc_a_syn	0.06038	0.0116		20
il_6_pg_per_mg	0.05812	0.0112		21
ab42_pg_per_mg	0.05681	0.0109		22
ifn_g_pg_per_mg	0.04439	0.0085		23
ihc_at8	0.02626	0.0051		24
bdnf_pg_per_mg	0.02059	0.0040		25
mcp_1_pg_per_mg	0.00279	0.0005		26
ihc_a_beta_ffpe	0.00000	0.0000		27
tnf_a_pg_per_mg	0.00000	0.0000		28
isoprostane_pg_per_mg	0.00000	0.0000		29
il_1b_pg_per_mg	0.00000	0.0000		30

Figure 23. Differential alterations in expression of excitatory and inhibitory postsynaptic density proteins are associated with dementia in AD. **a.** The transcriptional E/I ratio for DLG4 to GPHN (DLG4/GPHN) using RNA-Seq datasets from the Aging, Dementia and Traumatic Brain Injury study (ADTBI), was significantly increased in cases with clinical evidence of dementia (n= 46 cognitive healthy controls and 28 subjects with a DSM-IV clinical diagnosis of dementia of the AD disease type). **b.** The DLG4/GPHN ratio varied according to the severity of the amyloid deposition observed in the tissue and was stronger at the early and late stages of pathology severity. **c.** Random forest analysis indicates that the DLG4/GPHN ratio is a good predictor of clinical dementia compared to other histopathological metrics. For a list of abbreviations please see supplementary data 2.

CHAPTER 5. CONCLUSION

In our rat model of AD, the administration of Aβ-42 oligomer aggregates in the dorsal hippocampus led to neuroinflammation, via the activation of glial immune system, and memory impairment as evaluated by the NOR test. The short treatment with IFN-β1a was able to reverse memory impairment and to suppress microglia activation and the upregulation of pro-inflammatory cytokine (IL-6, IL-1β) levels and oxidative stress in the hippocampus. All together, these data suggest a protective effect of IFN-β1a against Aβ-42-induced functional alterations in the hippocampus of our rat AD model. The anti-inflammatory effect and the glutamatergic modulation of IFN-β1a in the CNS of experimental rats reasonably explains part of the recovery from memory impairment caused by hippocampal Aβ-42 peptide injection. These results highlight the strong link between inflammation and synaptic dysfunction in AD; however limited information of the type of postsynaptic alterations in the human brains affected by AD pathology is available. Even less information exists about the relationship of glutamatergic and GABAergic postsynaptic signaling in the same individual. The study of global synaptic excitation to inhibition (E/I ratio) imbalances, thought to underlie many human brain diseases has been hampered by time-dependent postmortem degradation of synaptic receptors. Here it is shown that the near-simultaneous recording of synaptic receptors after simulated morgue conditions allows the determination of the global E/I ratio with no changes in receptors affinity for at least 120h after death, expanding the availability and use of human diseased tissue stored in brain banks and allowing the direct evaluation of synaptic imbalance in a particular brain region of each subject. Finally, we provided the first evidence of a marked pro-excitatory perturbation of global synaptic E/I balance in AD parietal cortex a region within the default mode network that is overly active in the disorder and support the hypothesis that E/I imbalances disrupt cognition related shifts in cortical activity which contribute to the intellectual decline in AD. The ultimate goal will be to disrupt the positive feedback loop between oligomers, synaptic dysfunction and neuroinflammation by developing a combinatorial therapy that pair anti-inflammatory drug (IFN-β1a) and a drug capable to reduce hyperexcitability re-establishing the E/I balance.

Future Direction

Based on the previous data, due to limitations associated with techniques and time restriction, some questions remain open: (i) Can we observe the same synaptic imbalance in the AD rat model used in this project? If so, would anti-inflammatory treatment using IFN-β1a preserve the normal E/I balance? To address these questions we could perform TEVC in microtransplanted receptors from rats injected with Aβ-42 aggregates in the dorsal hippocampus. (ii) Another important point, that we are proposing is that the E/I

balance shifting toward pro-excitatory changes may explain the hyperactivity observed in AD. While we cannot directly link those two processes together, imbalance of the E/I ratio and hyperactivity were recently observed simultaneously in a AD mouse model [207]. (iii) Whether these excitability impairments, known to underlie MCI and pre-clinical AD, are present in early regions affected by AD pathogenesis and in early stages of the pathology are still unknown. Our future direction will be to determine the E/I ratio in brain regions that are early affected by AD pathogenesis, such as the temporal lobe, hippocampus and entorhinal cortex. In addition, we will test for first time the initial electrophysiological changes of human synaptic receptors elicited by Aβ and Tau toxic oligomers, and whether synaptic receptors from resilient people, stage Braak VI and no dementia, are susceptible to these oligomers. Finally, we will use MSM for the screening of compounds capable of reestablishing the E/I balance in early AD patients, to prevent the progression, or in full AD, to ameliorate or control the symptoms.

REFERENCES

[1] "2019 ALZHEIMER'S DISEASE FACTS AND FIGURES Includes a Special Report on Alzheimer's Detection in the Primary Care Setting: Connecting Patients and Physicians," Chicago, IL 60601.

[2] A. Serrano-Pozo, M. P. Frosch, E. Masliah, and B. T. Hyman, "Neuropathological alterations in Alzheimer disease.," *Cold Spring Harb. Perspect. Med.*, vol. 1, no. 1, p. a006189, Sep. 2011.

[3] M.-K. Chen *et al.*, "Assessing Synaptic Density in Alzheimer Disease With Synaptic Vesicle Glycoprotein 2A Positron Emission Tomographic Imaging," *JAMA Neurol.*, vol. 75, no. 10, p. 1215, Oct. 2018.

[4] F. Kamenetz *et al.*, "APP processing and synaptic function.," *Neuron*, vol. 37, no. 6, pp. 925–37, Mar. 2003.

[5] H. A. Pearson and C. Peers, "Physiological roles for amyloid beta peptides.," *J. Physiol.*, vol. 575, no. Pt 1, pp. 5–10, Aug. 2006.

[6] "Tau - an overview | ScienceDirect Topics." [Online]. Available: https://www.sciencedirect.com/topics/medicine-and-dentistry/tau#targetText=Tau,stability and regulating axonal transport. [Accessed: 29-Oct-2019].

[7] L. M. Fox and A. Yamamoto, "Macroautophagy of Aggregation-Prone Proteins in Neurodegenerative Disease," in *Autophagy: Cancer, Other Pathologies, Inflammation, Immunity, Infection, and Aging*, vol. 7, Elsevier Inc., 2015, pp. 117–137.

[8] M. Marquié *et al.*, "[F-18]-AV-1451 binding correlates with postmortem neurofibrillary tangle Braak staging.," *Acta Neuropathol.*, vol. 134, no. 4, pp. 619–628, Oct. 2017.

[9] P. T. Nelson *et al.*, "Correlation of Alzheimer disease neuropathologic changes with cognitive status: a review of the literature.," *J. Neuropathol. Exp. Neurol.*, vol. 71, no. 5, pp. 362–81, May 2012.

[10] P. Vemuri and C. R. Jack, "Role of structural MRI in Alzheimer's disease," *Alzheimers. Res. Ther.*, vol. 2, no. 4, p. 23, Aug. 2010.

[11] G. M. McKhann *et al.*, "The diagnosis of dementia due to Alzheimer's disease: recommendations from the National Institute on Aging-Alzheimer's Association workgroups on diagnostic guidelines for Alzheimer's disease.," *Alzheimers. Dement.*, vol. 7, no. 3, pp. 263–9, May 2011.

[12] "How Is Alzheimer's Disease Diagnosed?," *NIH*, *2019*. [Online]. Available: https://www.nia.nih.gov/health/how-alzheimers-disease-diagnosed. [Accessed: 23-Sep-2019].

[13] L. E. Hebert, J. Weuve, P. A. Scherr, and D. A. Evans, "Alzheimer disease in the United States (2010-2050) estimated using the 2010 census," *Neurology*, vol. 80, no. 19, pp. 1778–1783, May 2013.

[14] "Alzheimer's Facts and Figures Report | Alzheimer's Association." [Online]. Available: https://www.alz.org/alzheimers-dementia/facts-figures. [Accessed: 03-Sep-2019].

[15] "Alzheimer's & Dementia | Alzheimer's Association," *2019*, 2019. [Online]. Available: https://www.alz.org/alzheimer_s_dementia. [Accessed: 03-Sep-2019].

[16] M. T. Heneka *et al.*, "Neuroinflammation in Alzheimer's disease," *Lancet Neurol.*, vol. 14, no. 4, pp. 388–405, Apr. 2015.

[17] Y. T. Quiroz *et al.*, "Hippocampal hyperactivation in presymptomatic familial Alzheimer's disease," *Ann. Neurol.*, vol. 68, no. 6, pp. 865–875, Dec. 2010.

[18] S. Y. Bookheimer *et al.*, "Patterns of Brain Activation in People at Risk for Alzheimer's Disease," *N. Engl. J. Med.*, vol. 343, no. 7, pp. 450–456, Aug. 2000.

[19] S. Rossi *et al.*, "Interleukin-1b Causes Synaptic Hyperexcitability in Multiple Sclerosis," *ANN NEUROL*, vol. 71, pp. 76–83, 2012.

[20] B. D. S. Clarkson, R. J. Kahoud, C. B. McCarthy, and C. L. Howe, "Inflammatory cytokine-induced changes in neural network activity measured by waveform analysis of high-content calcium imaging

in murine cortical neurons," *Sci. Rep.*, vol. 7, no. 1, p. 9037, Dec. 2017.
[21] M. A. Busche and A. Konnerth, "Impairments of neural circuit function in Alzheimer's disease.," *Philos. Trans. R. Soc. Lond. B. Biol. Sci.*, vol. 371, no. 1700, 2016.
[22] J. K. Holth *et al.*, "Tau loss attenuates neuronal network hyperexcitability in mouse and Drosophila genetic models of epilepsy.," *J. Neurosci.*, vol. 33, no. 4, pp. 1651–9, Jan. 2013.
[23] J. R. Cirrito *et al.*, "Synaptic Activity Regulates Interstitial Fluid Amyloid-β Levels In Vivo," *Neuron*, vol. 48, no. 6, pp. 913–922, Dec. 2005.
[24] A. Salminen, J. Ojala, A. Kauppinen, K. Kaarniranta, and T. Suuronen, "Inflammation in Alzheimer's disease: Amyloid-β oligomers trigger innate immunity defence via pattern recognition receptors," *Prog. Neurobiol.*, vol. 87, no. 3, pp. 181–194, Feb. 2009.
[25] L. E. Rojo, J. A. Fernández, A. A. Maccioni, J. M. Jimenez, and R. B. Maccioni, "Neuroinflammation: Implications for the Pathogenesis and Molecular Diagnosis of Alzheimer's Disease," *Arch. Med. Res.*, vol. 39, no. 1, pp. 1–16, Jan. 2008.
[26] H. Hippius and G. Neundörfer, "The discovery of Alzheimer's disease.," *Dialogues Clin. Neurosci.*, vol. 5, no. 1, pp. 101–8, Mar. 2003.
[27] G. McKhann, D. Drachman, M. Folstein, R. Katzman, D. Price, and E. M. Stadlan, "Clinical diagnosis of Alzheimer's disease: report of the NINCDS-ADRDA Work Group under the auspices of Department of Health and Human Services Task Force on Alzheimer's Disease.," *Neurology*, vol. 34, no. 7, pp. 939–44, Jul. 1984.
[28] D. P. Perl, "Neuropathology of Alzheimer's disease.," *Mt. Sinai J. Med.*, vol. 77, no. 1, pp. 32–42, 2010.
[29] H. Braak and E. Braak, "Neuropathological stageing of Alzheimer-related changes," 1991.
[30] D. Mehta, R. Jackson, G. Paul, J. Shi, and M. Sabbagh, "Why do trials for Alzheimer's disease drugs keep failing? A discontinued drug perspective for 2010-2015," *Expert Opin. Investig. Drugs*, vol. 26, no. 6, pp. 735–739, Jun. 2017.
[31] "Alzheimer's: Drugs help manage symptoms - Mayo Clinic." [Online]. Available: https://www.mayoclinic.org/diseases-conditions/alzheimers-disease/in-depth/alzheimers/art-20048103#targetText=Alzheimer's still has no cure,manage symptoms of the disease.&targetText=Unfortunately%2C Alzheimer's drugs don't,time%2C their effects wear off. [Accessed: 29-Oct-2019].
[32] "Medications for Memory Loss | Alzheimer's Association." [Online]. Available: https://www.alz.org/alzheimers-dementia/treatments/medications-for-memory#targetText=The U.S. Food and Drug,and reasoning) of Alzheimer's disease. [Accessed: 29-Oct-2019].
[33] M. A. Meraz-Ríos, D. Toral-Rios, D. Franco-Bocanegra, J. Villeda-Hernández, and V. Campos-Peña, "Inflammatory process in Alzheimer's Disease.," *Front. Integr. Neurosci.*, vol. 7, p. 59, 2013.
[34] C. Reitz and R. Mayeux, "Alzheimer disease: epidemiology, diagnostic criteria, risk factors and biomarkers.," *Biochem. Pharmacol.*, vol. 88, no. 4, pp. 640–51, Apr. 2014.
[35] H. K. Dong, J.-A. Gim, S. H. Yeo, and H.-S. Kim, "Integrated late onset Alzheimer's disease (LOAD) susceptibility genes: Cholesterol metabolism and trafficking perspectives," *Gene*, vol. 597, pp. 10–16, Jan. 2017.
[36] L. M. Bekris, C.-E. Yu, T. D. Bird, and D. W. Tsuang, "Genetics of Alzheimer disease.," *J. Geriatr. Psychiatry Neurol.*, vol. 23, no. 4, pp. 213–27, Dec. 2010.
[37] H. Potter, A. Granic, and J. Caneus, "Role of Trisomy 21 Mosaicism in Sporadic and Familial Alzheimer's Disease.," *Curr. Alzheimer Res.*, vol. 13, no. 1, pp. 7–17, 2016.
[38] K. Blennow, M. J. De Leon, and H. Zetterberg, "Alzheimer's disease," 2006.
[39] J. L. Cummings, "Alzheimer's Disease," *N. Engl. J. Med.*, vol. 351, no. 1, pp. 56–67, Jul. 2004.
[40] M. V. F. Silva, C. D. M. G. Loures, L. C. V. Alves, L. C. De Souza, K. B. G. Borges, and M. D. G. Carvalho, "Alzheimer's disease: Risk factors and potentially protective measures," *J. Biomed. Sci.*, vol. 26, no. 1, May 2019.
[41] N. Scarmeas, Y. Stern, M. X. Tang, R. Mayeux, and J. A. Luchsinger, "Mediterranean diet and risk for Alzheimer's disease," *Ann. Neurol.*, vol. 59, no. 6, pp. 912–921, Jun. 2006.

[42] C. Y. Santos, P. J. Snyder, W. C. Wu, M. Zhang, A. Echeverria, and J. Alber, "Pathophysiologic relationship between Alzheimer's disease, cerebrovascular disease, and cardiovascular risk: A review and synthesis," *Alzheimer's and Dementia: Diagnosis, Assessment and Disease Monitoring*, vol. 7. Elsevier Inc, pp. 69–87, 2017.
[43] C. R. Jack *et al.*, "NIA-AA Research Framework: Toward a biological definition of Alzheimer's disease.," *Alzheimers. Dement.*, vol. 14, no. 4, pp. 535–562, 2018.
[44] I. Koychev *et al.*, "PET Tau and Amyloid-β Burden in Mild Alzheimer's Disease: Divergent Relationship with Age, Cognition, and Cerebrospinal Fluid Biomarkers," *J. Alzheimer's Dis.*, vol. 60, no. 1, pp. 283–293, Aug. 2017.
[45] A. Bakker, M. S. Albert, G. Krauss, C. L. Speck, and M. Gallagher, "Response of the medial temporal lobe network in amnestic mild cognitive impairment to therapeutic intervention assessed by fMRI and memory task performance.," *NeuroImage. Clin.*, vol. 7, pp. 688–98, 2015.
[46] R. J. Bateman *et al.*, "Clinical and biomarker changes in dominantly inherited Alzheimer's disease.," *N. Engl. J. Med.*, vol. 367, no. 9, pp. 795–804, Aug. 2012.
[47] A. G. Vlassenko, T. L. S. Benzinger, and J. C. Morris, "PET amyloid-beta imaging in preclinical Alzheimer's disease.," *Biochim. Biophys. Acta*, vol. 1822, no. 3, pp. 370–9, Mar. 2012.
[48] S. Y. Bookheimer *et al.*, "Patterns of Brain Activation in People at Risk for Alzheimer's Disease," *N. Engl. J. Med.*, vol. 343, no. 7, pp. 450–456, Aug. 2000.
[49] M. Bolós, M. Llorens-Martín, J. Jurado-Arjona, F. Hernández, A. Rábano, and J. Avila, "Direct Evidence of Internalization of Tau by Microglia In Vitro and In Vivo," *J. Alzheimer's Dis.*, vol. 50, no. 1, pp. 77–87, Nov. 2015.
[50] Y. Li, X. F. Du, C. S. Liu, Z. L. Wen, and J. L. Du, "Reciprocal Regulation between Resting Microglial Dynamics and Neuronal Activity In Vivo," *Dev. Cell*, vol. 23, no. 6, pp. 1189–1202, Dec. 2012.
[51] L. Dissing-Olesen, J. M. LeDue, R. L. Rungta, J. K. Hefendehl, H. B. Choi, and B. A. MacVicar, "Activation of neuronal NMDA receptors triggers transient ATP-mediated microglial process outgrowth," *J. Neurosci.*, vol. 34, no. 32, pp. 10511–10527, Aug. 2014.
[52] U. B. Eyo and L.-J. Wu, "Bidirectional microglia-neuron communication in the healthy brain.," *Neural Plast.*, vol. 2013, p. 456857, 2013.
[53] D. G. Walker, J. E. Dalsing-Hernandez, N. A. Campbell, and L.-F. Lue, "Decreased expression of CD200 and CD200 receptor in Alzheimer's disease: a potential mechanism leading to chronic inflammation.," *Exp. Neurol.*, vol. 215, no. 1, pp. 5–19, Jan. 2009.
[54] M. M. Varnum, T. Kiyota, K. L. Ingraham, S. Ikezu, and T. Ikezu, "1. Varnum MM, Kiyota T, Ingraham KL, Ikezu S, Ikezu T. The anti-inflammatory glycoprotein, CD200, restores neurogenesis and enhances amyloid phagocytosis in a mouse model of Alzheimer's disease. Neurobiol Aging. 2015;36(11):2995–3007. The anti-inflammator," *Neurobiol. Aging*, vol. 36, no. 11, pp. 2995–3007, 2015.
[55] M. Hernangómez *et al.*, "CD200-CD200R1 interaction contributes to neuroprotective effects of anandamide on experimentally induced inflammation," *Glia*, vol. 60, no. 9, pp. 1437–1450, Sep. 2012.
[56] Z. Chen *et al.*, "Microglial displacement of inhibitory synapses provides neuroprotection in the adult brain," *Nat. Commun.*, vol. 5, 2014.
[57] H. Phatnani and T. Maniatis, "Astrocytes in neurodegenerative disease.," *Cold Spring Harb. Perspect. Biol.*, vol. 7, no. 6, p. a020628, Apr. 2015.
[58] A. Gomez-Arboledas *et al.*, "Phagocytic clearance of presynaptic dystrophies by reactive astrocytes in Alzheimer's disease.," *Glia*, vol. 66, no. 3, pp. 637–653, 2018.
[59] A. Araque, V. Parpura, R. P. Sanzgiri, and P. G. Haydon, "Tripartite synapses: glia, the unacknowledged partner," *Trends Neurosci.*, vol. 22, no. 5, pp. 208–215, May 1999.
[60] G. Perea, M. Navarrete, and A. Araque, "Tripartite synapses: astrocytes process and control synaptic information," *Trends Neurosci.*, vol. 32, no. 8, pp. 421–431, Aug. 2009.
[61] W.-S. Chung and B. A. Barres, "The role of glial cells in synapse elimination," *Curr. Opin.*

Neurobiol., vol. 22, no. 3, pp. 438–445, Jun. 2012.
[62] M. A. Galic, K. Riazi, and Q. J. Pittman, "Cytokines and brain excitability.," *Front. Neuroendocrinol.*, vol. 33, no. 1, pp. 116–25, Jan. 2012.
[63] J. Peltola *et al.*, "Interleukin-6 and Interleukin-1 receptor antagonist in cerebrospinal fluid from patients with recent tonic–clonic seizures," *Epilepsy Res.*, vol. 41, no. 3, pp. 205–211, Oct. 2000.
[64] S. Balosso *et al.*, "A novel non-transcriptional pathway mediates the proconvulsive effects of interleukin-1beta.," *Brain*, vol. 131, no. Pt 12, pp. 3256–65, Dec. 2008.
[65] W.-Y. Wang, M.-S. Tan, J.-T. Yu, and L. Tan, "Role of pro-inflammatory cytokines released from microglia in Alzheimer's disease.," *Ann. Transl. Med.*, vol. 3, no. 10, p. 136, Jun. 2015.
[66] L. C. Katz and C. J. Shatz, "Synaptic activity and the construction of cortical circuits," *Science*, vol. 274, no. 5290. pp. 1133–1138, 15-Nov-1996.
[67] D. J. Selkoe, "Alzheimer's disease is a synaptic failure," *Science*, vol. 298, no. 5594. pp. 789–791, 25-Oct-2002.
[68] R. A. Rissman and W. C. Mobley, "Implications for treatment: GABAA receptors in aging, Down syndrome and Alzheimer's disease," *Journal of Neurochemistry*, vol. 117, no. 4. pp. 613–622, May-2011.
[69] S. Luchetti, I. Huitinga, and D. F. Swaab, "Neurosteroid and GABA-A receptor alterations in Alzheimer's disease, Parkinson's disease and multiple sclerosis.," *Neuroscience*, vol. 191, pp. 6–21, Sep. 2011.
[70] E. Alberdi *et al.*, "Amyloid β oligomers induce Ca 2+ dysregulation and neuronal death through activation of ionotropic glutamate receptors."
[71] W. Sieghart and M. M. Savić, "International Union of Basic and Clinical Pharmacology. CVI: GABAA Receptor Subtype- and Function-selective Ligands: Key Issues in Translation to Humans.," *Pharmacol. Rev.*, vol. 70, no. 4, pp. 836–878, 2018.
[72] D. Ulrich, "Amyloid-β impairs synaptic inhibition via GABAA receptor endocytosis," *J. Neurosci.*, vol. 35, no. 24, pp. 9205–9210, Jun. 2015.
[73] S. Sahara, Y. Yanagawa, D. D. M. O'Leary, and C. F. Stevens, "The fraction of cortical GABAergic neurons is constant from near the start of cortical neurogenesis to adulthood.," *J. Neurosci.*, vol. 32, no. 14, pp. 4755–61, Apr. 2012.
[74] B. Sun *et al.*, "Imbalance between GABAergic and Glutamatergic Transmission Impairs Adult Neurogenesis in an Animal Model of Alzheimer's Disease.," *Cell Stem Cell*, vol. 5, no. 6, pp. 624–33, Dec. 2009.
[75] T. P. Vogels, H. Sprekeler, F. Zenke, C. Clopath, and W. Gerstner, "Inhibitory plasticity balances excitation and inhibition in sensory pathways and memory networks.," *Science*, vol. 334, no. 6062, pp. 1569–73, Dec. 2011.
[76] S. Zhou and Y. Yu, "Synaptic E-I Balance Underlies Efficient Neural Coding.," *Front. Neurosci.*, vol. 12, p. 46, 2018.
[77] R. Gao and P. Penzes, "Common mechanisms of excitatory and inhibitory imbalance in schizophrenia and autism spectrum disorders.," *Curr. Mol. Med.*, vol. 15, no. 2, pp. 146–67, 2015.
[78] E. Vico Varela, G. Etter, and S. Williams, "Excitatory-inhibitory imbalance in Alzheimer's disease and therapeutic significance," *Neurobiology of Disease*, vol. 127. Academic Press Inc., pp. 605–615, 01-Jul-2019.
[79] H. I. Needs *et al.*, "Changes in excitatory and inhibitory receptor expression and network activity during induction and establishment of epilepsy in the rat Reduced Intensity Status Epilepticus (RISE) model," *Neuropharmacology*, vol. 158, p. 107728, Nov. 2019.
[80] A. Demuro, I. Parker, and G. E. Stutzmann, "Calcium Signaling and Amyloid Toxicity in Alzheimer Disease *," 2010.
[81] M. A. Busche *et al.*, "Clusters of Hyperactive Neurons Near Amyloid Plaques in a Mouse Model of Alzheimer's Disease," *Science (80-.).*, vol. 321, no. 5896, pp. 1686–1689, Sep. 2008.
[82] J. W. Ramadan, S. R. Steiner, C. M. O'Neill, and C. S. Nunemaker, "The central role of calcium in the effects of cytokines on beta-cell function: Implications for type 1 and type 2 diabetes," *Cell*

Calcium, vol. 50, no. 6. Elsevier Ltd, pp. 481–490, 2011.
[83] A. Calcium Hypothesis Workgroup, "Calcium Hypothesis of Alzheimer's disease and brain aging: A framework for integrating new evidence into a comprehensive theory of pathogenesis," 2017.
[84] D. Putcha *et al.*, "Hippocampal hyperactivation associated with cortical thinning in Alzheimer's disease signature regions in non-demented elderly adults.," *J. Neurosci.*, vol. 31, no. 48, pp. 17680–8, Nov. 2011.
[85] A. Bakker *et al.*, "Reduction of hippocampal hyperactivity improves cognition in amnestic mild cognitive impairment.," *Neuron*, vol. 74, no. 3, pp. 467–74, May 2012.
[86] D. Pandis and N. Scarmeas, "Seizures in Alzheimer disease: clinical and epidemiological data.," *Epilepsy Curr.*, vol. 12, no. 5, pp. 184–7, Sep. 2012.
[87] L. Pasquini *et al.*, "Medial Temporal Lobe Disconnection and Hyperexcitability Across Alzheimer's Disease Stages.," *J. Alzheimer's Dis. reports*, vol. 3, no. 1, pp. 103–112, May 2019.
[88] L. Pasquini *et al.*, "Increased Intrinsic Activity of Medial-Temporal Lobe Subregions is Associated with Decreased Cortical Thickness of Medial-Parietal Areas in Patients with Alzheimer's Disease Dementia," *J. Alzheimer's Dis.*, vol. 51, no. 1, pp. 313–326, Feb. 2016.
[89] M. E. Raichle, A. M. MacLeod, A. Z. Snyder, W. J. Powers, D. A. Gusnard, and G. L. Shulman, "A default mode of brain function," *Proc. Natl. Acad. Sci. U. S. A.*, vol. 98, no. 2, pp. 676–682, Jan. 2001.
[90] R. A. Sperling *et al.*, "Amyloid deposition is associated with impaired default network function in older persons without dementia.," *Neuron*, vol. 63, no. 2, pp. 178–88, Jul. 2009.
[91] K. Mevel, G. Chételat, F. Eustache, and B. Desgranges, "The default mode network in healthy aging and Alzheimer's disease.," *Int. J. Alzheimers. Dis.*, vol. 2011, p. 535816, Jun. 2011.
[92] P. Hagmann *et al.*, "Mapping the structural core of human cerebral cortex.," *PLoS Biol.*, vol. 6, no. 7, p. e159, Jul. 2008.
[93] M. E. Raichle, "The Brain's Default Mode Network," *Annu. Rev. Neurosci.*, vol. 38, no. 1, pp. 433–447, Jul. 2015.
[94] B. J. Harrison *et al.*, "Task-Induced Deactivation from Rest Extends beyond the Default Mode Brain Network," *PLoS One*, vol. 6, no. 7, p. e22964, Jul. 2011.
[95] J. S. Mayer, A. Roebroeck, K. Maurer, and D. E. J. Linden, "Specialization in the default mode: Task-induced brain deactivations dissociate between visual working memory and attention," *Hum. Brain Mapp.*, vol. 31, no. 1, p. NA-NA, Jan. 2009.
[96] K. D. Singh and I. P. Fawcett, "Transient and linearly graded deactivation of the human default-mode network by a visual detection task," *Neuroimage*, vol. 41, no. 1, pp. 100–112, May 2008.
[97] S. Palmqvist *et al.*, "Earliest accumulation of β-amyloid occurs within the default-mode network and concurrently affects brain connectivity," *Nat. Commun.*, vol. 8, no. 1, p. 1214, Dec. 2017.
[98] R. L. Buckner, J. R. Andrews-Hanna, and D. L. Schacter, "The Brain's Default Network Anatomy, Function, and Relevance to Disease," *Am. Psychol. Assoc.*, 2008.
[99] N. Lubina-Dąbrowska, A. Stepień, G. Sulkowski, B. Dąbrowska-Bouta, J. Langfort, and M. Chalimoniuk, "Effects of IFN-β1a and IFN-β1b treatment on the expression of cytokines, inducible NOS (NOS type II), and myelin proteins in animal model of multiple sclerosis," *Arch. Immunol. Ther. Exp. (Warsz).*, vol. 65, no. 4, pp. 325–338, Aug. 2017.
[100] N. Lubina-Dąbrowska, A. Stepień, G. Sulkowski, B. Dąbrowska-Bouta, J. Langfort, and M. Chalimoniuk, "Effects of IFN-β1a and IFN-β1b treatment on the expression of cytokines, inducible NOS (NOS type II), and myelin proteins in animal model of multiple sclerosis.," *Arch. Immunol. Ther. Exp. (Warsz).*, vol. 65, no. 4, pp. 325–338, Aug. 2017.
[101] M. Di Filippo *et al.*, "Interferon-β1a modulates glutamate neurotransmission in the CNS through CaMKII and GluN2A-containing NMDA receptors," *Neuropharmacology*, vol. 100, pp. 98–105, Jan. 2016.
[102] S. J. Coultrap and K. U. Bayer, "CaMKII regulation in information processing and storage," *Trends Neurosci.*, vol. 35, no. 10, pp. 607–618, Oct. 2012.

[103] G. Hadjilambreva, E. Mix, A. Rolfs, J. Müller, and U. Strauss, "Neuromodulation by a Cytokine: Interferon-β Differentially Augments Neocortical Neuronal Activity and Excitability," *J. Neurophysiol.*, vol. 93, no. 2, pp. 843–852, Feb. 2005.
[104] D. A. Costello and M. A. Lynch, "Toll-like receptor 3 activation modulates hippocampal network excitability, via glial production of interferon-β," *Hippocampus*, vol. 23, no. 8, pp. 696–707, Aug. 2013.
[105] O. Reetz, K. Stadler, and U. Strauss, "Protein kinase C activation mediates interferon-β-induced neuronal excitability changes in neocortical pyramidal neurons," *J. Neuroinflammation*, vol. 11, no. 1, p. 185, Dec. 2014.
[106] N. Mokhber *et al.*, "Cognitive dysfunction in patients with multiple sclerosis treated with different types of interferon beta: A randomized clinical trial," *J. Neurol. Sci.*, vol. 342, no. 1–2, pp. 16–20, Jul. 2014.
[107] F. Patti *et al.*, "Effects of immunomodulatory treatment with subcutaneous interferon beta-1a oncognitive decline in mildly disabled patients with relapsing—remitting multiple sclerosis," *Mult. Scler. J.*, vol. 16, no. 1, pp. 68–77, Jan. 2010.
[108] M. Calabrese *et al.*, "Effect of disease-modifying drugs on cortical lesions and atrophy in relapsing–remitting multiple sclerosis," *Mult. Scler. J.*, vol. 18, no. 4, pp. 418–424, Apr. 2012.
[109] L. M. E. Grimaldi *et al.*, "A pilot study on the use of interferon beta-1a in early Alzheimer's disease subjects," *J. Neuroinflammation*, vol. 11, Feb. 2014.
[110] J. M. Rubio-Perez and J. M. Morillas-Ruiz, "A review: inflammatory process in Alzheimer's disease, role of cytokines.," *ScientificWorldJournal.*, vol. 2012, p. 756357, 2012.
[111] C. Domingues, O. A. B. da Cruz e Silva, and A. G. Henriques, "Impact of Cytokines and Chemokines on Alzheimer's Disease Neuropathological Hallmarks," *Curr. Alzheimer Res.*, vol. 14, no. 8, pp. 870–882, Jul. 2017.
[112] P. L. Fernández, G. B. Britton, and K. S. Rao, "Potential Immunotargets for Alzheimer's Disease Treatment Strategies," *J. Alzheimer's Dis.*, vol. 33, no. 2, pp. 297–312, Dec. 2012.
[113] P. L. McGeer and E. G. McGeer, "The amyloid cascade-inflammatory hypothesis of Alzheimer disease: implications for therapy," *Acta Neuropathol.*, vol. 126, no. 4, pp. 479–497, Oct. 2013.
[114] K. Hensley, "Neuroinflammation in Alzheimer's disease: mechanisms, pathologic consequences, and potential for therapeutic manipulation.," *J. Alzheimers. Dis.*, vol. 21, no. 1, pp. 1–14, 2010.
[115] M. Etminan, S. Gill, and A. Samii, "Effect of non-steroidal anti-inflammatory drugs on risk of Alzheimer's disease: systematic review and meta-analysis of observational studies," *BMJ Br. Med. J.*, vol. 327, no. 7407, p. 128, Jul. 2003.
[116] S. Shadfar, C. J. Hwang, M.-S. Lim, D.-Y. Choi, and J. T. Hong, "Involvement of inflammation in Alzheimer's disease pathogenesis and therapeutic potential of anti-inflammatory agents," *Arch. Pharm. Res.*, vol. 38, no. 12, pp. 2106–2119, Dec. 2015.
[117] C. Balducci and G. Forloni, "Novel targets in Alzheimer's disease: A special focus on microglia," *Pharmacol. Res.*, vol. 130, pp. 402–413, Apr. 2018.
[118] J. J. Palop *et al.*, "Aberrant Excitatory Neuronal Activity and Compensatory Remodeling of Inhibitory Hippocampal Circuits in Mouse Models of Alzheimer's Disease," *Neuron*, vol. 55, no. 5, pp. 697–711, Sep. 2007.
[119] J. J. Palop and L. Mucke, "Epilepsy and cognitive impairments in Alzheimer disease.," *Arch. Neurol.*, vol. 66, no. 4, pp. 435–40, Apr. 2009.
[120] L. Verret *et al.*, "Inhibitory interneuron deficit links altered network activity and cognitive dysfunction in Alzheimer model.," *Cell*, vol. 149, no. 3, pp. 708–21, Apr. 2012.
[121] R. Goutagny and S. Krantic, "Hippocampal oscillatory activity in Alzheimer's disease: toward the identification of early biomarkers?," *Aging Dis.*, vol. 4, no. 3, pp. 134–40, Jun. 2013.
[122] B. Styr and I. Slutsky, "Imbalance between firing homeostasis and synaptic plasticity drives early-phase Alzheimer's disease," *Nat. Neurosci.*, vol. 21, no. 4, pp. 463–473, Apr. 2018.
[123] S. Jayadev *et al.*, "Alzheimer's disease phenotypes and genotypes associated with mutations in presenilin 2," *Brain*, vol. 133, no. 4, pp. 1143–1154, Apr. 2010.

[124] B. Zott, M. A. Busche, R. A. Sperling, and A. Konnerth, “What Happens with the Circuit in Alzheimer’s Disease in Mice and Humans?,” *Annu. Rev. Neurosci.*, vol. 41, pp. 277–297, 2018.
[125] M. Okun and I. Lampl, “Instantaneous correlation of excitation and inhibition during ongoing and sensory-evoked activities,” *Nat. Neurosci.*, vol. 11, no. 5, pp. 535–537, May 2008.
[126] C. M. Mazure and J. Swendsen, “Sex differences in Alzheimer’s disease and other dementias,” *The Lancet Neurology*, vol. 15, no. 5. Lancet Publishing Group, pp. 451–452, 01-Apr-2016.
[127] M. M. Mielke, P. Vemuri, and W. A. Rocca, “Clinical epidemiology of Alzheimer’s disease: Assessing sex and gender differences,” *Clinical Epidemiology*, vol. 6, no. 1. pp. 37–48, 08-Jan-2014.
[128] R. Carrotta *et al.*, “Toxicity of recombinant beta-amyloid prefibrillar oligomers on the morphogenesis of the sea urchin Paracentrotus lividus.,” *FASEB J.*, vol. 20, no. 11, pp. 1916–7, Sep. 2006.
[129] G. Mudò *et al.*, “Seizures increase trkC mRNA expression in the dentate gyrus of rat hippocampus. Role of glutamate receptor activation.,” *J. Mol. Neurosci.*, vol. 6, no. 1, pp. 11–22, 1995.
[130] V. Di Liberto *et al.*, “Existence of muscarinic acetylcholine receptor (mAChR) and fibroblast growth factor receptor (FGFR) heteroreceptor complexes and their enhancement of neurite outgrowth in neural hippocampal cultures.,” *Biochim. Biophys. acta. Gen. Subj.*, vol. 1861, no. 2, pp. 235–245, Feb. 2017.
[131] O. H. LOWRY, N. J. ROSEBROUGH, A. L. FARR, and R. J. RANDALL, “Protein measurement with the Folin phenol reagent.,” *J. Biol. Chem.*, vol. 193, no. 1, pp. 265–275, Nov. 1951.
[132] M. Frinchi, P. Scaduto, F. Cappello, N. Belluardo, and G. Mudò, “Heat shock protein (Hsp) regulation by muscarinic acetylcholine receptor (mAChR) activation in the rat hippocampus,” *J. Cell. Physiol.*, vol. 233, no. 8, 2018.
[133] M. G. Zizzo *et al.*, “Altered gastrointestinal motility in an animal model of Lesch-Nyhan disease.,” *Auton. Neurosci.*, vol. 210, pp. 55–64, 2018.
[134] V. Di Liberto *et al.*, “Anxiolytic effects of muscarinic acetylcholine receptors agonist oxotremorine in chronically stressed rats and related changes in BDNF and FGF2 levels in the hippocampus and prefrontal cortex.,” *Psychopharmacology (Berl).*, vol. 234, no. 4, pp. 559–573, Feb. 2017.
[135] T. M. Kelly and J. J. Mann, “Validity of DSM-III-R diagnosis by psychological autopsy: A comparison with clinician ante-mortem diagnosis,” *Acta Psychiatr. Scand.*, vol. 94, no. 5, pp. 337–343, 1996.
[136] E. G. Jones, S. H. Hendry, X. B. Liu, S. Hodgins, S. G. Potkin, and W. W. Tourtellotte, “A method for fixation of previously fresh-frozen human adult and fetal brains that preserves histological quality and immunoreactivity.,” *J. Neurosci. Methods*, vol. 44, no. 2–3, pp. 133–44, Sep. 1992.
[137] J. A. Blair *et al.*, “Individual Case Analysis of Postmortem Interval Time on Brain Tissue Preservation.,” *PLoS One*, vol. 11, no. 3, p. e0151615, 2016.
[138] J. R. Glausier, A. Konanur, and D. A. Lewis, “Factors Affecting Ultrastructural Quality in the Prefrontal Cortex of the Postmortem Human Brain,” *J. Histochem. Cytochem.*, vol. 67, no. 3, pp. 185–202, Mar. 2019.
[139] A. Limon *et al.*, “Electrophysiological evaluation of extracellular spermine and alkaline pH on synaptic human GABAA receptors,” *Transl. Psychiatry*, vol. 9, no. 1, p. 218, Dec. 2019.
[140] A. Limon, J. M. Reyes-Ruiz, and R. Miledi, “Microtransplantation of neurotransmitter receptors from postmortem autistic brains to Xenopus oocytes,” *Proc. Natl. Acad. Sci. U. S. A.*, vol. 105, no. 31, pp. 10973–10977, Aug. 2008.
[141] H. Braak and E. Braak, “Staging of alzheimer’s disease-related neurofibrillary changes,” *Neurobiol. Aging*, vol. 16, no. 3, pp. 271–278, 1995.
[142] S. S. Mirra *et al.*, “The consortium to establish a registry for Alzheimer’s disease (CERAD). Part II. Standardization of the neuropathologic assessment of Alzheimer’s disease,” *Neurology*, vol. 41, no. 4, pp. 479–486, 1991.
[143] M. B. Dick, E. Doran, M. Phelan, and I. T. Lott, “Cognitive profiles on the severe Impairment Battery are similar in Alzheimer disease and Down syndrome with dementia,” *Alzheimer Dis. Assoc.*

Disord., vol. 30, no. 3, pp. 251–257, Aug. 2016.
[144] J. C. Lauterborn, C. D. Cox, S. W. Chan, P. W. Vanderklish, G. Lynch, and C. M. Gall, "Synaptic actin stabilization protein loss in Down syndrome and Alzheimer disease," *Brain Pathol.*, Sep. 2019.
[145] L. Y. Chen, C. S. Rex, M. S. Casale, C. M. Gall, and G. Lynch, "Changes in synaptic morphology accompany actin signaling during LTP," *J. Neurosci.*, vol. 27, no. 20, pp. 5363–5372, May 2007.
[146] C. A. Hunt, L. J. Schenker, and M. B. Kennedy, "PSD-95 is associated with the postsynaptic density and not with the presynaptic membrane at forebrain synapses," *J. Neurosci.*, vol. 16, no. 4, pp. 1380–1388, Feb. 1996.
[147] C. S. Rex *et al.*, "Different Rho GTPase-dependent signaling pathways initiate sequential steps in the consolidation of long-term potentiation," *J. Cell Biol.*, vol. 186, no. 1, pp. 85–97, Jul. 2009.
[148] L. Y. Chen *et al.*, "Physiological activation of synaptic Rac>PAK (p-21 activated kinase) signaling is defective in a mouse model of fragile X syndrome," *J. Neurosci.*, vol. 30, no. 33, pp. 10977–10984, Aug. 2010.
[149] R. R. Seese *et al.*, "LTP induction translocates cortactin at distant synapses in wild-type but not Fmr1 knock-out mice," *J. Neurosci.*, vol. 32, no. 21, pp. 7403–7413, May 2012.
[150] K. H. Gylys, J. A. Fein, F. Yang, and G. M. Cole, "Enrichment of presynaptic and postsynaptic markers by size-based gating analysis of synaptosome preparations from rat and human cortex," *Cytometry*, vol. 60A, no. 1, pp. 90–96, Jul. 2004.
[151] M. M. Comerota, B. Krishnan, and G. Taglialatela, "Near infrared light decreases synaptic vulnerability to amyloid beta oligomers," *Sci. Rep.*, vol. 7, no. 1, Dec. 2017.
[152] K. H. Gylys, J. A. Fein, F. Yang, D. J. Wiley, C. A. Miller, and G. M. Cole, "Synaptic changes in alzheimer's disease: Increased amyloid-β and gliosis in surviving terminals is accompanied by decreased PSD-95 fluorescence," *Am. J. Pathol.*, vol. 165, no. 5, pp. 1809–1817, 2004.
[153] J. Marsal, G. Tigyi, and R. Miledi, "Incorporation of acetylcholine receptors and Cl- channels in Xenopus oocytes injected with Torpedo electroplaque membranes.," *Proc. Natl. Acad. Sci. U. S. A.*, vol. 92, no. 11, pp. 5224–8, May 1995.
[154] A. Limon, J. M. Reyes-Ruiz, and R. Miledi, "Loss of functional GABAA receptors in the Alzheimer diseased brain," *Proc. Natl. Acad. Sci.*, vol. 109, no. 25, pp. 10071–10076, Jun. 2012.
[155] P. Picone, R. Carrotta, G. Montana, M. R. Nobile, P. L. San Biagio, and M. Di Carlo, "Aβ oligomers and fibrillar aggregates induce different apoptotic pathways in LAN5 neuroblastoma cell cultures," *Biophys. J.*, vol. 96, no. 10, pp. 4200–4211, 2009.
[156] T. Yang, S. Li, H. Xu, D. M. Walsh, and D. J. Selkoe, "Large soluble oligomers of amyloid β-protein from alzheimer brain are far less neuroactive than the smaller oligomers to which they dissociate," *J. Neurosci.*, vol. 37, no. 1, pp. 152–163, Jan. 2017.
[157] R. Ghasemi, A. Zarifkar, K. Rastegar, N. Maghsoudi, and M. Moosavi, "Repeated intra-hippocampal injection of beta-amyloid 25-35 induces a reproducible impairment of learning and memory: Considering caspase-3 and MAPKs activity," *Eur. J. Pharmacol.*, vol. 726, no. 1, pp. 33–40, Mar. 2014.
[158] J. Q. Tong *et al.*, "Leptin attenuates the detrimental effects of β-amyloid on spatial memory and hippocampal later-phase long term potentiation in rats," *Horm. Behav.*, vol. 73, pp. 125–130, Jul. 2015.
[159] C. M. Maier, F. Yu, T. Nishi, S. J. Lathrop, and P. H. Chan, "Interferon-β fails to protect in a model of transient focal stroke," *Stroke*, vol. 37, no. 4, pp. 1116–1119, Apr. 2006.
[160] S. Floris *et al.*, "Interferon-beta directly influences monocyte infiltration into the central nervous system.," *J. Neuroimmunol.*, vol. 127, no. 1–2, pp. 69–79, Jun. 2002.
[161] P. H. van der Meide *et al.*, "Discontinuation of treatment with IFN-beta leads to exacerbation of experimental autoimmune encephalomyelitis in Lewis rats. Rapid reversal of the antiproliferative activity of IFN-beta and excessive expansion of autoreactive T cells as disease promoting mechanisms.," *J. Neuroimmunol.*, vol. 84, no. 1, pp. 14–23, Apr. 1998.
[162] S. Gong *et al.*, "Dynamics and correlation of serum cortisol and corticosterone under different physiological or stressful conditions in mice," *PLoS One*, vol. 10, no. 2, Feb. 2015.

[163] J. Meunier, J. Ieni, and T. Maurice, “The anti-amnesic and neuroprotective effects of donepezil against amyloid B 25-35 peptide-induced toxicity in mice involve an interaction with the σ 1 receptor,” *Br. J. Pharmacol.*, vol. 149, no. 8, pp. 998–1012, Dec. 2006.
[164] J. J. Graber, D. Ford, M. Zhan, G. Francis, H. Panitch, and S. Dhib-Jalbut, “Cytokine changes during interferon-beta therapy in multiple sclerosis: Correlations with interferon dose and MRI response,” *J. Neuroimmunol.*, vol. 185, no. 1–2, pp. 168–174, Apr. 2007.
[165] Y. Liu, I. Teige, I. Ericsson, V. Navikas, and S. Issazadeh-Navikas, “Suppression of EAE by oral tolerance is independent of endogenous IFN-β whereas treatment with recombinant IFN-β ameliorates EAE,” *Immunol. Cell Biol.*, vol. 88, no. 4, pp. 468–476, May 2010.
[166] J. Río and X. Montalban, “Interferon-β $_{1b}$ in the treatment of multiple sclerosis,” *Expert Opin. Pharmacother.*, vol. 6, no. 16, pp. 2877–2886, Dec. 2005.
[167] S. R. Ruuls *et al.*, “The length of treatment determines whether IFN-beta prevents or aggravates experimental autoimmune encephalomyelitis in Lewis rats.,” *J. Immunol.*, vol. 157, no. 12, pp. 5721–31, Dec. 1996.
[168] M. Yu, A. Nishiyama, B. D. Trapp, and V. K. Tuohy, “Interferon-β inhibits progression of relapsing-remitting experimental autoimmune encephalomyelitis,” *J. Neuroimmunol.*, vol. 64, no. 1, pp. 91–100, 1996.
[169] A. Deczkowska *et al.*, “Mef2C restrains microglial inflammatory response and is lost in brain ageing in an IFN-I-dependent manner,” *Nat. Commun.*, vol. 8, no. 1, Dec. 2017.
[170] R. G. Thorne, L. R. Hanson, T. M. Ross, D. Tung, and W. H. Frey, “Delivery of interferon-β to the monkey nervous system following intranasal administration,” *Neuroscience*, vol. 152, no. 3, pp. 785–797, Mar. 2008.
[171] N. H. Greig, W. R. Fredericks, H. W. Holloway, T. T. Soncrant, and S. I. Rapoport, “Delivery of human interferon-alpha to brain by transient osmotic blood-brain barrier modification in the rat.,” *J. Pharmacol. Exp. Ther.*, vol. 245, no. 2, 1988.
[172] W. Pan, W. A. Banks, and A. J. Kastin, “Permeability of the blood-brain and blood-spinal cord barriers to interferons,” *J. Neuroimmunol.*, vol. 76, no. 1–2, pp. 105–111, Jun. 1997.
[173] L. Capuron and A. H. Miller, “Immune system to brain signaling: Neuropsychopharmacological implications,” *Pharmacology and Therapeutics*, vol. 130, no. 2. pp. 226–238, May-2011.
[174] B. Weinstock-Guttman, R. M. Ransohoff, R. P. Kinkel, and R. A. Rudick, “The interferons: Biological effects, mechanisms of action, and use in multiple sclerosis,” *Ann. Neurol.*, vol. 37, no. 1, pp. 7–15, Jan. 1995.
[175] G. G. Turrigiano, K. R. Leslie, N. S. Desai, L. C. Rutherford, and S. B. Nelson, “Activity-dependent scaling of quantal amplitude in neocortical neurons,” *Nature*, vol. 391, no. 6670, pp. 892–896, Feb. 1998.
[176] R. C. Froemke, “Plasticity of Cortical Excitatory-Inhibitory Balance,” *Annu. Rev. Neurosci.*, vol. 38, no. 1, pp. 195–219, Jul. 2015.
[177] G. Turrigiano, “Homeostatic synaptic plasticity: local and global mechanisms for stabilizing neuronal function.,” *Cold Spring Harb. Perspect. Biol.*, vol. 4, no. 1, p. a005736, Jan. 2012.
[178] A. Bernareggi, M. Grilli, M. Marchi, C. Limatola, F. Ruzzier, and F. Eusebi, “Characterization of GABAA receptors expressed in glial cell membranes of adult mouse neocortex using a Xenopus oocyte microtransplantation expression system,” *J. Neurosci. Methods*, vol. 198, no. 1, pp. 77–83, May 2011.
[179] E. Sanna, C. Motzo, A. Murgia, F. Amato, T. Deserra, and G. Biggio, “Expression of Native GABAA Receptors in Xenopus Oocytes Injected With Rat Brain Synaptosomes,” *J. Neurochem.*, vol. 67, no. 5, pp. 2212–2214, Nov. 2002.
[180] F. Mazzo *et al.*, “Reconstitution of synaptic Ion channels from rodent and human brain in *Xenopus* oocytes: a biochemical and electrophysiological characterization,” *J. Neurochem.*, vol. 138, no. 3, pp. 384–396, Aug. 2016.
[181] E. Murenzi, A. C. Toltin, S. B. Symington, M. M. Morgan, and J. M. Clark, “Evaluation of microtransplantation of rat brain neurolemma into Xenopus laevis oocytes as a technique to study

the effect of neurotoxicants on endogenous voltage-sensitive ion channels," *Neurotoxicology*, vol. 60, pp. 260–273, May 2017.
[182] L. K. Siew, S. Love, D. Dawbarn, G. K. Wilcock, and S. J. Allen, "Measurement of pre- and post-synaptic proteins in cerebral cortex: effects of post-mortem delay.," *J. Neurosci. Methods*, vol. 139, no. 2, pp. 153–9, Oct. 2004.
[183] V. Tretter, T. C. Jacob, J. Mukherjee, J.-M. Fritschy, M. N. Pangalos, and S. J. Moss, "The clustering of GABA(A) receptor subtypes at inhibitory synapses is facilitated via the direct binding of receptor alpha 2 subunits to gephyrin.," *J. Neurosci.*, vol. 28, no. 6, pp. 1356–65, Feb. 2008.
[184] D. Keith and A. El-Husseini, "Excitation Control: Balancing PSD-95 Function at the Synapse.," *Front. Mol. Neurosci.*, vol. 1, p. 4, 2008.
[185] M. Xue, B. V Atallah, and M. Scanziani, "Equalizing excitation-inhibition ratios across visual cortical neurons.," *Nature*, vol. 511, no. 7511, pp. 596–600, Jul. 2014.
[186] R. Tatti, M. S. Haley, O. K. Swanson, T. Tselha, and A. Maffei, "Neurophysiology and Regulation of the Balance Between Excitation and Inhibition in Neocortical Circuits.," *Biol. Psychiatry*, vol. 81, no. 10, pp. 821–831, 2017.
[187] B. Sommer *et al.*, "Flip and flop: a cell-specific functional switch in glutamate-operated channels of the CNS," *Science (80-.).*, vol. 249, no. 4976, pp. 1580–1585, Sep. 1990.
[188] K. A. Yamada and C. M. Tang, "Benzothiadiazides inhibit rapid glutamate receptor desensitization and enhance glutamatergic synaptic currents.," *J. Neurosci.*, vol. 13, no. 9, pp. 3904–15, Sep. 1993.
[189] K. M. Partin, M. W. Fleck, and M. L. Mayer, "AMPA receptor flip/flop mutants affecting deactivation, desensitization, and modulation by cyclothiazide, aniracetam, and thiocyanate.," *J. Neurosci.*, vol. 16, no. 21, pp. 6634–47, Nov. 1996.
[190] L. Verret *et al.*, "Inhibitory Interneuron Deficit Links Altered Network Activity and Cognitive Dysfunction in Alzheimer Model," *Cell*, vol. 149, no. 3, pp. 708–721, Apr. 2012.
[191] J. Noebels, "A perfect storm: Converging paths of epilepsy and Alzheimer's dementia intersect in the hippocampal formation," *Epilepsia*, vol. 52, pp. 39–46, Jan. 2011.
[192] J. Barral and A. D'Reyes, "Synaptic scaling rule preserves excitatory-inhibitory balance and salient neuronal network dynamics," *Nat. Neurosci.*, vol. 19, no. 12, pp. 1690–1696, Dec. 2016.
[193] L. Q. Uddin, A. M. C. Kelly, B. B. Biswal, F. X. Castellanos, and M. P. Milham, "Functional Connectivity of Default Mode Network Components: Correlation, Anticorrelation, and Causality," *Hum. Brain Mapp.*, vol. 30, no. 2, pp. 625–637, Feb. 2009.
[194] C. Lustig *et al.*, "Functional deactivations: Change with age and dementia of the Alzheimer type," *Proc. Natl. Acad. Sci. U. S. A.*, vol. 100, no. SUPPL. 2, pp. 14504–14509, Nov. 2003.
[195] E. Head, D. Powell, B. T. Gold, and F. A. Schmitt, "Alzheimer's Disease in Down Syndrome."
[196] F. Eusebi, E. Palma, M. Amici, and R. Miledi, "Microtransplantation of ligand-gated receptor-channels from fresh or frozen nervous tissue into Xenopus oocytes: A potent tool for expanding functional information," *Progress in Neurobiology*, vol. 88, no. 1. pp. 32–40, May-2009.
[197] R. Zwart, F. Mazzo, and E. Sher, "Microtransplantation of human brain receptors into oocytes to tackle key questions in drug discovery," *Drug Discovery Today*, vol. 24, no. 2. Elsevier Ltd, pp. 533–543, 01-Feb-2019.
[198] S. Agarwal, R. K. Tannenberg, and P. R. Dodd, "Reduced expression of the inhibitory synapse scaffolding protein gephyrin in Alzheimer's disease.," *J. Alzheimers. Dis.*, vol. 14, no. 3, pp. 313–21, Jul. 2008.
[199] C. M. Hales *et al.*, "Abnormal Gephyrin immunoreactivity associated with Alzheimer disease pathologic changes," *J. Neuropathol. Exp. Neurol.*, vol. 72, no. 11, pp. 1009–1015, Nov. 2013.
[200] S. Mondragón-Rodríguez *et al.*, "Interaction of endogenous tau protein with synaptic proteins is regulated by N-methyl-D-aspartate receptor-dependent tau phosphorylation," *J. Biol. Chem.*, vol. 287, no. 38, pp. 32040–32053, Sep. 2012.
[201] A. Ittner and L. M. Ittner, "Dendritic Tau in Alzheimer's Disease," *Neuron*, vol. 99, no. 1. Cell Press, pp. 13–27, 11-Jul-2018.
[202] M. D. Greicius, G. Srivastava, A. L. Reiss, and V. Menon, "Default-mode network activity

distinguishes Alzheimer's disease from healthy aging: evidence from functional MRI.," *Proc. Natl. Acad. Sci. U. S. A.*, vol. 101, no. 13, pp. 4637–42, Mar. 2004.
[203] E. S. Lee *et al.*, "Default Mode Network Functional Connectivity in Early and Late Mild Cognitive Impairment: Results from the Alzheimer's Disease Neuroimaging Initiative," *Alzheimer Dis. Assoc. Disord.*, vol. 30, no. 4, pp. 289–296, 2016.
[204] N. L. Bjorklund, L. C. Reese, V. M. Sadagoparamanujam, V. Ghirardi, R. L. Woltjer, and G. Taglialatela, "Absence of amyloid β oligomers at the postsynapse and regulated synaptic Zn2+in cognitively intact aged individuals with Alzheimer's disease neuropathology," *Mol. Neurodegener.*, vol. 7, no. 1, May 2012.
[205] O. Zolochevska and G. Taglialatela, "Non-Demented Individuals with Alzheimer's Disease Neuropathology: Resistance to Cognitive Decline May Reveal New Treatment Strategies.," *Curr. Pharm. Des.*, vol. 22, no. 26, pp. 4063–8, 2016.
[206] J. N. Vega, T. J. Hohman, J. R. Pryweller, E. M. Dykens, and T. A. Thornton-Wells, "Resting-state functional connectivity in individuals with down syndrome and williams syndrome compared with typically developing controls," *Brain Connect.*, vol. 5, no. 8, pp. 461–475, Oct. 2015.
[207] T. Nuriel *et al.*, "Neuronal hyperactivity due to loss of inhibitory tone in APOE4 mice lacking Alzheimer's disease-like pathology," *Nat. Commun.*, vol. 8, no. 1, Dec. 2017.